

Dynamic wind farm layout optimization.

To find the optimal spots for movable floating offshore wind turbines through dynamic repositioning.

OE54030: Master Thesis (TU Delft)

TMR5950: Wind Turbine Energy - Offshore Engineering,
Master Thesis (NTNU)

Ufuktan Kilinc

Dynamic wind farm layout optimization.

To find the optimal spots for movable floating
offshore wind turbines through dynamic
repositioning.

by

Ufuktan Kilinc

University	Student Number
TU Delft	4538625
NTNU	557407

Thesis committee

Dr. ir. M. B. Zaaijer

Prof. D. T. Nguyen

Prof. E. E. Bachynski-Polic

Dr. ir. A. C. Viré

Prof. Z. Gao

Delft University of Technology

Norwegian University of Science and Technology

Norwegian University of Science and Technology

Delft University of Technology

Norwegian University of Science and Technology

Sunday 28th August, 2022

Cover Image: Wind Farm Fryslân by Ufuktan Kilinc.



Preface

This document, titled “Dynamic wind farm layout optimization,” describes the potential of a novel wind farm control concept based on movable wind turbines to increase a wind farm’s energy yield. It is part of the Master’s Thesis Project and a requirement to successfully finish the European Wind Energy Master (EWEM) programme with Offshore Engineering as a specialization. Upon finalizing this Master’s Thesis, I will be awarded with two degrees; MSc. Offshore and Dredging Engineering (TU Delft) & MSc. Technology—Wind Energy (NTNU). From January to August 2022, during the fourth and last semester of the EWEM programme, I worked on this document and its contents.

The first time I heard about the idea of wind turbine repositioning was in the Systems and Control class during my BSc. Mechanical Engineering at the TU Delft. In one of the lectures, Jan-Willem van Wingerden mentioned the concept of movable floating offshore wind turbines to reduce the effects of the wake. This idea intrigued me due to its novelty and technological challenges. While discussing a suitable Master’s Thesis topic together with Michiel Zaaijer, he mentioned the idea of wind farm layout optimization with dynamically repositionable floating wind turbines. We agreed that this was an interesting topic to investigate further.

From September to December 2021, NTNU hosted the third semester of the EWEM program. I took the course “TMR4590—Specialization Project Wind Turbine Energy—Offshore Engineering,” for which I conducted a literature study on the wind turbine repositioning concept. This Master’s Thesis Project was based on and guided by the conclusions of the literature review.

I am very grateful to my supervisors, Michiel Zaaijer, Dong Trong Nguyen, and Erin Bachynski-Polić, who guided me throughout the project. Their availability, support, feedback, and interest in my research are much appreciated. Many of the ideas and methods in this research came from the good discussions we had. I also wish to thank the Thesis committee members, Axelle Viré and Zhen Gao, for their time and interest.

I wish you a good reading experience!

*Ufuktan Kilinc
Delft, August 2022*

Abstract

Recently, there has been an increase in interest in floating wind turbines that are located offshore. These turbines allow for the harvesting of the power of the wind far offshore, where wind speeds are often higher.

Compared to their fixed counterparts, floating wind turbines allow for a certain mobility after the installation. This allows wind farm developers to consider layouts that change throughout the wind farm's operational phase. The change in layout can increase the energy yield of the wind farm, which may reduce the cost of floating wind energy.

This Master's Thesis presents a new method for wind farm layout optimization with movable floating offshore wind turbines. The objective function that is maximized is the annual energy production (AEP). The proposed method first finds the optimal installation locations of the turbines, then searches for the optimal wind farm layout for each wind direction while considering the movable range of the turbines. Different movable range sizes are considered in the analysis. These sizes range from small (there is almost no mobility allowed) to large (the turbine is allowed to move anywhere in the wind farm). The results show that the steepest gains are achieved for a movable range size of up to two rotor diameters (i.e., the turbine is allowed to move two rotor diameters in each direction, evaluated from the installation position). Above this range, a large additional movement is required for a minor increase in AEP. Moreover, for this movable range size, repositioning turbines is so effective that their installation positions almost do not affect the AEP.

In addition to the previous method, this Master's Thesis also presents a novel method to assess the movable range of floating offshore wind turbines. In this method, it is assumed that the mobility is achieved by adjusting the mooring line lengths through a winch system on board of the floater. The proposed method optimizes the line lengths such that an equilibrium is obtained in the relocated position. Various locations are selected for the analysis that cover most of the mooring system footprint on the seabed. The results show that the assumed movable range shape is not the same as the actual movable range shape.

For a 15MW floating offshore reference turbine, the movable range size with the steepest gains in terms of AEP (two rotor diameters) and the actual movable range are compared. The results show that the actual shape covers large parts of the circular shape.

In conclusion, large gains are expected in terms of AEP for movable floating offshore wind turbines. This brings us one step closer to reducing the cost of floating wind energy, which in turn increases its competitiveness with other energy resources.

Contents

Preface	i
Abstract	ii
Nomenclature	vi
List of Figures	vii
List of Tables	ix
1 Introduction	1
1.1 Background	1
1.1.1 Offshore wind	1
1.1.2 Floating wind	1
1.1.3 Levelized Cost of Energy	2
1.1.4 Description of the wake effect	2
1.1.5 A unique wake effect mitigation approach for floating offshore wind farms	3
1.2 Problem analysis	5
1.3 Objective	5
1.4 Approach	5
1.5 Organization of thesis	6
2 Wind farm layout optimization problem definition for AEP maximization	7
2.1 Traditional wind farm layout design	7
2.2 General description of wind farm layout optimization	8
2.3 Static and dynamic wind farm layout optimization	8
2.3.1 Definition of a static and dynamic wind farm layout	8
2.3.2 Description of static and dynamic wind farm layout optimization	9
2.3.3 Reference and restricted dynamic wind farm layout optimization methods	9
2.4 Mathematical formulations and workflows for AEP maximization	10
2.4.1 General optimization problem	10
2.4.2 Movable range and wind farm boundary constraints	10
2.4.3 Reference wind farm layout optimization problems	12
2.4.4 Restricted dynamic wind farm layout optimization problems	15
2.5 Wind farm AEP calculation using PyWake	19
2.5.1 Formulation of AEP	19
2.5.2 Definition of wind farm efficiency	19
2.5.3 AEP calculation using PyWake	20
2.5.4 PyWake model validation through an example layout	20
2.6 Constrained optimization algorithms	22
2.6.1 Introduction of four optimization algorithms	22
2.6.2 Covariance matrix adaptation evolution strategy	22
2.6.3 Constrained optimization by linear approximation	23
2.6.4 Trust-region interior point method	23
2.6.5 Sequential least squares programming	23
3 Optimized dynamic wind farm layouts for a case study	24
3.1 Description of wind farm case study	24
3.1.1 Wind farm case study selection	24
3.1.2 IEA37 3.35 MW turbine	25
3.1.3 Wind farm site	26
3.1.4 Wind resource	26

3.1.5	Wake model.	27
3.2	Optimized reference wind farm layouts	28
3.2.1	Static layout optimization.	29
3.2.2	Unrestricted dynamic layout optimization	33
3.3	Optimized restricted dynamic wind farm layouts	34
3.3.1	Sequential optimization	34
3.3.2	Nested optimization	37
3.4	Optimized dynamic wind layouts for three different static layouts	40
3.4.1	Introduction to the optimization study	40
3.4.2	Optimization approach	40
3.4.3	Dynamic layout for IEA37 example layout.	41
3.4.4	Dynamic layout for sequential optimization static layout	42
3.4.5	Dynamic layout for nested optimization static layout	43
3.5	Comparison of dynamic layout optimization results.	44
3.6	Discussion	45
3.6.1	The interpretations and implications of key findings	45
3.6.2	Limitations	46
4	Repositioning mechanism for a movable floating offshore wind turbine	47
4.1	Repositioning mechanism objectives	47
4.2	Description, comparison, and selection of repositioning mechanism(s)	48
4.2.1	Description of four different repositioning mechanisms.	48
4.2.2	Comparison and selection of repositioning mechanism(s)	50
4.3	Characteristics of position mooring	51
4.3.1	Turbine repositioning using position mooring	51
4.3.2	Example position mooring system and its main components	51
4.4	Position mooring performance	52
4.4.1	Introduction to position mooring performance assessment.	52
4.4.2	Methodology for position mooring performance assessment.	53
4.4.3	Case study: UMaine VoltturnUS-S floater for IEA 15MW turbine.	57
4.5	Discussion	63
4.5.1	The interpretations and implications of key findings	63
4.5.2	Limitations	63
5	Discussion	65
5.1	Introduction to the discussion	65
5.2	Movable range	65
5.3	Limitations	66
6	Conclusion and further work	67
6.1	Conclusion	67
6.2	Further work	68
A	Optimized dynamic layout for IEA 37 example layout	74
A.1	Convergence study with four different optimization algorithms.	74
A.2	Convergence study with COBYLA for different parameter values	76
B	Additional results for position mooring of UMaine VoltturnUS-S	79
B.1	Fairlead tension.	79
B.2	Vertical fairlead tension	80
B.3	Absolute error in yaw angle	80

Nomenclature

List of Abbreviations

AEP	Annual Energy Production
CapEx	Capital Expenditure
CMA-ES	Covariance Matrix Adaptation Evolution Strategy
COBYLA	Constrained Optimization By Linear Approximation
CoE	Cost of Energy
DecEx	Decommissioning Expenditure
DoF	Degrees of Freedom
DP	Dyanmic positioning
EA	Evolutionary Algorithms
EP	Evolutionary Programs
ES	Evolution Strategies
ES	Evolutionary Strategy
FB	Financial Balance
FOWT	Floating Offshore Wind Turbine
GA	Genetic Algorithm
GWEC	Global Wind Energy Council
IEA	International Energy Agency
LCoE	Levelized Cost of Energy
LPC	Levelized Production Cost
MIP	Mixed Integer Programming
NPV	Net Present Value
O&M	Operation and Maintenance
OpEx	Operational and maintenance Expenditure
PM	Position Mooring
PSO	Particle Swarm Optimization
SA	Simulated Annealing
SLSQP	Sequential Least Squares Programming
TAPM	Thruster Assisted Position Mooring
TI	Turbulence Intensity
trust-constr	Trust-region interior point method
TSP	Travelling Salesman Problem
WFLO	Wind Farm Layout Optimization

WFLOP	Wind Farm Layout Optimization Problem
YITuR	Yaw and Induction-based Turbine Repositioning

List of Figures

1.1	Search results on Google Scholar per publication period for the keyword “floating offshore wind”	2
1.2	The four main types of floating offshore wind turbines, including the related terminology [10].	3
1.3	Illustration of the turbine repositioning control strategy for a two-turbine scenario [29].	4
1.4	Overview of the chapters and their contents in this Master’s Thesis report.	6
2.1	An illustration of a traditional wind farm layout with the corresponding terminology [16].	7
2.2	Example of static and dynamic layouts for different wind directions.	9
2.3	Circular movable range boundary of a wind turbine inside a circular wind farm boundary.	11
2.4	Flowchart of the static wind farm layout optimization.	13
2.5	Flowchart of the unrestricted dynamic wind farm layout optimization.	14
2.6	Flowchart of the sequential wind farm layout optimization.	16
2.7	Flowchart of the nested wind farm layout optimization.	18
2.8	A simple illustration of the workflow used to calculate the AEP and power per wind direction in PyWake.	20
2.9	An example of a wind farm layout that consists of 16 wind turbines.	21
3.1	IEA37 3.35MW power curve.	25
3.2	Wind distribution frequency of the IEA 37 case studies.	26
3.3	Wake expansion of a single wind turbine using the simplified version of the Bastankhah’s Gaussian wake model.	28
3.4	Convergence study of the static WFLO for four different optimization algorithms (feasible function values only).	29
3.5	Optimized static wind farm layouts for four different optimization algorithms.	30
3.6	Convergence study of the static WFLOP solved 200 times using CMA-ES with the feasible function values in blue and the final optima in red.	31
3.7	Histogram of the optimized AEP values for the static WFLOP solved 200 times with CMA-ES.	32
3.8	Best found optimum static wind farm layout from 200 runs.	32
3.9	Optimized unrestricted dynamic wind farm layout shown for four different wind directions, with the green arrow indicating where the wind is coming from.	33
3.10	Wind farm efficiency for various movable range sizes obtained by solving the sequential WFLOP.	35
3.11	Optimized static wind farm layout obtained by solving the sequential WFLOP.	36
3.12	Optimized dynamic wind farm layout obtained by solving the sequential WFLOP.	36
3.13	Convergence path of the feasible static layouts and their corresponding dynamic layouts, obtained by solving the nested WFLOP.	38
3.14	Final static wind farm layout obtained by solving the nested WFLOP.	39
3.15	Optimized dynamic wind farm layout obtained by solving the nested WFLOP.	39
3.16	Optimized dynamic wind farm layout for the IEA 37 example layout.	41
3.17	Optimized dynamic wind farm layout for the static layout obtained by solving the sequential WFLOP.	42
3.18	Optimized dynamic wind farm layout for the static layout obtained by solving the nested WFLOP.	43
3.19	Wind farm efficiency for various dynamic layout optimization results.	44
4.1	Four different repositioning mechanisms for a movable floating offshore wind turbine.	48

4.2	Position mooring repositioning mechanism concept for a movable floating offshore wind turbine.	51
4.3	Example position mooring system and its main components for a movable floating offshore wind turbine.	52
4.4	Movable range shapes for mobile floating offshore wind turbines for various mooring configurations.	53
4.5	Required definitions for a floater (represented by a square) to assess position mooring (top view).	54
4.6	Illustration of a single catenary mooring line.	55
4.7	Illustrations of the UMaine VoltturnUS-S floater for the IEA 15MW turbine.	57
4.8	Illustration of the position mooring repositioning mechanism concept for the UMaine VoltturnUS-S floater.	59
4.9	Desired coordinates for the UMaine VoltturnUS-S floater.	59
4.10	Example of a desired position and the actual position for the UMaine VoltturnUS-S floater.	60
4.11	Contour plot of the mooring line length for various desired positions.	61
4.12	Contour plot of the horizontal tension at the fairlead for various desired positions.	62
4.13	Contour plot of the absolute error in position for various desired positions.	62
5.1	Comparison of the circular movable range shape and the movable range shape for the UMaine VoltturnUS-S floater.	65
A.1	Convergence study of the dynamic layout for 4 of the 16 wind directions, only showing the feasible function values.	75
A.2	Convergence study of the dynamic layout for 4 of the 16 wind directions, with a looser tolerance on the constraint violations.	76
A.3	Convergence study of the dynamic layout for 4 of the 16 wind directions using the COBYLA algorithm, only showing the feasible function values.	77
A.4	Convergence study of the dynamic layout for 4 of the 16 wind directions using the COBYLA algorithm, showing all function values (including infeasible function values).	78
B.1	Contour plot of the tension at the fairlead for various desired positions.	79
B.2	Contour plot of the vertical tension at the fairlead for various desired positions.	80
B.3	Contour plot of the absolute error in yaw angle (rotation around z -axis) for various desired positions.	80

List of Tables

2.1	Wind farm power output per wind direction for the example layout.	21
3.1	IEA37 3.35MW wind turbine characteristics [67].	26
3.2	Wind attributes of the IEA 37 case studies.	27
3.3	The optimum AEP and the number of function value evaluations for the convergence study of the static WFLOP for four different optimization algorithms.	30
4.1	Comparison of four different repositioning mechanisms for a movable floating offshore wind turbine.	50
A.1	Best found AEP values of the dynamic wind farm layout for the IEA37 example layout. .	74

Introduction

This Master's Thesis Report details the benefits of movable floating offshore wind turbines (FOWTs) on the energy yield of a wind farm and describes an approach that enables turbines to move around. This chapter provides a general introduction to floating offshore wind farms and describes a means to increase their competitiveness with other renewable energy systems. Subsequently, a problem analysis is provided, which leads to the two objectives of this Master's Thesis and the approach to achieving each objective. Lastly, a breakdown of the organization of this Master's Thesis Report is provided.

1.1. Background

1.1.1. Offshore wind

The Global Wind Energy Council (GWEC) presented in the Global Offshore Wind Report 2021, that offshore wind will be a large contributor to the global goals to mitigate climate change [1]. The International Energy Agency (IEA), in its roadmap for the global energy sector to reach net-zero by 2050, reported key deployment milestones for renewables [2]. Annual offshore wind capacity additions will need to increase from 5 GW/yr in 2020 to 80 GW/yr in 2030 and 70 GW/yr in 2050. To reach these milestones, the offshore wind energy sector will have to grow enormously in the coming 30 years. This brings many opportunities and challenges with it.

Over the past few years, offshore wind has already witnessed enormous growth in both annual and cumulative installed capacity. The total installed capacity reported for 2020 is approximately 33 GW. The United Kingdom, Germany, and China occupy the largest share of the total installed capacity [3].

1.1.2. Floating wind

Currently, the majority of the installed wind turbines have a bottom-fixed foundation [4]. FOWTs, however, are expected to play a larger role in offshore wind from around 2030, in the IEA's milestones to reach net-zero [2]. There is also a growing scientific interest in floating offshore wind, which is illustrated in Figure 1.1. This is not surprising given that the vast majority (80%) of offshore wind resource potential is located in waters deeper than 60 meters [1].

FOWTs are not necessarily direct competitors of bottom-fixed turbines, but could complement them. Especially in deeper waters, where bottom-fixed turbines are simply not feasible (yet) or the costs of deployment are excessively large, FOWTs might provide the solution. They can be deployed in deeper waters and at increasing distances from shore [5], which were previously inaccessible locations. Countries with these deeper waters can now consider floating wind as a renewable energy resource [6], and it can help them contribute to the IEA's targets. This opens up a whole new, possibly bigger markets [7].

FOWTs, however, are more costly than bottom-fixed wind turbines. The support structure alone is four to six times as costly as the bottom-fixed support structure [8]. Nonetheless, it can be expected that with

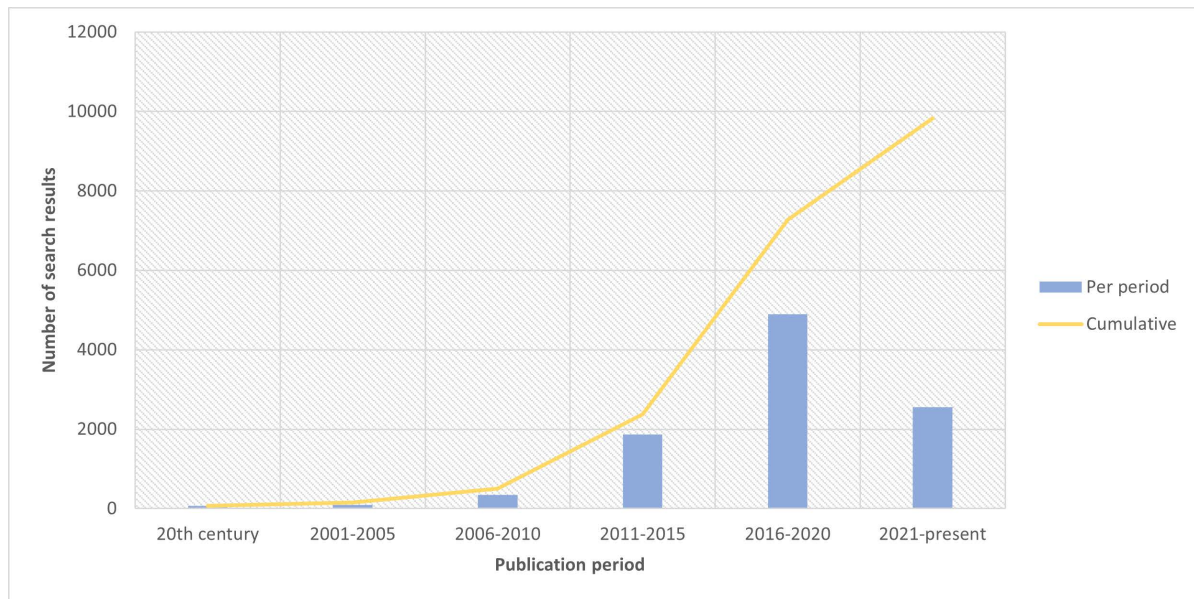


Figure 1.1: Search results on Google Scholar per publication period for the keyword “floating offshore wind”.

increased maturity of the technology and mass production, FOWTs will become economically viable. They are especially attractive for deep waters with high mean wind speeds, sites with good connections to the grid, and locations close to densely populated areas with large demands for energy [9].

An illustration of several types of FOWTs is shown in Figure 1.2. The rotor-nacelle assembly (RNA) is supported by the tower, which is fixed on the floating platform. This platform is referred to as a floater and is kept in place by the station keeping system. The main components of this system are the mooring lines and the anchors.

1.1.3. Levelized Cost of Energy

To make floating wind turbines competitive with other (renewable) energy resources, the LCoE has to be decreased [1]. The LCoE estimates the price per unit of generated energy and is an often used metric by techno-economic analysts to compare and assess different (renewable) energy systems [11–13]. The Capital Expenditure (CapEx), Operational and maintenance Expenditure (OpEx), and Annual Energy Production (AEP) are part of the LCoE [14]. For a floating wind farm system, the CapEx consists, for a large part, of the capital cost of the wind turbine, the substructure, the foundations, and the electrical infrastructure; the OpEx consists of the Operation and Maintenance (O&M) cost of the system. The AEP is the total wind farm energy output in a year. Another contributor to the LCoE is the Decommissioning Expenditure (DecEx), which is not further considered in this work.

There are multiple ways to decrease the LCoE of floating offshore wind. One approach is to reduce the CapEx through economies of scale, support structure design optimization, material reduction of electrical cables, and better installation vessels. Another approach is to reduce OpEx by improving O&M techniques, improving access to vessels and/or equipment, and implementing remote O&M strategies. Lastly, the AEP can be increased through turbine scaling, increased availability of turbines, decreased electrical power cable losses, and decreased wind farm wake losses [11, 14, 15]. The latter has large impacts on the AEP and is described in more detail next.

1.1.4. Description of the wake effect

A group of wind turbines that are clustered together to productively use the available area and wind resources is called a wind farm or wind park [16]. These wind farms are an environmentally friendly way to convert energy, since the wind is an inexhaustible clean energy resource. They often operate for multiple years and are able to provide large amounts of energy [17]. They also reduce the average O&M and capital cost per wind turbine [16].

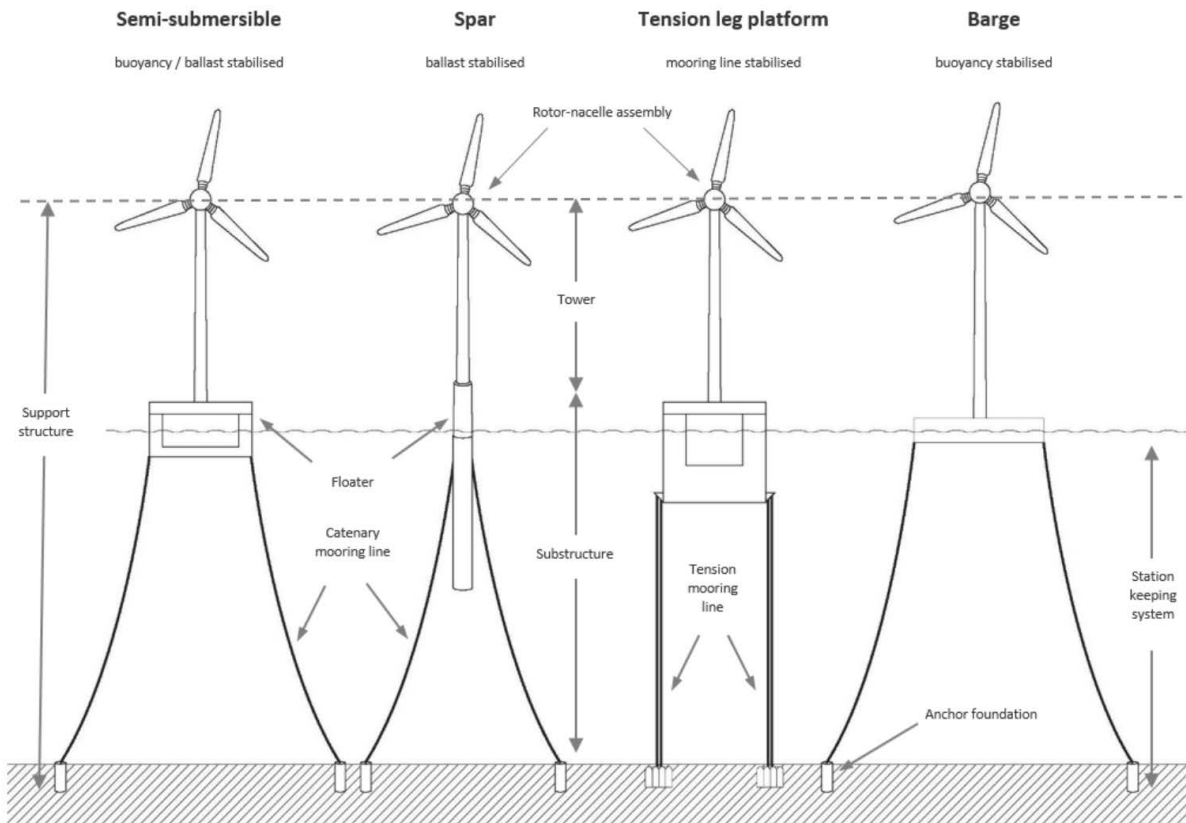


Figure 1.2: The four main types of floating offshore wind turbines, including the related terminology [10].

Grouping turbines also has adverse effects since the turbines impact each other aerodynamically [18, 19]. The wind turbines extract kinetic energy from the wind and convert it to electrical energy [20], which disrupts the flow of the wind. Therefore, the downstream wind must have a reduced amount of energy compared with the upstream wind [21]. Turbines located in the downstream wind region, where the flow has not recovered from the disruption, consequently receive a decreased incoming velocity. This downstream region of a wind turbine is called a wake [22]. Within the wake, the turbulence intensity (TI) is notably larger. For a better understanding of the downstream development of the TI in the wake, the reader is referred to Neunaber et al. (2020) [23]. The phenomenon of upstream turbines causing downstream turbines to receive low-speed, turbulent wind is called the wake effect [21]. It results in less power converted from the wind and more high-frequency loading [24]. In large offshore wind farms, the wake effect is estimated to cause energy losses ranging from 10% to 20% [25]. Moreover, the added loads can increase the fatigue of structural components, which is associated with more maintenance and a decreased operational lifespan of the turbines [23].

Wind farms have three different conditions that should be fulfilled: (i) low cost, (ii) long-lasting, and (iii) low service requirements [26]. The main objective of wind farms is to maximize the power converted while simultaneously minimizing the fatigue and loads on the structural components. Therefore, the wake effect must be minimized.

1.1.5. A unique wake effect mitigation approach for floating offshore wind farms

Wind farm control

Studies related to wind farm control can be separated into two fields: (i) electrical engineering; and (ii) mechanical and/or aerodynamic engineering [27]. In this Master's Thesis, only the latter is considered.

Wind farm control considers the effects of individual wind turbines on each other and improves the performance of the overall wind farm [26]. The main objective of wind farm control is to decrease the cost of energy through increased wind farm power output and reduced fatigue of the structural components [28]. This can be achieved by controlling individual wind turbines such that the wake

effects are mitigated [18].

In the literature, there exist multiple different control strategies, such as power de-rating/axial induction-based control, yaw-based wake redirection, tilt control, and turbine repositioning [18, 29]. In this Master's Thesis, the wind farm control strategy is limited to turbine repositioning. This strategy is described in more detail next.

Turbine repositioning

Turbine repositioning is a wake avoidance control strategy that improves the wind turbine location such that the effects of the wake are mitigated [18]. In simple terms, the upstream and/or downstream wind turbines are moved in such a way that the incoming wind speed at the downstream turbines is higher. Therefore, more power can be converted by the downstream wind turbines. Figure 1.3 demonstrates the wind turbine repositioning control strategy for a two turbine case.

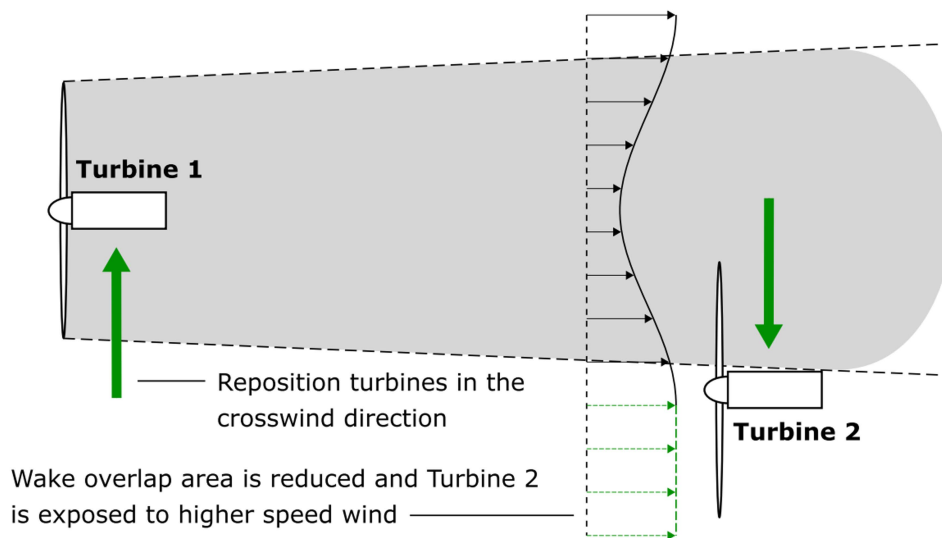


Figure 1.3: Illustration of the turbine repositioning control strategy for a two-turbine scenario [29].

Not all wind turbine designs allow for turbine repositioning. The design must:

1. be floating;
2. be capable of producing the force required to move to and stay in the desired position;
3. allow for an adequate mobility.

Turbine repositioning is something that is done after the installation of the wind farm. To get the most out of this strategy, it must be considered during the design phase of the wind farm.

Wind farm layout optimization with movable floating offshore wind turbines

Wind farm layout optimization (WFLO) aims to find the ideal position of the wind turbines within the given environment [30]. The ideal wind farm layout depends on what it is optimized for and how that is done. Nonetheless, it is, at least, desirable to reduce the wake losses and to decrease the capital and operational costs.

An assumption that is made in WFLO is that the wind turbines have one fixed position over the wind farm's lifespan. This fixed position is the installation location of the turbine. FOWTs, however, could potentially allow for a change in their positions within the wind farm [31]. This makes it possible to consider a layout that changes throughout the period of operation. The change in layout would be possible through the turbine repositioning wind farm control strategy. The wind farm layout is no longer fixed, but could be adapted based on what is best for different wind directions. This results in a further reduction of the wake losses compared with a fixed layout [6].

1.2. Problem analysis

In WFLO for bottom-fixed wind turbines, the wind farm layout is optimized considering all wind directions. Wind turbines can no longer be moved once they have been installed in their optimal positions. These turbines will be located at these positions for the entire operational phase of the wind farm. The best layout considering all wind directions, however, is not necessarily the best layout considering each wind direction separately. Therefore, a wind farm with bottom-fixed turbines will likely never use the full potential of the wind.

A big difference between bottom-fixed and FOWTs is that the latter is able to move after installation [31]. This mobility could enable the turbines to find better locations in the wind farm to increase the AEP and use the full potential of the wind resource [6]. Wind farm layouts with movable FOWTs, however, are only financially appealing if the additional wind farm AEP gains outweigh the additional costs to achieve the mobility [6]. Depending on the technology required to reposition the turbine, the CapEx and OpEx might increase as well.

There are thus two important aspects to wind farm layout optimization with movable floating offshore wind turbines that, ideally, need to be considered together. One is the increase in the wind farm's AEP, and the other is the increase in costs to achieve the movability. These aspects are both dependent on the technical implementations required to enable the movability of turbines. Currently, there is not much known about the technology and its characteristics that make turbine repositioning possible. As a result, the overall impact of the two aspects on the LCoE is difficult to assess and currently unknown.

1.3. Objective

As mentioned in the previous section, the impact of movable floating offshore wind turbines on a wind farm's LCoE is challenging to evaluate. It is, however, possible to consider separate parts of the problem: the impact of movable turbines on a wind farm's AEP; the technology and its characteristics required to allow for movable turbines. Therefore, in this Master's Thesis Project, the objective is twofold:

1. To provide insight into the ability of movable floating offshore wind turbines to increase a wind farm's AEP;
2. To gain an understanding of repositioning mechanisms and their characteristics for movable floating offshore wind turbines.

1.4. Approach

To reach each objective in Section 1.3, a set of actions has to be carried out. The activities to achieve the first objective are:

1. Define wind farm layout optimization problems for AEP maximization, both for fixed and movable wind turbines;
2. Select a wind farm case study;
3. Solve the wind farm layout optimization problem for fixed wind turbines;
4. Solve the wind farm layout optimization problem for floating offshore wind turbines with various degrees of movability.

The activities to reach the second objective are:

1. Investigate and compare previous repositioning mechanisms in the floating wind and offshore/marine industries;
2. Select one repositioning mechanism and further characterize it;
3. Propose a method to assess the movability and station-keeping performance of the selected repositioning mechanism;
4. Evaluate the proposed method for a case study.

1.5. Organization of thesis

An overview of the chapters and their contents is presented in Figure 1.4. In Chapter 2, definitions of the wind farm layout optimization problem are provided for AEP maximization of a wind farm with fixed and movable wind turbines. Subsequently, in Chapter 3, the optimization problems defined in the previous chapter are solved for a case study. In Chapter 4, various repositioning mechanisms are looked into and one is selected to be further characterized. The results from Chapter 3 and Chapter 4 are discussed jointly in Chapter 5. The final conclusions are provided in Chapter 6 together with the proposed further work that can be done regarding wind farms with movable FOWTs.

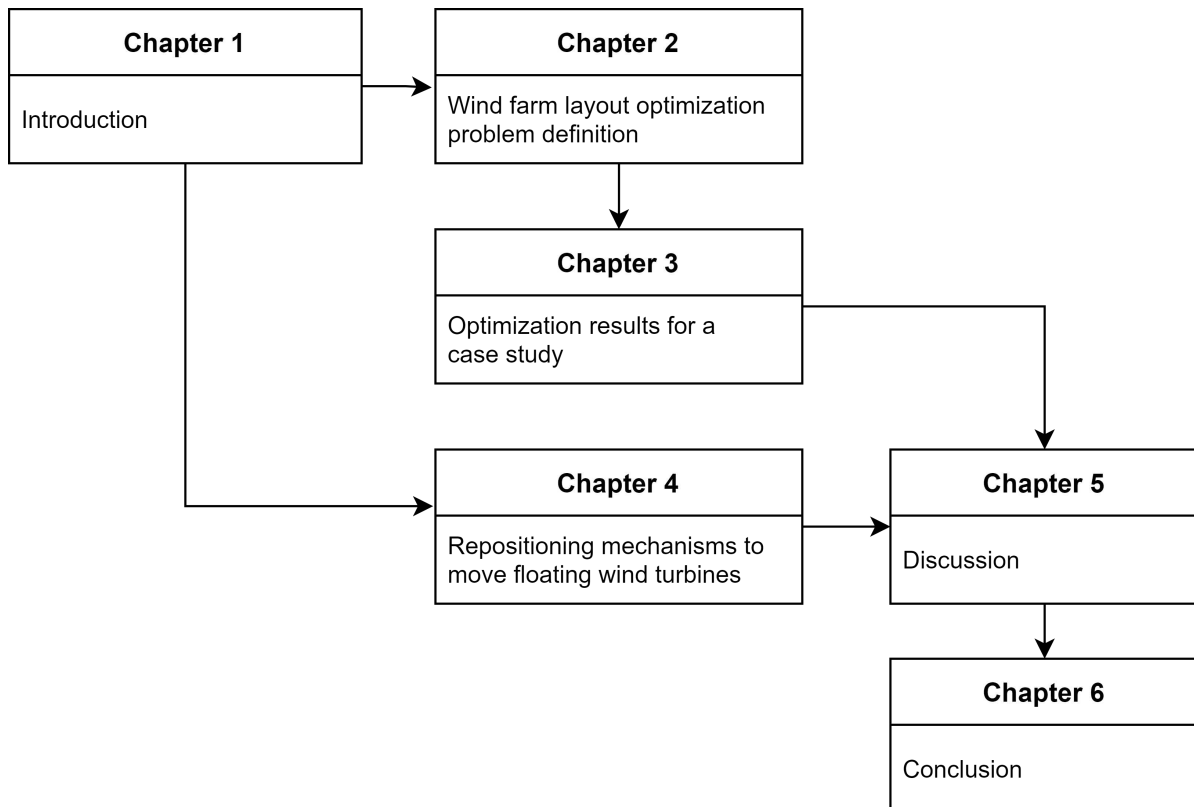


Figure 1.4: Overview of the chapters and their contents in this Master's Thesis report.

2

Wind farm layout optimization problem definition for AEP maximization

In this chapter, wind farm layout optimization problems are defined for AEP maximization of a wind farm with fixed and movable wind turbines. The chapter starts with a description of how a traditional wind farm layout was designed (Section 2.1), and follows up with the more calculated method of doing it: wind farm layout optimization (Section 2.2). Next, the division made in this Master's Thesis in wind farm layout optimization for a fixed and mobile layout is explained (Section 2.3). Hereafter, the mathematical formulations and workflows for AEP maximization are provided (Section 2.4). Subsequently, a mathematical description of the AEP is given, as well as a description of how PyWake can be used to evaluate the AEP (Section 2.5). Lastly, the four different optimization algorithms used in this Master's Thesis to solve optimization problems are explained (Section 2.6).

2.1. Traditional wind farm layout design

Wind turbines in conventional wind farms were installed with basic spacing guidelines [32]. These guidelines depend on the prevailing wind, which is the predominant wind direction [19]. The spacing between the turbines in the prevailing wind direction is called the downwind spacing, and the spacing between the turbines perpendicular to the prevailing wind direction is called the crosswind spacing [16]. A schematic demonstration of a traditional wind farm layout is given in Figure 2.1.

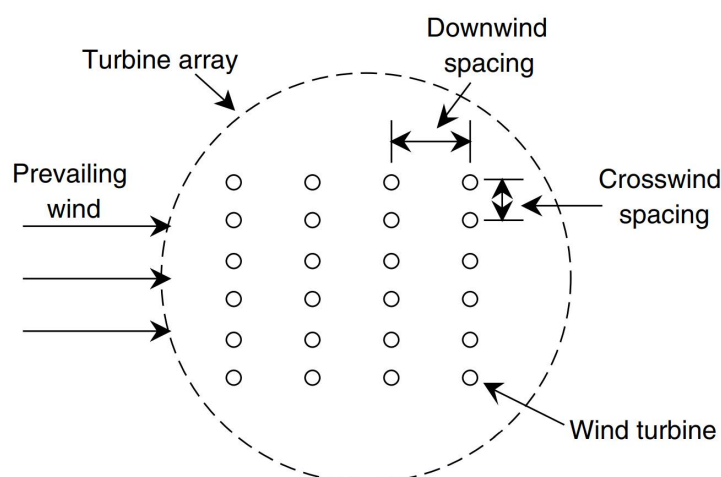


Figure 2.1: An illustration of a traditional wind farm layout with the corresponding terminology [16].

There are rules of thumb for the downwind and crosswind spacing that can be used to plan the layout

of a wind farm. Typically, the downwind spacing of the turbines is in the range of 5 to 9 rotor diameters, and the crosswind spacing is in the range of 3 to 5 rotor diameters [19]. According to [33], a downwind spacing of 8 to 12 rotor diameters and a crosswind spacing of 2 to 4 rotor diameters seems to be ideal.

No matter what the sweet spot seems to be for the spacing rules, a relatively large downwind spacing seems to be desired. This large downwind spacing allows the wake to recover through turbulent mixing [23]. However, increasing the downwind spacing too much leads to large inter-array cables and high area rental costs [34]. This, in turn, results in higher capital costs for the wind farm. So, increasing the downwind spacing alone might not be the best way to reduce the wake effect.

Another issue with the conventional wind farm is that all other wind directions are not accounted for. This will lead to a wind farm layout design that is not optimal [19]. The wind resource is most utilized by designing a wind farm layout that is unique to the location [35]. Mitigating the wake effect in only one direction is not the most desirable option, especially at sites with often varying wind directions [36].

The reader can guess, by now, that there exist better solutions for the wind farm layout than the simple spacing rules for the prevailing wind. These solutions can be found by solving the wind farm layout optimization problem (WFLOP) [19].

2.2. General description of wind farm layout optimization

Wind farm layout optimization aims to find the ideal position of the wind turbines within the given environment [30]. To obtain the ideal position, an objective function has to be minimized (or maximized, depending on the formulation of the function) within the constraints of the wind farm. Several objective functions have been considered in solving the WFLOP, for example, AEP, power, Cost of Energy (CoE), Levelized Production Cost (LPC), Financial Balance (FB), and Net Present Value (NPV) [37]. When considering AEP and power as objective functions, the main goal is to minimize wake losses. The other objective functions do consider costs related to the wind farm layout as well. Solely mitigating the wake effect might, for example, not necessarily be financially attractive.

The first investigation into the optimal location of wind turbines within a wind farm site was performed by Mosetti et al. (1994) [38]. Every wind farm site has different environmental characteristics [34]. Therefore, many academic studies that followed used the same three wind scenarios and the basic optimization problem as described by Mosetti et al. (1994) [38]. This allowed the researchers to compare their optimization algorithms with their predecessors.

In recent studies, more practical optimization problems have been solved that contain a better economic description of the wind farm [39]. This is a positive development since it could help advance the implementation of WFLO in practice [30]. Some relevant aspects for wind farm developers are the cost of the connection to the grid; cabling costs; blade damage due to turbulence; maintenance cost; and installation cost [19].

Most scholarly works on WFLO assume a fixed wind farm layout. This means that once the optimal wind turbine positions are found by solving the WFLOP, these will be the desired installation positions. For bottom-fixed wind turbines, these positions are fixed. FOWTs, however, allow for a certain mobility after installation [31]. This makes it possible to consider WFLO with movable floating wind turbines, resulting in a mobile wind farm layout [6].

2.3. Static and dynamic wind farm layout optimization

In this section, the division made in this Master's Thesis in WFLO with fixed and mobile turbines is explained, and several layout optimization methods are introduced.

2.3.1. Definition of a static and dynamic wind farm layout

In this Master's Thesis, we refer to a static wind farm layout when it is assumed that the turbine position is fixed during the operational phase of the wind farm and to a dynamic wind farm layout when it is assumed that the turbine position is varied. In a static layout the turbine positions are thus the same for all wind directions, while in a dynamic layout for each wind direction a different layout is allowed. The difference between the static and dynamic layouts for a changing wind direction is illustrated in Figure 2.2.

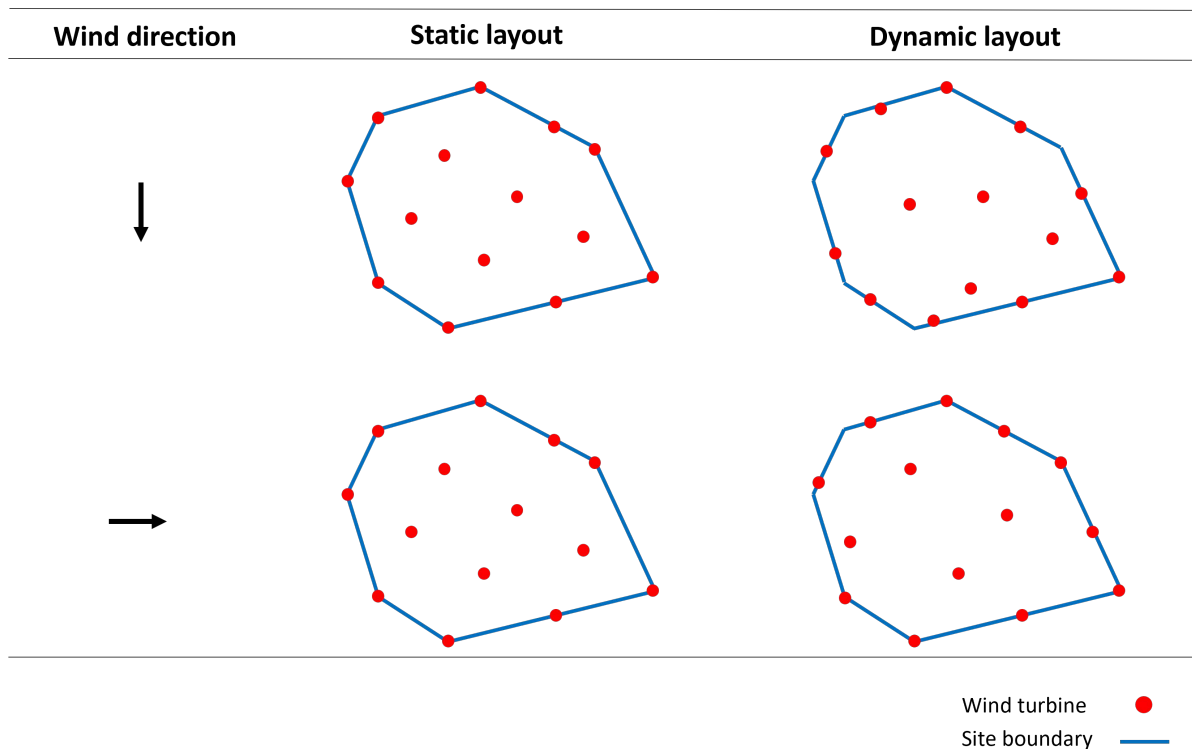


Figure 2.2: Example of static and dynamic layouts for different wind directions.

2.3.2. Description of static and dynamic wind farm layout optimization

In static WFLO, fixed layouts are evaluated based on their performance over the entire lifetime of the wind farm. The optimum is the single layout that has the best cumulative effect over all wind directions.

Dynamic WFLO optimizes multiple layouts that may differ per wind direction. The optimum is the set of layouts for which the lifetime performance is best when it is evaluated with each respective layout per wind direction. When only AEP is considered, the procedure of dynamic WFLO can be simplified. Instead of optimizing all layouts simultaneously, one layout can be optimized for each wind direction separately. The layouts within the final set have to be consistent with the movability of the turbines. The installation positions and mobility range of the movable turbines must, therefore, be taken into account. The installation positions are the mobility range centres of the movable turbines. These positions, together with the mobility range, define where each turbine is able to move to inside the dynamic wind farm. It should be noted that, throughout this work, the “installation,” “static,” and “neutral” positions of the movable turbines are used interchangeably.

2.3.3. Reference and restricted dynamic wind farm layout optimization methods

In this work, two reference layout optimization methods are considered: static and unrestricted dynamic WFLO. These two methods serve as a reference for the two restricted dynamic WFLO methods that are considered in this research: sequential and nested WFLO.

The static WFLO method assumes that there is one fixed layout in which turbines have no mobility at all. When mobile layouts are considered, this method is the worst in terms of energy yield and thus serves as a lower bound. The unrestricted dynamic WFLO method assumes that the wind turbines are free to move anywhere in the wind farm. The installation positions do not have to be taken into account, and the turbines are not constrained by their mobility range since it is unlimited. Therefore, this method is the best in terms of energy yield and thus serves as an upper bound for mobile layouts.

To obtain a realistic dynamic wind farm layout, the turbine installation positions have to be taken into account. As a result, the sequential and nested optimization both include the following two steps:

1. Establish a static wind farm layout consisting of turbine installation positions;

2. Optimize the dynamic wind farm layout for the layout in the previous step.

The sequential WFLO method involves the evaluation of both a static and a dynamic wind farm layout. From the word “sequential,” it could already be understood that the optimization of the two layouts is done consecutively: first, optimize the static wind farm layout; second, optimize the dynamic wind farm layout.

The nested WFLO method also involves the evaluation of both a static and a dynamic wind farm layout. This method is based on the nested optimization framework proposed by Rodrigues et al. (2015) [6]. It involves an optimization inside another optimization: a dynamic layout is optimized for each iteration of the static layout optimization. Thus, for each generated static layout, the best achievable performance under dynamic repositioning is evaluated.

2.4. Mathematical formulations and workflows for AEP maximization

After giving a brief introduction of a general optimization problem, the constraints used in this work are introduced. This leads to the mathematical optimization problem statements and workflows used in this work to maximize AEP.

2.4.1. General optimization problem

Here follows a brief description of an optimization problem as explained in Martins and Ning (2021) [40].

In an optimization problem, there are three important components that need to be carefully defined: the design variable(s), the objective function, and the constraint(s).

Design variables are the variables that characterize the system. The dimensionality of a problem is determined by the number of design variables n_x . The design variable x might be bounded. An upper bound is given by \bar{x} and a lower bound is given by \underline{x} .

An objective function is required in order to obtain the optimum design. The objective function is represented by the symbol $f(x)$. The definition of the objective function is of paramount importance since it decides what will be minimized (or maximized). If the objective function is not a proper description of the problem that has to be solved, the solution found by the optimizer will be suboptimal from an engineering perspective.

Most problems in engineering involve constraints. These constraints are functions of the design variables. Two types of constraints can be distinguished: (i) inequality constraints and (ii) equality constraints. The inequality constraint is expressed as $g(x) \leq 0$, while the equality constraint is expressed as $h(x) = 0$.

The optimization problem statement in mathematical form is described by:

$$\begin{array}{ll} \text{minimize} & f(x) \\ \text{by varying} & \underline{x}_i \leq x_i \leq \bar{x}_i \quad i = 1, \dots, n_x \\ \text{subject to} & g_j(x) \leq 0 \quad j = 1, \dots, n_g \\ & h_l(x) = 0 \quad l = 1, \dots, n_h. \end{array}$$

2.4.2. Movable range and wind farm boundary constraints

There are two constraints considered in this work: the movable range (the mobility area of the movable FOWTs) and the wind farm boundary. The former constraint applies only to sequential and nested WFLOPs, whereas the latter applies to all WFLOPs. Turbines are allowed to be within or on these boundaries.

For simplicity, the movable range and wind farm boundary have been chosen as circular. Figure 2.3 depicts these boundaries and their associated variables. The neutral position of the wind turbine is the installation position and the centre of the movable range. Several example positions are provided for a relocated wind turbine within the movable range.

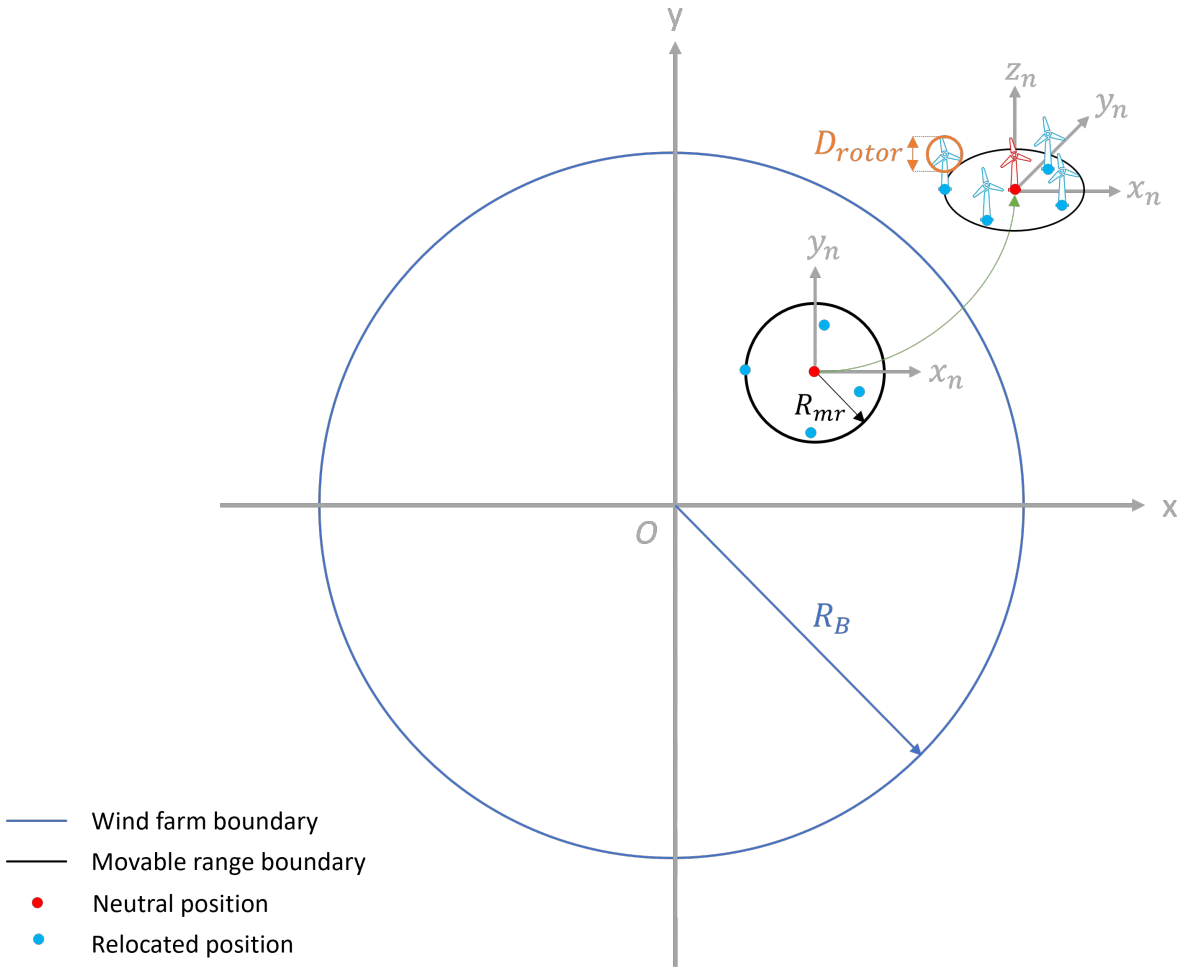


Figure 2.3: Circular movable range boundary of a wind turbine inside a circular wind farm boundary.

The ratio between the movable range boundary radius and the turbine rotor diameter is given by:

$$\frac{R_{mr}}{D_{rotor}} = C, \quad (2.1)$$

where R_{mr} is the boundary radius of the circular movable range shape, D_{rotor} is the rotor diameter, and C is the ratio between the two variables. If C is small, the movable range of the wind turbine is small, and if C is large, the movable range of the wind turbine is large.

Wind turbines that are installed near or on the wind farm boundary, have movable ranges outside the wind farm boundary. Rodrigues et al. (2015) assumed in their wind farm layout optimization study with movable turbines, that the turbines installed close to the wind farm boundary are allowed to cross it [6]. For two reasons, this assumption is not made in this Master's Thesis:

1. The design space is increased compared to WFLO without movable turbines, which might exaggerate the possible gains in terms of AEP;
2. When large movable range sizes are considered, turbines might be located far outside the wind farm boundary. In practice, this might not be possible or not be allowed. The wind farm boundary is defined for a reason.

It is also possible to consider other constraints. Baker et al. (2019), for example, considered the separation distance, which is a constraint for the distance between the turbines. In their work, this distance must be larger than or equal to two rotor diameters. The separation distance constraint is used by

Rodrigues et al. (2015) as well, but then with four rotor diameters [6]. In this Master's Thesis, the separation distance constraint is neglected because it adds computational time and might not even be necessary. The goal of the optimization is to maximize the AEP. Having a small separation distance between the turbines increases the wake effect for certain wind directions and usually does not help in increasing the AEP. Therefore, WFLO is not likely to provide solutions for wind turbines that are close to each other. If it does, the turbines that violate the separation constraint could be moved to another location. This can be done either manually or by solving another optimization problem wherein only the turbines that violate the constraint are moved. It could even be the case that by doing this, the AEP increases if the optimizer did not find the global minimum.

2.4.3. Reference wind farm layout optimization problems

Static wind farm layout optimization problem

The optimization problem that is solved in the static WFLO is given below:

$$\begin{array}{ll}
 \text{maximize} & \text{AEP}(X) \\
 \text{by varying} & X_i \\
 \text{subject to} & x_j^2 + y_j^2 \leq R_B^2
 \end{array}
 \quad
 \begin{array}{l}
 X = [x_1 \ \dots \ x_{n_{wt}} \ y_1 \ \dots \ y_{n_{wt}}] \\
 i = 1, \dots, n_X \\
 j = 1, \dots, n_{wt},
 \end{array}
 \quad (2.2)$$

where:

- AEP is the Annual Energy Production in GWh;
- X is the design variable vector consisting of the wind turbine coordinates;
- n_{wt} is the number of wind turbines;
- x_j is the x-coordinate of the wind turbine;
- y_j is the y-coordinate of the wind turbine;
- n_X is the number of design variables;
- R_B is the circular wind farm boundary radius.

Note that in Section 2.4.1, the design variable was given by x , whereas in this problem statement it is given by X . This is done to prevent a mix-up between the wind turbine coordinate and the design variable. Furthermore, it may be noted that there are two times the number of design variables n_X as the number of wind turbines n_{wt} , because each turbine has two coordinates that describe its location.

The workflow of static WFLO is displayed in Figure 2.4.

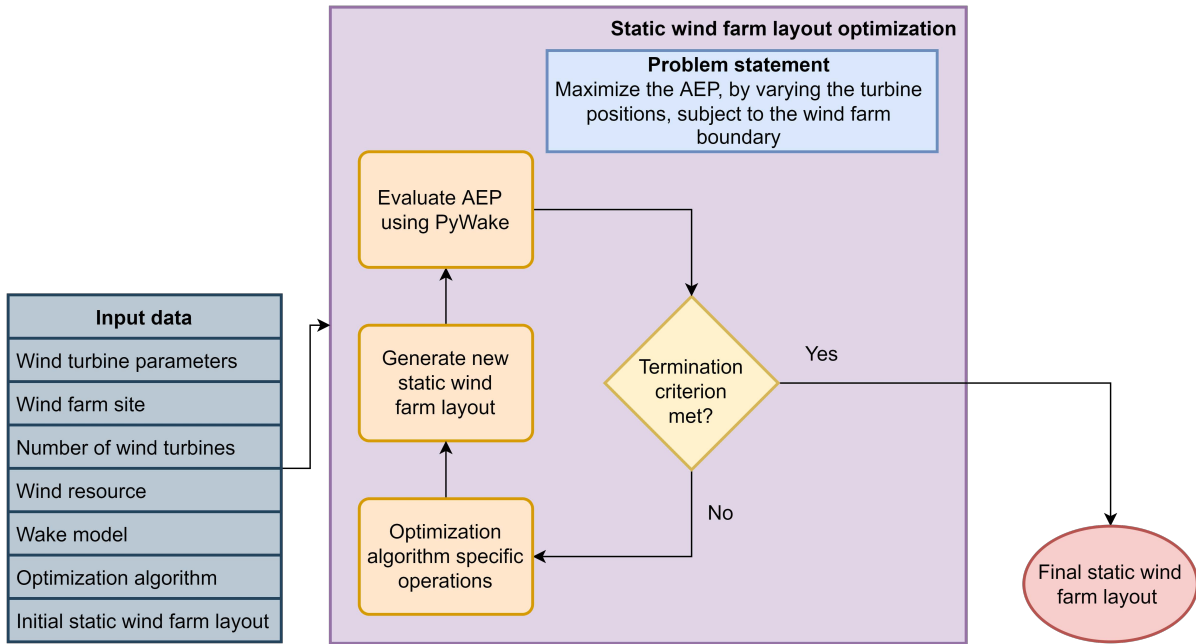


Figure 2.4: Flowchart of the static wind farm layout optimization.

The goal of the static WFLO is to maximize the AEP by varying the wind turbine coordinates subject to the wind farm boundary. To maintain simplicity, a circular wind farm boundary with a radius of R_B is assumed. The circular wind farm boundary, however, could be easily changed to a more realistic boundary. This would change the constraints of the optimization problem.

The optimization loop is continued until the algorithm's specific termination criteria are met. The output is a static wind farm layout that has an optimal AEP and satisfies the constraints.

Unrestricted dynamic wind farm layout optimization problem

The optimization problems that are solved in the unrestricted dynamic WFLO are given below:

$$\begin{aligned}
 & \text{maximize} && P_1(X^{(1)}) && X^{(1)} = [x_1 \quad \dots \quad x_{n_{wt}} \quad y_1 \quad \dots \quad y_{n_{wt}}] \\
 & \text{by varying} && X_i^{(1)} && i = 1, \dots, n_X \\
 & \text{subject to} && x_j^2 + y_j^2 \leq R_B^2 && j = 1, \dots, n_{wt} \\
 & \vdots && && \\
 & \text{maximize} && P_{n_{wd}}(X^{(n_{wd})}) && X^{(n_{wd})} = [x_1 \quad \dots \quad x_{n_{wt}} \quad y_1 \quad \dots \quad y_{n_{wt}}] \\
 & \text{by varying} && X_i^{(n_{wd})} && i = 1, \dots, n_X \\
 & \text{subject to} && x_j^2 + y_j^2 \leq R_B^2 && j = 1, \dots, n_{wt},
 \end{aligned} \tag{2.3}$$

where, P_k is the wind farm power output per wind direction. The wind direction number k ranges from 1 to n_{wd} , where the latter is the number of wind directions that are considered. Each wind direction number corresponds with a certain wind direction. If, for example, $n_{wd} = 16$, then $k = 1$ corresponds with a wind direction of 0 degrees and $k = 16$ corresponds with a wind direction of 337.5 degrees.

The workflow of unrestricted dynamic WFLO is displayed in Figure 2.5.

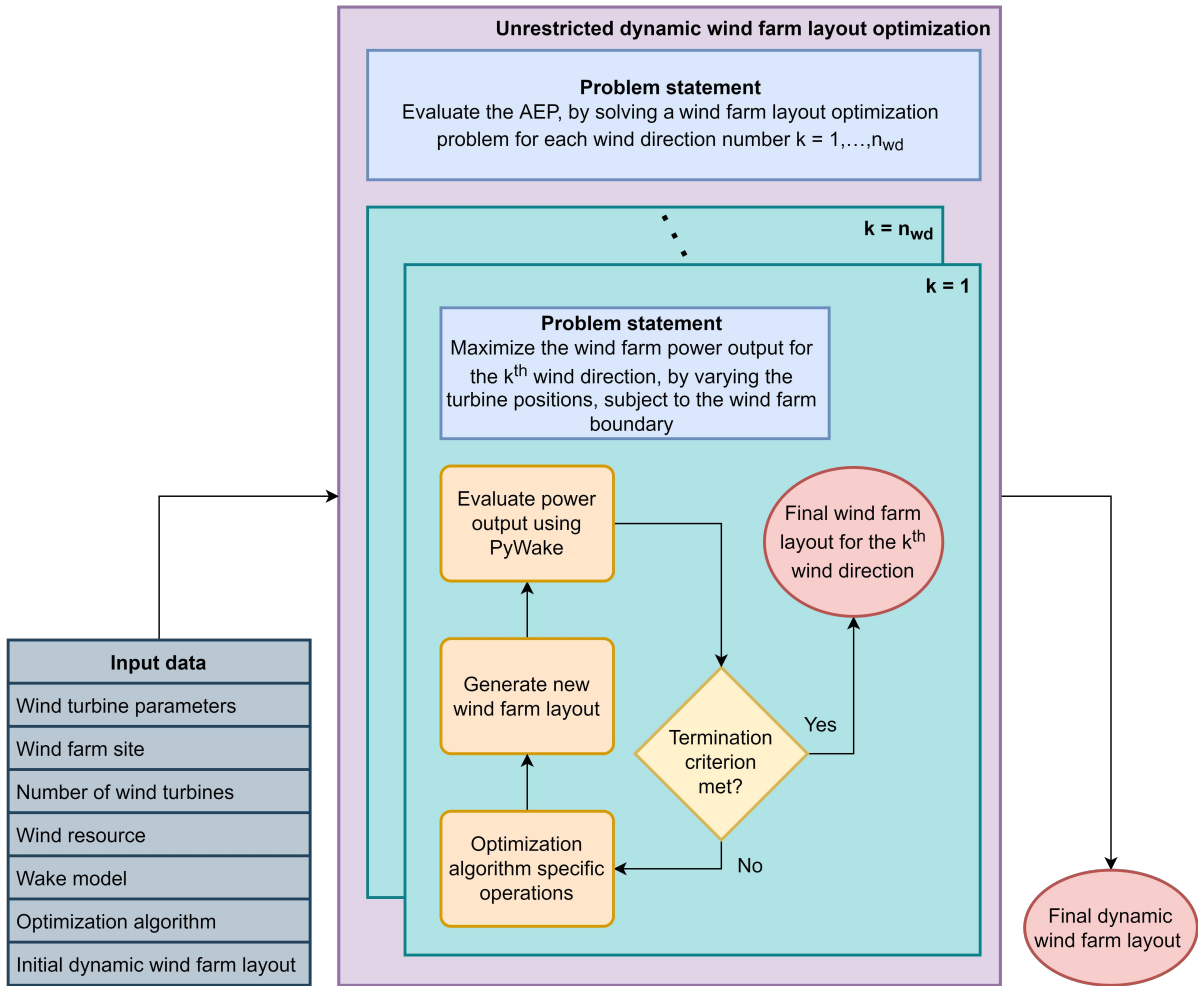


Figure 2.5: Flowchart of the unrestricted dynamic wind farm layout optimization.

The desired goal of the unrestricted dynamic WFLO is to maximize the AEP of the dynamic wind farm layout. This is done indirectly by solving n_{wd} optimization subproblems. The goals of the subproblems are to maximize the wind farm power output for each considered wind direction by varying the wind turbine positions subject to the wind farm boundary. The power output per wind direction P_k can be evaluated with PyWake if the turbine positions for that wind direction (X^k) are known (see Figure 2.8). The whole optimization process is finished once all subproblems are solved. The AEP is then simply calculated by using Equation 2.9. The final result is a dynamic wind farm layout that results in an optimal AEP. The dynamic wind farm layout consists of an optimal wind farm layout for each wind direction. There are a total of n_{wd} different wind farm layouts, each optimized for the considered wind direction.

For a circular wind farm boundary, the unrestricted dynamic WFLO should result in identical, but rotated, layouts for all wind directions. The optimum for each wind direction should thus be the same.

2.4.4. Restricted dynamic wind farm layout optimization problems

Sequential optimization

There are two steps in the sequential WFLO. The optimization problem that is solved in step 1 is given below:

$$\begin{array}{ll}
 \text{maximize} & \text{AEP}_s(X_s) \\
 \text{by varying} & X_{s,i} \\
 \text{subject to} & x_{s,j}^2 + y_{s,j}^2 \leq R_B^2 \\
 & X_s = [x_{s,1} \ \dots \ x_{s,n_{wt}} \ y_{s,1} \ \dots \ y_{s,n_{wt}}] \\
 & i = 1, \dots, n_X \\
 & j = 1, \dots, n_{wt}.
 \end{array} \tag{2.4}$$

The optimization problem in step 1 is the same as the static WFLOP given in Equation 2.2. The only difference between the two problems is in the notation. In step 1, use is made of the subscript 's', which stands for static. This difference in notation is useful for avoiding misunderstanding in step 2 of the sequential WFLO.

By solving the optimization problem in step 1, the optimal static wind farm layout is obtained. This static layout consists of the wind turbine installation positions. These installation positions are required to define the movable range of the turbines. The movable range confines the dynamic layout that is optimized in step 2. As a result, the optimal static wind farm layout (X_s) of step 1 is an input to step 2. The optimization problems that are solved in step 2 are given below:

$$\begin{array}{ll}
 \text{maximize} & P_1(X^{(1)}) \\
 \text{by varying} & X_i^{(1)} \\
 \text{subject to} & x_j^2 + y_j^2 \leq R_B^2 \\
 & (x_j - x_{s,j})^2 + (y_j - y_{s,j})^2 \leq R_{mr}^2 \\
 & \vdots \\
 \text{maximize} & P_{n_{wd}}(X^{(n_{wd})}) \\
 \text{by varying} & X_i^{(n_{wd})} \\
 \text{subject to} & x_j^2 + y_j^2 \leq R_B^2 \\
 & (x_j - x_{s,j})^2 + (y_j - y_{s,j})^2 \leq R_{mr}^2 \\
 & X^{(1)} = [x_1 \ \dots \ x_{n_{wt}} \ y_1 \ \dots \ y_{n_{wt}}] \\
 & i = 1, \dots, n_X \\
 & j = 1, \dots, n_{wt} \\
 & j = 1, \dots, n_{wt}.
 \end{array} \tag{2.5}$$

The optimization problems in step 2 are similar to the unrestricted dynamic WFLOP given in Equation 2.3, except for the addition of the circular movable range constraints on the wind turbines. For this additional constraint, the turbine installation positions are required from step 1. Each turbine must remain within or on the circular movable range boundary. The radius of this boundary is given by R_{mr} .

The workflow of sequential WFLO is displayed in Figure 2.6.

The desired goal in the sequential WFLOP is to maximize the AEP of the dynamic wind farm layout. There are two steps to reach this desired goal. Each step has its own optimization problem that needs to be solved. The goals for each of these problems are as follows:

1. Maximize the AEP of the static wind farm layout by varying the static turbine positions (installation positions) subject to the wind farm boundary;
2. For each considered wind direction, maximize the wind farm power output by varying the wind turbine positions subject to the wind farm boundary and movable range boundary.

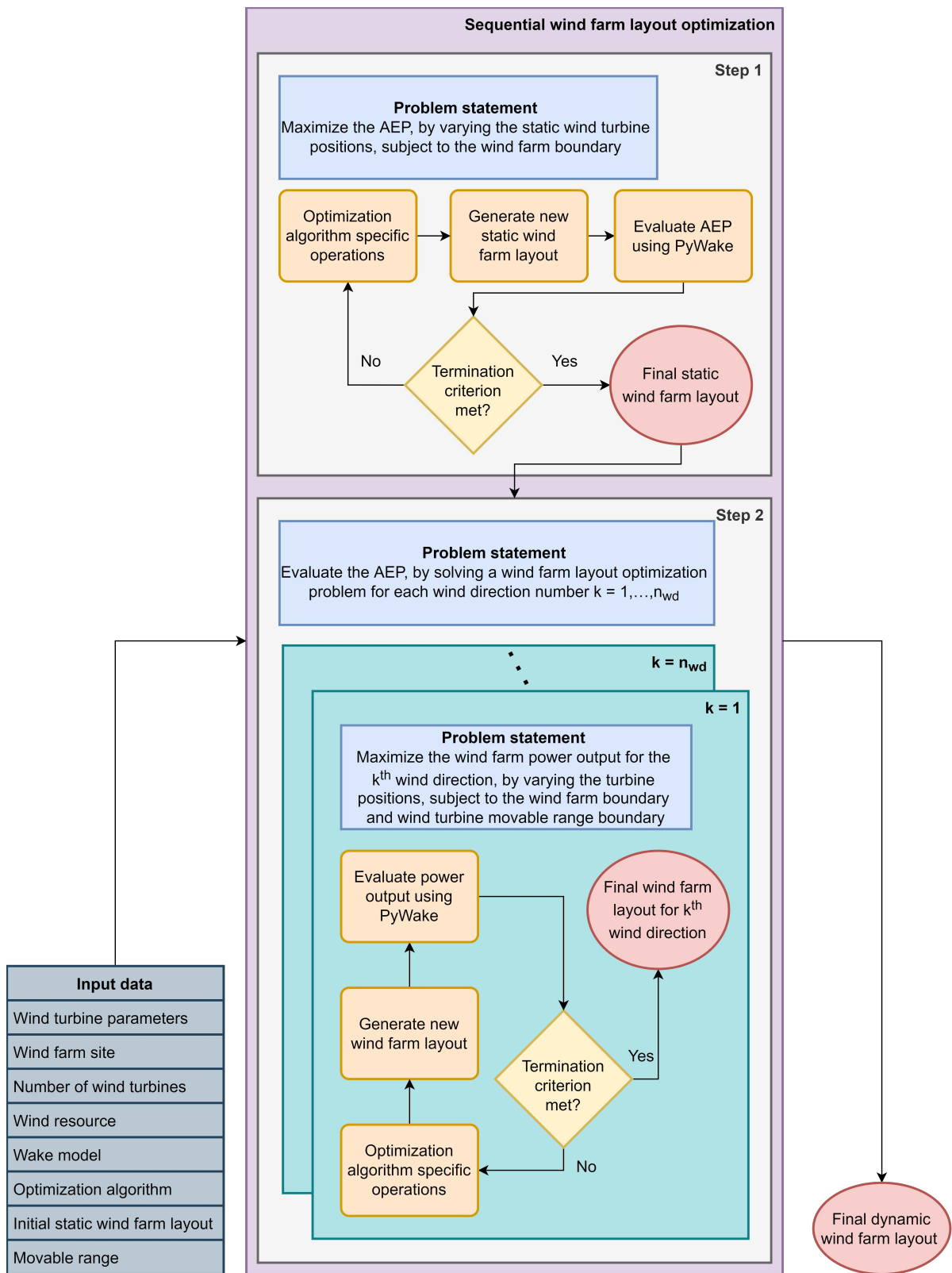


Figure 2.6: Flowchart of the sequential wind farm layout optimization.

In the first step, the goal is to maximize the AEP of the static wind farm layout. This layout consists of the wind turbine static positions. An example of a static wind turbine position can be seen in Figure 2.3. In this illustration, the static position is referred to as the neutral position. This neutral position is the

installation position of the FOWT, which does not change over the operational phase of the wind farm. The first step of optimization is completed when the AEP of the static wind farm layout is optimized and the positions of the static wind turbines are found.

The static wind farm layout obtained in step 1 is necessary for step 2 of the sequential WFLO. The static positions of the turbines are located in the centre of the movable range. These positions are, thus, essential to define the movable range of the wind turbines. The mobility of the wind turbines in step 2 is constrained by the movable range boundary.

In the second step, the desired goal is to maximize the AEP of the dynamic wind farm layout. This is done indirectly by solving n_{wd} optimization subproblems. Each subproblem is solved for a specific wind direction. For each considered wind direction, the goal is to maximize the wind farm power output in that direction. PyWake can be used to calculate the power output of a wind farm for a specific wind direction by inputting the turbine positions $X^{(k)}$. The AEP of the dynamic wind farm layout is evaluated once all subproblems are solved.

The whole optimization process is finished once step 2 is completed, that is, when all subproblems are solved and the AEP of the dynamic wind farm layout is evaluated. The final result is a dynamic wind farm layout that has an optimal AEP and satisfies the constraints. The dynamic wind farm layout consists of n_{wd} different wind farm layouts. There is thus an optimum wind farm layout for each considered wind direction.

Nested optimization

A nested optimization problem is also known as a multi-level optimization problem. In such problems, the constraints of an optimization problem are computed by solving another optimization problem [42, 43]. If there are only two levels to the optimization problem, it is called a bi-level optimization problem. This problem includes an upper level problem and a lower level problem. The lower level problem is a constraint to the upper level problem.

The optimization problem that is solved in the nested WFLO is given below:

$$\begin{array}{ll}
 \text{maximize} & \text{AEP}_d(X_s) \\
 \text{by varying} & X_{s,i} \\
 \text{subject to} & x_{s,j}^2 + y_{s,j}^2 \leq R_B^2 \\
 & \text{maximize} \\
 & \text{by varying} \\
 & \text{subject to} \\
 & \vdots \\
 & \text{maximize} \\
 & \text{by varying} \\
 & \text{subject to}
 \end{array}
 \begin{array}{l}
 X_s = [x_{s,1} \quad \dots \quad y_{s,n_{wt}}] \\
 i = 1, \dots, n_X \\
 j = 1, \dots, n_{wt} \\
 P_1(X^{(1)}) \\
 X_i^{(1)} \\
 x_j^2 + y_j^2 \leq R_B^2 \\
 (x_j - x_{s,j})^2 + (y_j - y_{s,j})^2 \leq R_{mr}^2 \\
 \vdots \\
 P_{n_{wd}}(X^{(n_{wd})}) \\
 X_i^{(n_{wd})} \\
 x_j^2 + y_j^2 \leq R_B^2 \\
 (x_j - x_{s,j})^2 + (y_j - y_{s,j})^2 \leq R_{mr}^2
 \end{array}
 \begin{array}{l}
 X^{(1)} = [x_1 \quad \dots \quad y_{n_{wt}}] \\
 i = 1, \dots, n_X \\
 j = 1, \dots, n_{wt} \\
 j = 1, \dots, n_{wt} \\
 \\
 X^{(n_{wd})} = [x_1 \quad \dots \quad y_{n_{wt}}] \\
 i = 1, \dots, n_X \\
 j = 1, \dots, n_{wt} \\
 j = 1, \dots, n_{wt}.
 \end{array}
 \quad (2.6)$$

In the nested optimization problem, considered in this work, there is an upper level problem and multiple lower level problems. Each lower level optimization problem is a constraint on the upper level optimization problem. The desired goal in the nested optimization problem is to maximize the AEP of the dynamic wind farm layout. As already stated, the optimization problem consists of two levels:

1. Maximize the AEP of the dynamic wind farm layout by varying the static turbine positions (installation positions) subject to the wind farm boundary and to the lower level optimization problems;
2. For each considered wind direction, maximize the wind farm power output by varying the wind turbine positions subject to the wind farm and movable range boundary.

The workflow of nested WFLO is displayed in Figure 2.7.

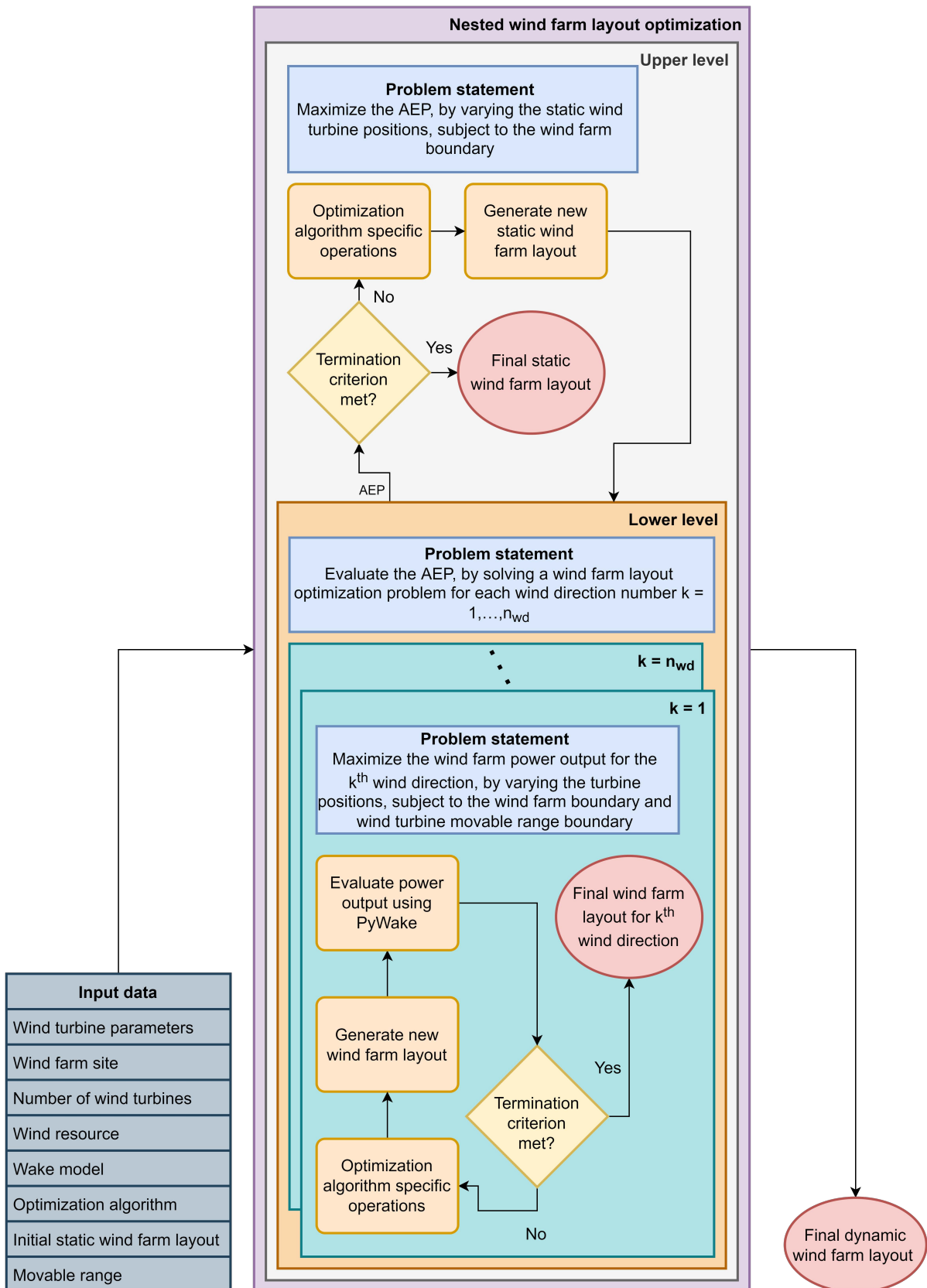


Figure 2.7: Flowchart of the nested wind farm layout optimization.

For the upper level optimization, the goal is to maximize the AEP of the dynamic wind farm layout. The

upper level only varies the static turbine positions, also known as the installation positions. For each static wind farm layout that is generated in the upper level optimization, n_{wd} lower level problems are solved. Each lower level problem corresponds with a specific wind direction. The AEP of the dynamic layout can be evaluated once all lower level problems are solved. The upper level optimization is finished once the generated static layout and its corresponding optimal dynamic layout meet the upper level termination criteria. The final result is a static layout that gives the best dynamic layout.

The main difference between the sequential and nested WFLO is in the evaluation of the static wind farm layout. In the first step of the sequential optimization, a static WFLOP is solved by varying the wind turbine static positions. Hereafter, the static positions are fixed and the second step of the optimization problem is solved. In the nested optimization, the wind turbine static positions, generated in the upper level, are evaluated on their ability to produce the optimal dynamic wind farm layout in the lower level. In other words, the performance of the static turbine positions is not assessed by their ability to result in the best static layout, as is the case in sequential optimization, but in their ability to result in the best dynamic layout.

2.5. Wind farm AEP calculation using PyWake

A mathematical description of the AEP and wind farm efficiency is provided, and the use of PyWake to calculate the AEP for a given wind farm layout is described. The PyWake model is then validated through an example layout provided in the literature.

2.5.1. Formulation of AEP

Baker et al. (2019) used the following formulation of the AEP to maximize the objective function in their study [44]:

$$\text{AEP} = \left(\sum_{k=1}^{n_{wd}} \sum_{l=1}^{n_{ws}} f_k w_{k,l} P_{k,l} \right) 8760 \frac{\text{hrs}}{\text{yr}}, \quad (2.7)$$

where:

- n_{wd} is the number of wind direction bins;
- n_{ws} is the number of wind speed bins;
- f_k is the frequency of occurrence of a wind direction bin;
- $w_{k,l}$ is the frequency of occurrence of a wind speed bin for each wind direction bin;
- $P_{k,l}$ is the total wind farm power output at the midpoint value of a wind direction bin;
- 8760 is the number of hours in a year.

To obtain the total wind farm power output for a certain wind direction, the power outputs of all individual wind turbines for all wind speed samples for that wind direction have to be computed. For each wind speed sample, the power output of all wind turbines can be calculated once the effective wind speed V_e of the turbines is known. The effective wind speed is the incoming wind speed at a wind turbine while accounting for the wake losses. This incoming wind speed is dependent on the wind turbine coordinates (x,y) because the wake losses are position dependent. By using the power curve of a wind turbine, the power output of each individual wind turbine can be computed for a certain effective wind speed.

Simply put, if all wind turbine coordinates are known, the total wind farm power output for a certain wind direction can be calculated and, in turn, the AEP can be evaluated. For a more detailed explanation of the formulation and calculation of the AEP, the reader is referred to Baker et al. (2019) [44].

2.5.2. Definition of wind farm efficiency

The wind farm efficiency helps in the understanding and comparison of what can be gained in terms of AEP for various wind farm layouts. The wind farm efficiency is described by the following equation:

$$\eta = \frac{\text{AEP}}{\text{AEP}_{\text{freestanding}}}, \quad (2.8)$$

where η is the wind farm efficiency, AEP is the calculated annual energy production of the wind farm, and $\text{AEP}_{\text{freestanding}}$ is the annual energy production of n_{wt} freestanding wind turbines, i.e., no wake losses.

2.5.3. AEP calculation using PyWake

PyWake is a free-to-use wind farm modelling software implemented in Python [45]. It has the ability to compute the annual energy production, the effective local wind speed at a wind turbine, the effective local turbulence intensity, the power output, the thrust coefficient, and the wind farm flow fields. It includes different inbuilt wind farm sites, wind turbines, and wake deficit models.

Pywake is used to calculate the AEP or power of a given layout (see Figure 2.8). In order to do this, PyWake needs some important input data, such as the wind turbine characteristics, wind resource, and the wake deficit model. In the case of the AEP, the wind turbine coordinates are given as input to PyWake, which evaluates and returns the AEP. In the case of the power, the wind turbine coordinates and wind direction are given as inputs to PyWake, which evaluates and returns the power per wind direction. The latter case can be used to obtain the wind farm power outputs for all considered wind directions in the dynamic WFLOP. The AEP of the dynamic wind farm layout can then simply be evaluated, outside PyWake, with the following equation [46]:

$$\text{AEP} = \left(\sum_{k=1}^{n_{\text{wd}}} f_k P_k \right) 8760 \frac{\text{hrs}}{\text{yr}}. \quad (2.9)$$

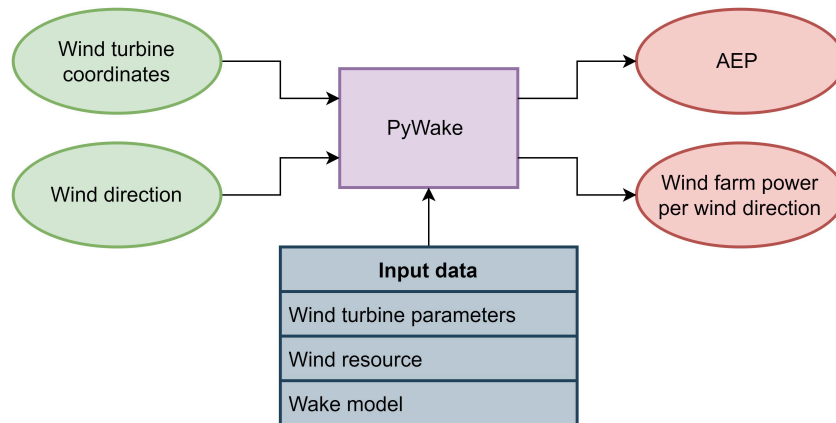


Figure 2.8: A simple illustration of the workflow used to calculate the AEP and power per wind direction in PyWake.

2.5.4. PyWake model validation through an example layout

An example wind farm layout is provided by Baker et al. (2019) for a 16 wind turbine scenario, with an AEP of 366.94 GWh [47]. By using the methodology described in their work, the same results (in terms of AEP) are expected to be obtained with PyWake. Hence, the PyWake model can be validated.

Figure 2.9 demonstrates the example layout. Each turbine has a location that is described by an x- and y-coordinate (x_j, y_j) , where j is the turbine number.

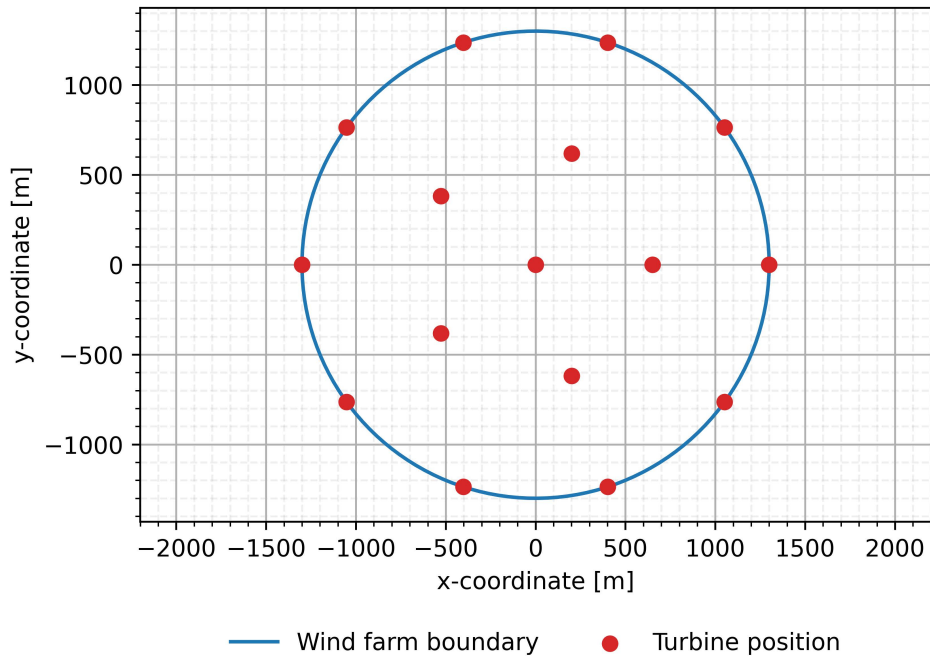


Figure 2.9: An example of a wind farm layout that consists of 16 wind turbines.

The PyWake model can be easily validated with the example layout since both the wind turbine positions and the AEP are already known. By providing the wind turbine locations and the necessary input data to the PyWake model, the same AEP value is obtained as mentioned above. To be more precise, the AEP value provided by Baker et al. (2019) is 366.9415712 GWh [47], and the AEP value obtained with the PyWake model is 366.94157116 GWh.

It is also possible to obtain the wind farm power per wind direction and calculate the AEP with Equation 2.9. The wind farm power output for each considered wind direction, obtained with PyWake, is shown in Table 2.1. By multiplying the power output for the considered wind direction with the wind directional bin frequency (see Figure 3.2 for the wind distribution frequency), taking the sum, and multiplying it by the number of hours in a year, the AEP can be calculated. The same AEP value directly obtained with the PyWake model can be indirectly obtained with the described method.

Wind direction [deg]	Power [MW]	Wind directional bin frequency [-]
0.0	43.126	0.025
22.5	40.420	0.024
45.0	44.809	0.029
67.5	44.944	0.036
90.0	38.014	0.063
112.5	44.944	0.065
135.0	44.809	0.100
157.5	40.420	0.122
180.0	43.126	0.063
202.5	40.673	0.038
225.0	43.973	0.039
247.5	44.898	0.083
270.0	38.136	0.213
292.5	44.898	0.046
315.0	43.973	0.032
337.5	40.673	0.022

Table 2.1: Wind farm power output per wind direction for the example layout.

2.6. Constrained optimization algorithms

Four different constraint optimization algorithms used in this Master's Thesis are introduced and a short high-level description of each algorithm is given.

2.6.1. Introduction of four optimization algorithms

Many algorithms have been used to solve the WFLOP. Some notable algorithms are, but not limited to: Genetic Algorithm (GA), Evolutionary Strategy (ES), Particle Swarm Optimization (PSO), Mixed Integer Programming (MIP), Simulated Annealing (SA), and Travelling Salesman Problem (TSP) [34, 37].

The optimization of a wind farm layout is known to be a complex problem to solve due to its high dimensionality and multimodal design space [48]. In case study 1 in Baker et al. (2019), for example, many optimization algorithms were used, while keeping all other variables in the WFLOP fixed [47]. Even though some algorithms found similar results, none of them found the same result. This indicates the difficulty and multimodality of the WFLOP. The use of multiple optimizers aids in verification of the obtained results from solving the optimization problem. Therefore, in this Master's Thesis, multiple optimization algorithms are used.

The optimization problem that is solved in this work includes constraints on the turbine position. Therefore, the optimizers need to handle constraints. The algorithms that are used in this work are:

- Covariance matrix adaptation evolution strategy (CMA-ES);
- Constrained optimization by linear approximation (COBYLA);
- Trust-region interior point method (trust-constr);
- Sequential least squares programming (SLSQP).

All these algorithms are freely accessible in Python and can handle constraints. Considering that PyWake is implemented in Python as well, using optimizers available in Python is quite convenient.

CMA-ES was the algorithm used in the first study that considered WFLO with movable FOWTs [8]. It is an often used evolutionary strategy, which is freely available on GitHub for Python [49]. The other algorithms are in-built optimizers of the widely used SciPy open-source Python library [50]. SciPy offers several optimization methods. Not all of them are able to solve optimization problems subject to inequality constraints, but these three are.

The four algorithms used in this Master's Thesis are explained in more detail next. Readers that are not interested in these explanations are referred to the subsequent chapter, where the optimization problems defined in this chapter are solved for a case study.

2.6.2. Covariance matrix adaptation evolution strategy

Evolutionary Programs (EP) or Evolutionary Algorithms (EA) are the general terms for solving optimization problems based on evolutionary and genetic principles [51]. One such EA-technique is Evolution Strategies (ES) [52, 53]. An ES-method usually starts by creating a population of candidates or individuals, which are then evaluated on their performance. The best candidate(s) from the population are then selected as parents. Hereafter, offspring are generated from the parents through duplication or recombination. The offspring undergo a mutation based on probability and are then added to the population. The population, which is now larger, has to be decreased through survival strategies. The above-mentioned process is repeated until the termination criteria are met [54].

CMA-ES is one of the most often used EA's [55], and was originally proposed by Hansen et al. (1995) [56]. The CMA-ES method involves the adaptation of the eigenvectors in the covariance matrix to create a nonisotropic distribution of the mutations that is known to be more efficient than an isotropic distribution [57]. In other words, a deliberately calculated multivariate normal distribution of the mutations is able to generate populations with better solutions. By favouring the probability of occurrence of mutations, which are developed by chance, in certain directions, the optimization method becomes more effective. The goal of the optimizer is to deal with an objective function that is non-linear, non-separable, and moderately or highly dimensional (at least 10 design variables) [58]. Furthermore, the objective function can be non-convex, multimodal, non-smooth, discontinuous, ill-conditioned, and/or

noisy. These characteristics of the objective function are difficulties that can be faced in real-world optimization problems.

2.6.3. Constrained optimization by linear approximation

COBYLA is the Fortran software implementation of Powell's method [59, 60], proposed by Powell (1994) and developed for Westland Helicopters [61]. COBYLA, which is also implemented in SciPy [50], is a derivative-free optimization method, which is particularly helpful when derivatives are not available, difficult to obtain, or not useful. It is a non-linear constrained optimization problem-solving algorithm that is able to handle both equality and inequality constraints.

COBYLA works by linearly approximating the objective function and the constraint functions, by interpolating between vertices of simplices [61]. A simplex is a convex hull that has $n_x + 1$ vertices and a volume that is non-zero [59]. A trust-region with a certain radius is applied to restrain the change of the design variables. The radius of this trust-region is decreased once the changes in design variables do not lead to better solutions. The radius is decreased a finite number of times, until it achieves a certain small value. The algorithm is then terminated.

2.6.4. Trust-region interior point method

Trust-constr is the SciPy implementation of a trust region method for large-scale constrained optimization problems [50]. For nonlinear inequality constraints, trust-constr uses the trust-region interior point method, as proposed by Byrd et al. (1999) [62]. The algorithm used for the interior point method is called the Nonlinear Interior point Trust Region Optimizer (NITRO). A comprehensive description of NITRO is provided in algorithm III of Byrd et al. (1999) [62].

NITRO makes use of barrier subproblems to handle inequality constraints. An estimate of the solution to the subproblems is provided by using Sequential Quadratic Programming (SQP) and trust region approaches. In each subproblem, the Lagrangian function is approximated by a quadratic function. Furthermore, the nonlinear constraints are approximated by linear constraints. This quadratic function is then minimized within a certain trust region boundary radius, where the approximations for the Lagrangian function and constraints can be relied upon. The final result of the optimization is a step towards a new point. If the decrease in merit function value at this point is reasonable, a new subproblem is solved. If this is not the case, the trust region boundary radius is decreased and another step is calculated. Readers that are familiar with such optimization methods could have noticed the nested optimization scheme in NITRO.

2.6.5. Sequential least squares programming

SLSQP is a gradient-based optimization method that is able to solve a multivariate (non)linear optimization problem that is subject to equality constraints, inequality constraints, and/or bounds. The initial algorithm was proposed by Kraft (1988) [63]. SciPy has an implementation of the SLSQP method that is freely available for general use [50].

The SLSQP optimizer solves a nonlinear optimization problem by using a quadratic subproblem to determine the step direction. In the quadratic subproblem, the Lagrangian function is approximated and minimized. Furthermore, within the subproblem, the nonlinear constraint is estimated by a linear constraint. The SLSQP solver makes use of a Quasi-Newton approach with a Broyden–Fletcher–Goldfarb–Shanno (BFGS) update to estimate the Hessian of the Lagrangian function by using first-order data. The step size is calculated by taking advantage of the Hessian approximation. For the computation of the step direction, a quadratic subproblem has to be solved. Three techniques are proposed by Kraft (1988) to solve the quadratic subproblem: i) the primal method; ii) the primal/dual method; and (iii) the dual method [63]. SLSQP makes use of the second technique, which is an adapted version of the Least Squares with Equality and Inequality Constraints (LSEI), which was originally implemented by Lawson and Hanson (1974) [64]. Kraft (1988) adapted the LSEI method, freely available to the public at the time, to solve a linear least squares subproblem instead of a quadratic subproblem [63].

3

Optimized dynamic wind farm layouts for a case study

This chapter presents and discusses optimized dynamic wind farm layouts for a wind farm case study. First, a description is provided of the wind farm case study that is used in this Master's Thesis (Section 3.1). Next, two reference WFLOPs are solved for this case study (Section 3.2). Hereafter, the dynamic WFLOP is solved with two different methods (Section 3.3): sequential and nested optimization. Subsequently, additional efforts are made to find even better dynamic layouts (Section 3.4). Following that, a comparison of the dynamic layout results is made (Section 3.5). Lastly, a discussion is provided regarding the key findings and the limitations of the studies in this chapter (Section 3.6).

3.1. Description of wind farm case study

In this section, the wind farm case study that is used in this Master's Thesis to solve the WFLOP is described. The section starts with the selection of the wind farm case study and a description of the wind turbines used in this case study. Next, a description of the wind farm site is provided. Hereafter, the wind resource is presented, and the wake deficit model used to calculate the incoming wind speeds of the wind turbine is explained.

3.1.1. Wind farm case study selection

There are many aspects to the WFLOP, such as the wind farm site, wind turbine type, number of wind turbines, wind resource, wake model, optimization algorithm, etc. Case studies help in reducing the number of variables such that specific aspects of the problem can be analysed in more detail. In this Master's Thesis, a wind farm case study is used to analyse the addition of movable turbines to the WFLOP. The increased complexity of dynamic WFLOP compared to static WFLOP makes the reduction of the number of variables essential.

IEA's Wind Task 37 has several goals to enhance system engineering methodology and application in wind energy [65]. One of their goals is to perform design optimization research to acquire knowledge of and expand on various methodologies [66]. Baker et al. (2019) performed such a study specifically for WFLO to obtain a set of best practices for optimization algorithms and wake deficit models [47]. Therefore, two case studies were developed to analyse these two aspects [46]. In case study 1, the optimization algorithm could be chosen at will, but the wake model was fixed. In case study 2, both the optimization algorithm and the wake model were free to choose. Several participants with various backgrounds were asked to solve the optimization problems in these case studies [47].

In this Master's Thesis, only case study 1 is considered to simplify the optimization problem. In this case study, participants were free to choose an optimization algorithm and every other aspect of the WFLOP was fixed. The objective function of the optimization problem was to maximize the AEP, subject to the wind farm boundary, by varying the turbine locations (x_j, y_j) , where j is the wind turbine number. The wind turbine used in this study was the IEA37 3.35 MW onshore reference turbine [67]. Three

different numbers of wind turbines were used, with a corresponding wind farm boundary size:

1. $n_{wt} = 16$ with $R_B = 1,300$ m;
2. $n_{wt} = 36$ with $R_B = 2,000$ m;
3. $n_{wt} = 64$ with $R_B = 3,000$ m.

Here, R_B is the boundary radius of a circular wind farm with its centre at $(0,0)$, and n_{wt} is the number of wind turbines.

To reduce the complexity of the optimization problem when considering a dynamic wind farm, only one of the three different scenarios is studied. To decrease the computational time, the scenario that consists of the lowest number of wind turbines is selected ($n_{wt} = 16$).

The selection of case study 1 is beneficial for the dynamic WFLOP in two ways: (i) developing and validating the complex optimization framework for dynamic WFLO; and (ii) comparing dynamic layout results to static layout results of multiple participants in case study 1.

It should be noted that all variables of the WFLOP are based on case study 1 of Baker et al. (2019) [47]. The wind turbine, wind farm site, number of wind turbines, wind resource, and wake model, used in the dynamic WFLOP, are all fixed. This simplifies the study of the addition of movability in the WFLOP. For the specific choice of these variables, the reader is referred to the related works of the authors [41, 46, 47].

3.1.2. IEA37 3.35 MW turbine

As mentioned in Section 3.1.1, the wind turbine that will be considered for the optimization problem in this Master's Thesis is the IEA37 3.35 MW onshore reference turbine [67]. The power output of this turbine for different wind speeds is presented in Figure 3.1. For a mathematical description of the power output for different wind speeds, the reader is referred to Eq. (1) in Baker et al. (2019) [47]. The important characteristics of this reference turbine considered in the WFLOP are shown in Table 3.1.

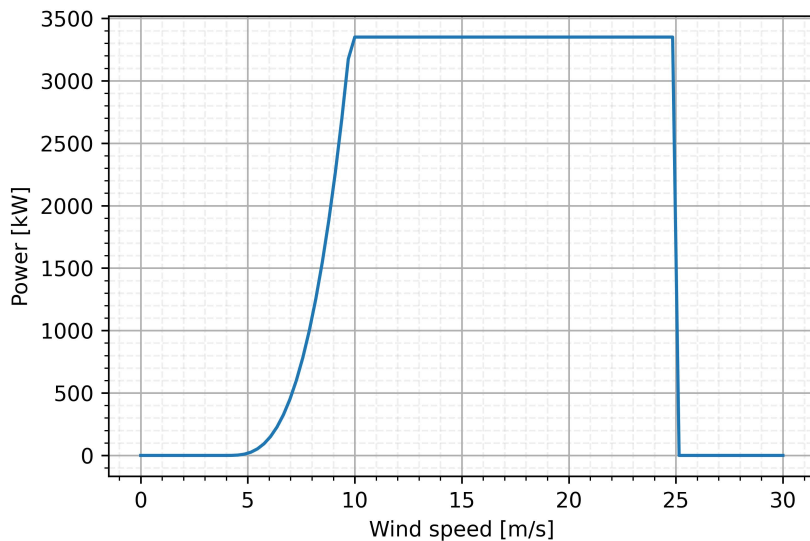


Figure 3.1: IEA37 3.35MW power curve.

The reader might have noticed that the turbine used in solving the dynamic WFLOP is land-based and not offshore. As stated in Section 1.1.5, to allow for turbine repositioning, the wind turbine must be floating. Therefore, an onshore turbine would not be suitable for turbine repositioning. The size and rated power of this land-based wind turbine is also relatively small. Offshore wind turbines often have a larger hub height, rotor diameter, and rated power than onshore wind turbines [68]. In solving the dynamic WFLOP, however, the use of an onshore turbine is not expected to cause a change in the character of the results. In other words, the conclusions that could be drawn from the results of the

dynamic WFLO for an onshore wind turbine are not expected to be much different than for an offshore wind turbine. The dynamic WFLOP is not dependent on one type of wind turbine, as it is merely an input to the optimization problem.

Description	Symbol	Value	Unit
Hub height	h_{hub}	110	[m]
Rotor diameter	D_{rotor}	130	[m]
Cut-in wind speed	$V_{\text{cut-in}}$	4	[m/s]
Rated wind speed	V_{rated}	9.8	[m/s]
Cut-out wind speed	$V_{\text{cut-out}}$	25	[m/s]

Table 3.1: IEA37 3.35MW wind turbine characteristics [67].

3.1.3. Wind farm site

As specified in Section 3.1.1, the wind farm site selected to study a dynamic layout is the 16 turbine scenario for case study 1 in Baker et al. (2019) [47]. The wind farm has a circular boundary with its centre at (0,0). The radius of the boundary is $R_B = 1,300$ m.

In reality, wind farm areas do not have circular wind farm boundaries. Wind farm boundaries often have an irregular shape and could even consist of multiple segments instead of a singular one. The wind farm area and boundary could, for example, be influenced by the environment and the constraints imposed by the regulatory authorities or by the law. However, to reduce the effect of the wind farm boundary on the layout, the circular wind farm boundary was chosen by Baker et al. (2019) [47]. The turbines were allowed to be on or inside this circular wind farm boundary.

3.1.4. Wind resource

Wind data obtained from a site is usually binned by the wind direction. The wind direction ranges from 0 degrees to 360 degrees, with 0 degrees representing North, 90 degrees representing East, 180 degrees representing South, and 270 degrees representing West. The number of bins used is often twelve or sixteen [35]. A higher number of bins would give a more accurate description of the wind resources. It should be noted that the value associated with a particular wind direction is the value where the wind is coming from, not where the wind is going to. If, for example, the largest bin is around 270 degrees, then the wind is coming from the west and going to the east. This example can be observed in Figure 3.2, which is the wind rose data used in the IEA37 case studies [47]. Each sector represents the frequency of occurrence for a certain wind direction bin.

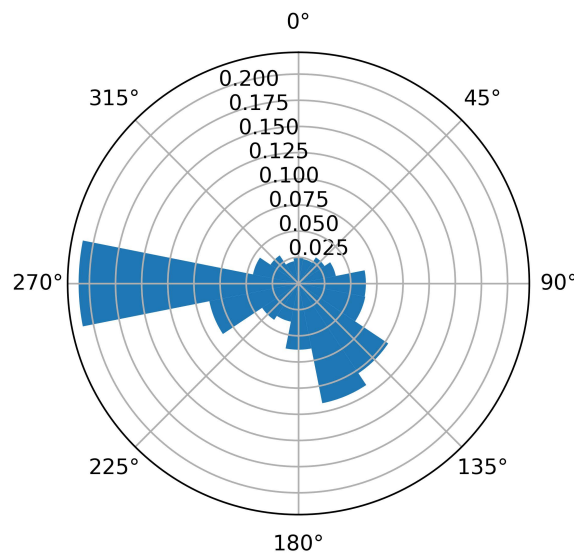


Figure 3.2: Wind distribution frequency of the IEA 37 case studies.

In the IEA37 case studies, the wind speed was assumed to be constant for all wind directions [47]. The value of this constant wind speed was set to be the same as the rated wind speed of the wind turbine, that is 9.8 m/s (see Table 3.1). In reality, the wind speed is not constant. The wind data would be better described by a Weibull distribution for each wind direction sector [35]. However, the goal of case study 1 was to compare different optimization algorithms with each other [47]. Therefore, Baker et al. (2019) strove to have a rough design space with many local optima. For a constant wind speed of 9.8 m/s, the wake effect causes the largest differences in incoming wind speed for turbines located in the disturbed flow of the wind. Other important wind characteristics are summarized in Table 3.2.

Description	Value	Unit
Number of wind direction bins	16	[-]
Wind direction step size	22.5	[°]
Constant wind speed in all wind directions	9.8	[m/s]

Table 3.2: Wind attributes of the IEA 37 case studies.

3.1.5. Wake model

General description of analytical wake models

There exist many analytical wake models that can be used to calculate the velocity deficit in the wake [69–79]. The reader is referred to the original works for a description of these wake deficit models. For a review and evaluation of several of these models, the reader is referred to Archer et al. (2018) and Kaldellis et al. (2021) [80, 81]. The most well-known of these models is the Jensen model, which has been widely used in literature and industry due to its simplicity [22].

Each model uses some of the following parameters to formulate an expression for the velocity deficit in the wake and the diameter of the wake [81]:

- Upstream wind speed V ;
- Rotor radius (or diameter) R_{rotor} (or D_{rotor});
- Downstream distance x ;
- Lateral coordinate y ;
- Spanwise coordinate z ;
- Wake expansion (or decay) coefficient k or k^* ;
- Thrust coefficient C_T ;
- Axial induction factor a ;
- Ambient turbulence I_a ;
- Wind turbine generated turbulence I_w ;
- Hub height h_{hub} ;
- Surface roughness z_0 ;
- Wake model specific coefficients.

For more information on how to use a wake model to calculate the wind speed deficit at a downstream turbine, the reader is referred to Hou et al. (2019) [82]. Once the velocity deficit for each wind turbine is known, the power can be easily calculated using the turbines' power curve.

Wake model used in IEA37 case studies

In case study 1 of the IEA37 case studies [47], the wake model was fixed, but the optimization algorithm was free to choose, as explained in Section 3.1.1. The wake deficit model, chosen for the case study, was a simplified version of the Bastankhah's Gaussian wake model [41], first used by Thomas and Ning (2018) [83]. The velocity deficit in the wake can be estimated with the adapted version of the Bastankhah and Porté-Agel wake model [74], which is described by the following equation [41]:

$$\frac{\Delta V}{V_\infty} = \left(1 - \sqrt{1 - \frac{C_T}{8\sigma_y^2/D_{rotor}^2}}\right) \exp\left(-0.5 \left(\frac{y_i - y_g}{\sigma_y}\right)^2\right), \quad (3.1)$$

where:

- C_T is the thrust coefficient, which for the case study was set 8/9;
- D_{rotor} is the rotor diameter of the IEA 37 3.35MW wind turbine;
- $y_i - y_g$ is the distance from hub to hub in the lateral direction, from the wind turbine where the wake is generated y_g to the wind turbine where the velocity deficit has to be determined y_i ;
- σ_y is the standard deviation of the generated wake deficit in the lateral direction that can be computed using Eq. (2) in Baker et al. (2019) [41].

In Figure 3.3 the development of a wake is shown obtained with the simplified version of the Bastankhah's Gaussian wake model.

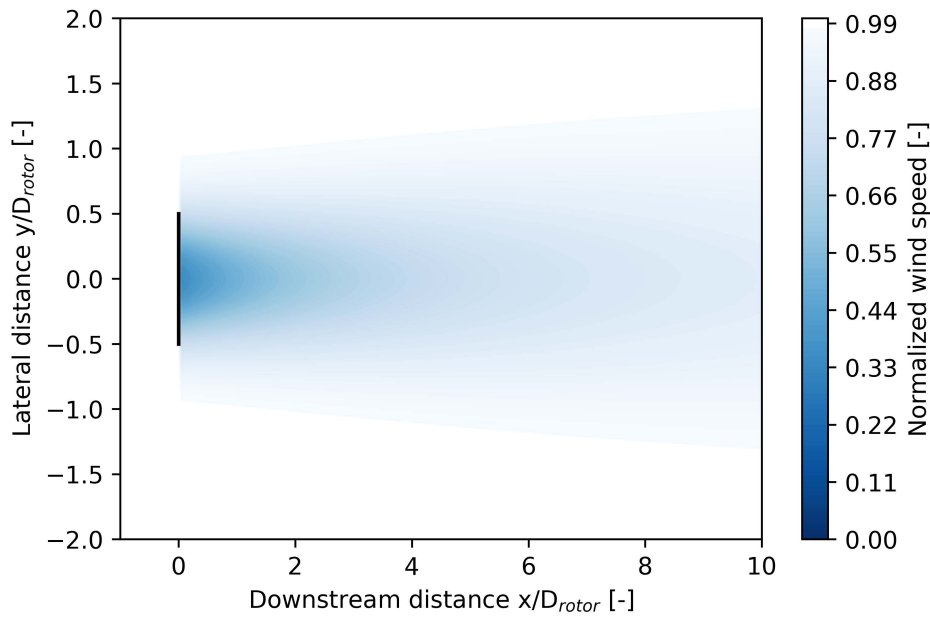


Figure 3.3: Wake expansion of a single wind turbine using the simplified version of the Bastankhah's Gaussian wake model.

The simplified version of Bastankhah's Gaussian wake deficit model is combined with a superposition model and a rotor-average model. For this wake deficit model, the default superposition model is the squared sum model, and the default rotor-average model is the rotor centre model [45]. The wake deficit model approximates the velocity deficit in the wake. The superposition model determines how the wakes from different turbines add up. The rotor-average model establishes a single or multiple points at the downstream wind turbine rotors, calculates the velocity deficit at these points, and determines the rotors' average wind speed. The rotor centre model only uses a single point, the rotor centre, to determine the rotor's average wind speed. Ideally, multiple points scattered over the rotor are used, since the rotor's average wind speed will be better approximated. More points, however, are also computationally more expensive.

3.2. Optimized reference wind farm layouts

In this section, the static WFLOP and the unrestricted dynamic WFLOP are solved to get a lower bound and an upper bound in terms of AEP.

3.2.1. Static layout optimization

Solving the static WFLOP with four different optimization algorithms

The four different optimization algorithms (explained in Section 2.6) are used to solve the static WFLOP. The convention used by the different optimizers is to minimize the objective function. Therefore, a minus sign is put in front of the objective function, which is to maximize the AEP.

The different optimization algorithms are compared by letting them run until the algorithms' specific termination criteria are met. Some examples of termination criteria include, but are not limited to: an absolute or relative tolerance on the value of the objective function; an absolute or relative tolerance on the design variables; a maximum number of function evaluations; and a maximum number of iterations. The termination criteria are different for each optimizer. To prevent early termination due to a maximum number of iterations, which is not a performance criterion, the termination criteria 'maxiter' is set high.

There are optimization algorithm-specific parameters that could be tuned to obtain possibly better optimization results. No such efforts are made in the comparison between the different optimizers.

All optimizers require an initial guess x_0 to start the optimization. This initial guess is a random wind farm layout that lies within the wind farm boundary. The same random layout is provided to the different optimizers. The performance of the different optimizers is then assessed more fairly, since some initial layouts might be a better starting point for the optimization than others. CMA-ES additionally requires an initial standard deviation, σ_0 , which is approximately 1/4 of the design space. Therefore, σ_0 is set to 1/4 times the wind farm boundary diameter ($2 \times R_B$).

The convergence paths of the four optimization algorithms are presented in Figure 3.4. Out of all the optimizers, CMA-ES finds the best optimum. It also has a relatively steep convergence rate. Furthermore, between 10^2 and a bit beyond 10^3 number of function evaluations, CMA-ES shows a large scatter in function values. This is due to the random processes involved in the Evolution Strategy. COBYLA and trust-constr converge to the same optimum, as can be seen in Table 3.3. This suggests that both optimization algorithms are highly influenced by their initial starting point. The convergence rate of COBYLA is steeper than that of trust-constr. The latter also requires a lot more function evaluations to meet the termination criteria. Although SLSQP is able to find a better wind farm layout than COBYLA and trust-constr, it is the worst at generating feasible solutions. This means that the generated layouts do not satisfy the wind farm boundary constraint most of the time.

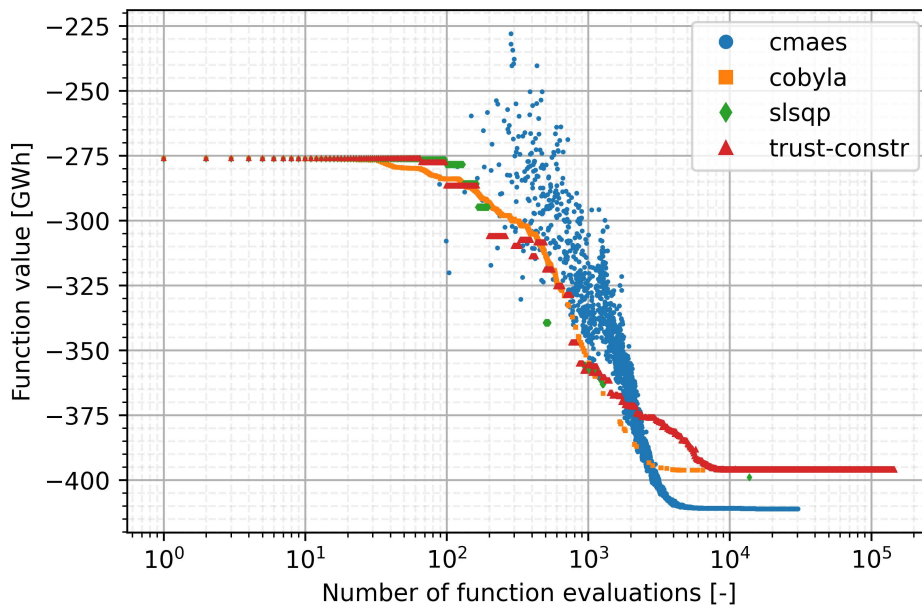


Figure 3.4: Convergence study of the static WFLO for four different optimization algorithms (feasible function values only).

Algorithm	AEP [GWh]	Function evaluations [-]
CMA-ES	411.07	30302
COBYLA	396.24	20552
SLSQP	398.97	13881
trust-constr	396.24	145763

Table 3.3: The optimum AEP and the number of function value evaluations for the convergence study of the static WFLOP for four different optimization algorithms.

Figure 3.5 illustrates the final optimized static wind farm layouts for the four different optimization algorithms. As mentioned earlier, both COBYLA and trust-constr found the same optimum. By looking at the final optimized wind farm layout of both algorithms, the same result can be seen as well.

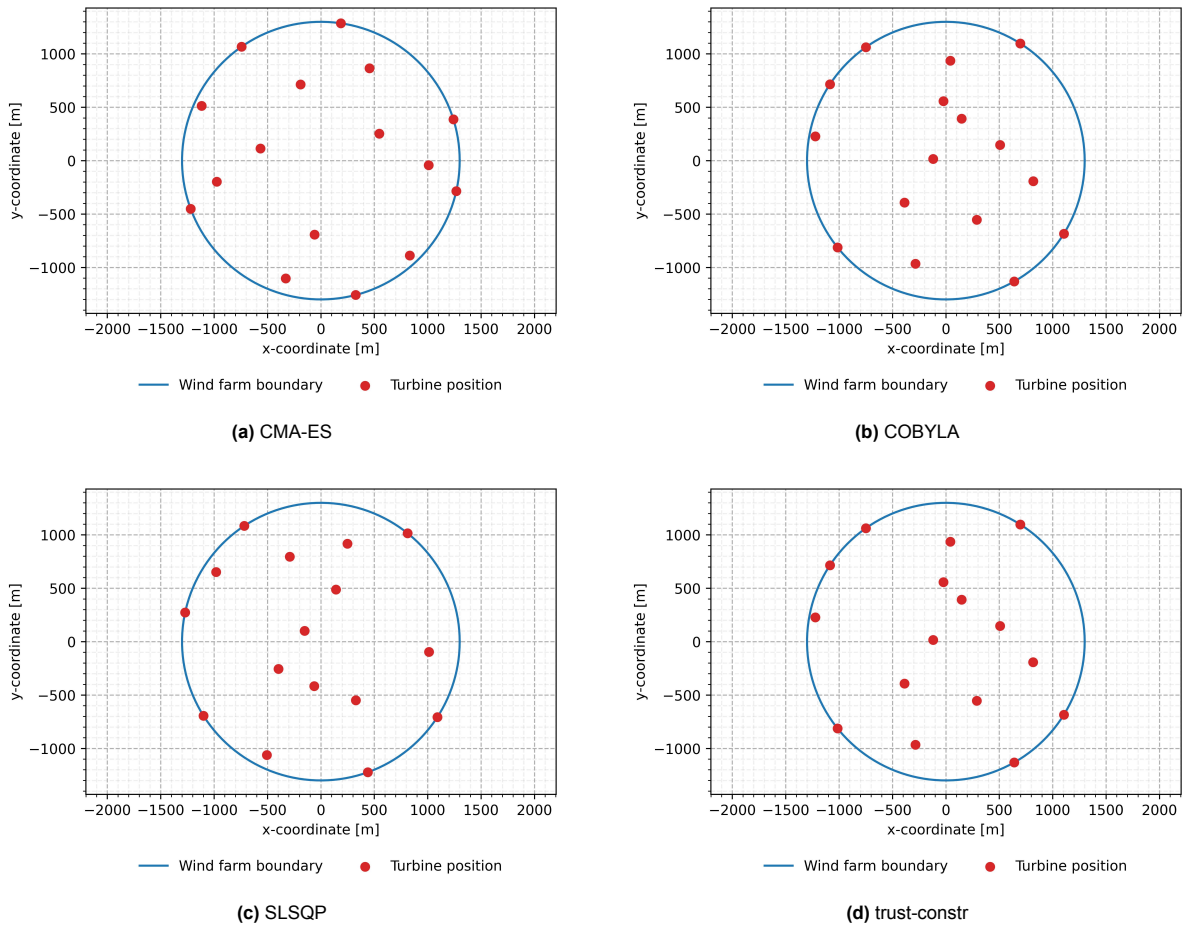


Figure 3.5: Optimized static wind farm layouts for four different optimization algorithms.

Of all the optimizers, the CMA-ES had the superior performance. By running the optimization multiple times, it might be the case that other algorithms would perform better or equally well. The convergence to the same optimum of COBYLA and trust-constr, however, indicates the influence of the initial starting point on the optimization results. Because it includes random processes, CMA-ES is able to overcome the influence of the starting layout on the optimization result. This makes CMA-ES a good choice for the optimization of static wind farm layouts.

It is also possible to compare the results of CMA-ES with the results of the different participants in Baker et al. (2019) that solved the same optimization problem [47]. The different participants were free to choose their own optimization algorithm. It is not well reported how they exactly solved the problem. It could be the case, for example, that an optimization was only run once; it could also be the case that

the optimization was run multiple times, as was done by participant 4, referred to as sub4 [47]. This participant solved the optimization problem 200 times with different starting points. This makes the comparison of results based on the final optimum alone rather difficult. Nonetheless, running CMA-ES once compares well with the top-ranked algorithms reported in Table 2 of Baker et al. (2019) [47].

Solving the static WFLOP 200 times using CMA-ES

A similar convergence study, as performed in the previous section, is done. Now, only one optimization algorithm is being studied: CMA-ES. The static WFLOP is solved 200 times with 200 different random starting points.

To reduce the computational time but still obtain a decent wind farm layout, the termination criterion 'tolfun' is set to 1 (the default is 1×10^{-11}). This termination criterion is met once the difference between the worst and best function value from the population in an iteration is smaller than the tolerance in the function value ('tolfun'). The population size is dependent on the number of design variables, which is 32 for 16 wind turbines. For 32 design variables, the population size calculated by CMA-ES is 14. Each candidate in this population has a function value. That means that there are 14 function values. Because these values are given in GWh, the optimization stops if the range of the values is less than 1 GWh.

Figure 3.6 shows the convergence graphs for the static WFLO solved 200 times with CMA-ES.

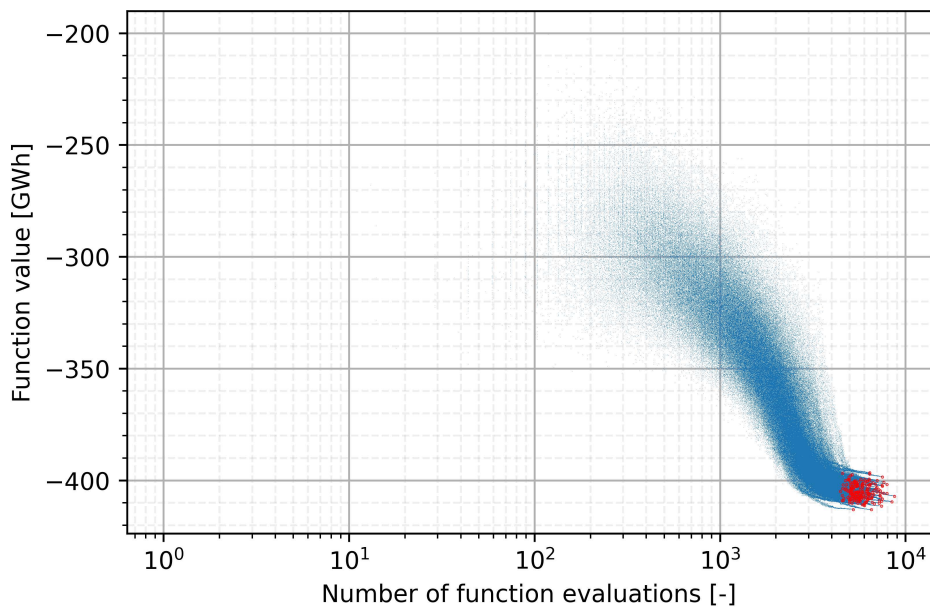


Figure 3.6: Convergence study of the static WFLOP solved 200 times using CMA-ES with the feasible function values in blue and the final optima in red.

There are several observations that could be made:

- The convergence rate for the different runs is quite similar;
- The number of function evaluations it takes to meet the termination criteria in each run is not the same;
- The optima for the different runs are not the same.

In Figure 3.7, a histogram is shown to visualize the optimal AEP values obtained by solving the static WFLOP 200 times. The minimum AEP value is 396.57 GWh and the mean AEP value is 405.10 GWh. The best found optimum from the 200 runs with a looser tolerance is better than the optimum found with stricter tolerance shown in Table 3.3 (413.14 GWh versus 411.07 GWh).

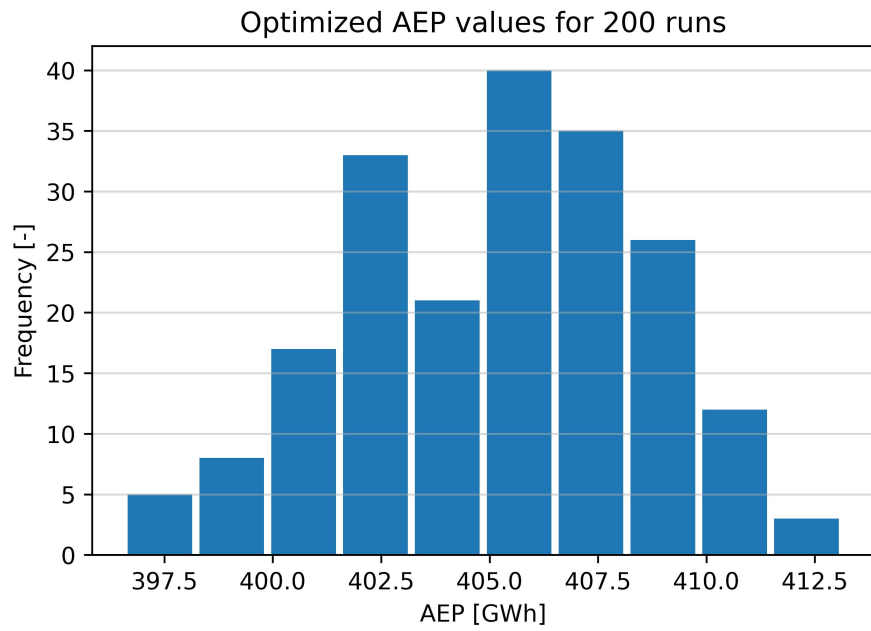


Figure 3.7: Histogram of the optimized AEP values for the static WFLOP solved 200 times with CMA-ES.

The resulting layout of the best found optimum from the 200 runs is shown in Figure 3.8. Many of the wind turbines are on or near the wind farm boundary.

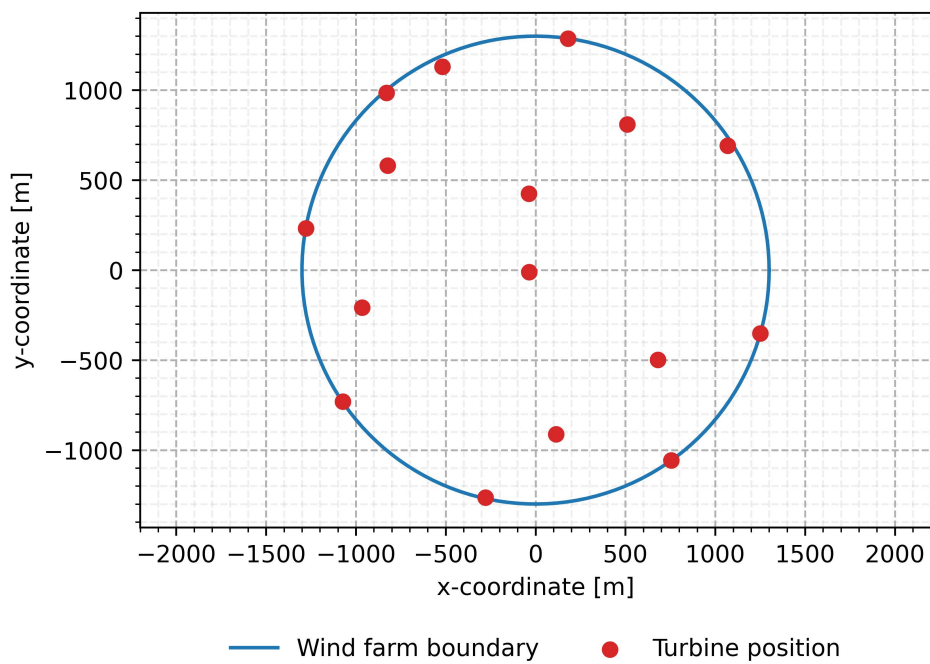


Figure 3.8: Best found optimum static wind farm layout from 200 runs.

3.2.2. Unrestricted dynamic layout optimization

The optimization algorithm used to solve the unrestricted dynamic WFLOP is the CMA-ES algorithm. Now, the 'tolfun' is set to 1×10^{-6} instead of 1 (as was done in Section 3.2.1). Because the unrestricted dynamic WFLOP is solved once, a stricter tolerance is applied.

The dynamic wind farm layout is presented in Figure 3.9 for 4 of the 16 different wind directions. The dynamic wind farm layout consists thus of 12 more wind farm layouts that follow the exact same trend: the wind turbines form a row perpendicular to the wind direction. In this way, there is no turbine located downstream of another turbine. Hence, the wake losses are minimized and the power output of the wind farm for that wind direction is maximized.

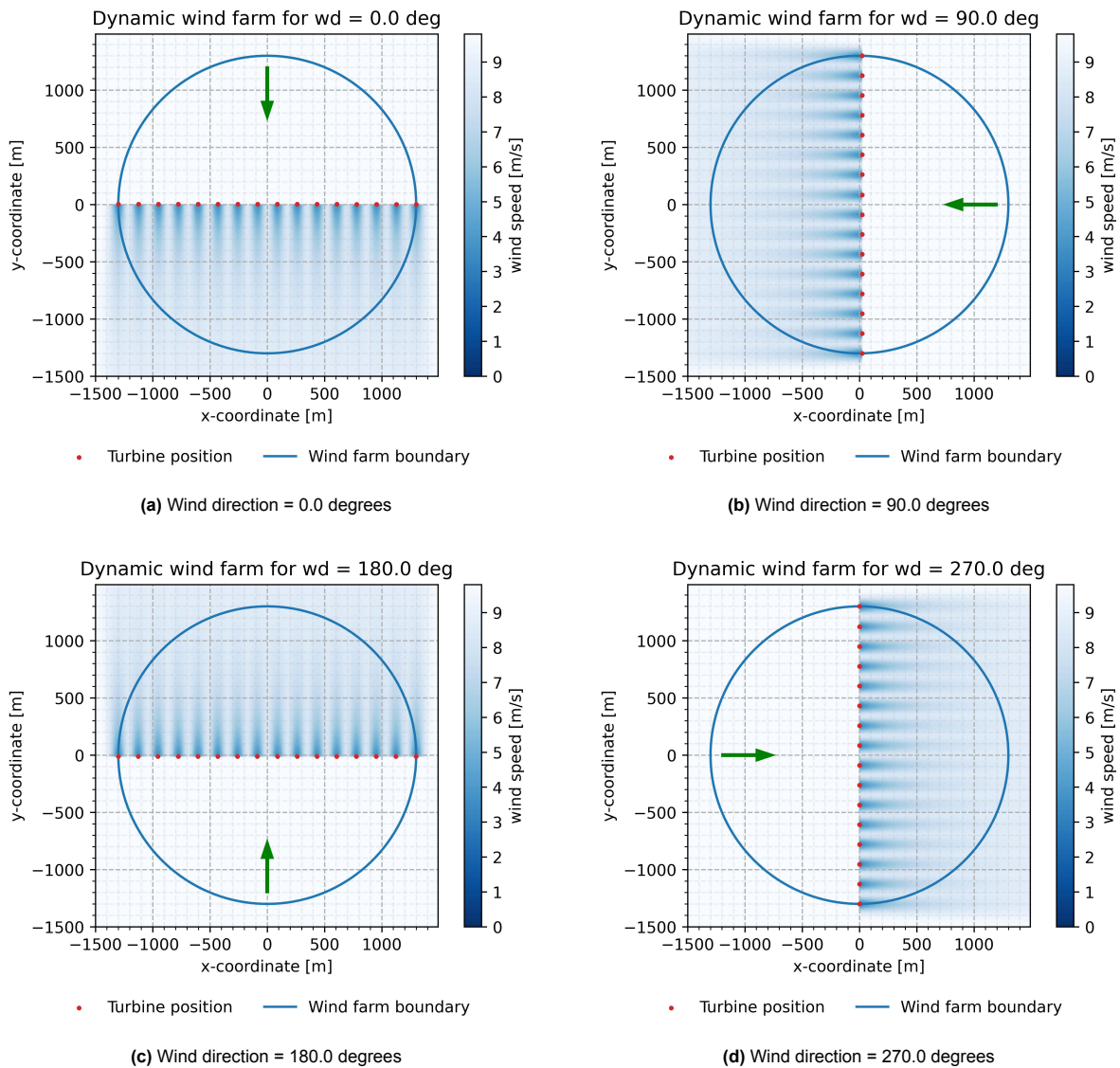


Figure 3.9: Optimized unrestricted dynamic wind farm layout shown for four different wind directions, with the green arrow indicating where the wind is coming from.

The CMA-ES algorithm, again, demonstrates itself to be an excellent optimizer. For each wind direction, the optimization starts with a random initial wind farm layout. The outcome for each wind direction, however, is the same: a row perpendicular to the wind direction. The optimizer is thus not dependent on the starting point and consistently finds the same outcome. This is also what would be expected from the optimum solution.

The AEP of 16 freestanding wind turbines, i.e., no wake losses, is 469.54 GWh. The AEP of the

dynamic wind farm layout, although very close, is not the same. The AEP value of the dynamic wind farm layout is 468.66 GWh, which indicates that there are still some wake losses.

Figure 3.9a is used as an example to describe how there are wake losses if there are no downstream wind turbines. In this wind farm layout, the wind is coming from the north. Therefore, the wind turbines align themselves perpendicular to this wind direction to minimize the wake losses. Although no visible difference in the y-coordinate of the wind turbines can be seen, there are still minor differences. Because of this, there are wind turbines downstream from other wind turbines, according to the wake model. The wake losses can then be attributed to the fact that the wake model, described in Section 3.1.5, has a deficit profile described by a Gaussian distribution. There is thus a velocity deficit in the crosswind direction as well. Even though the velocity deficit is minor, a small change in wind speed has a large effect on the power since it is proportional to the velocity cubed. Therefore, there is still a minor difference in the AEP.

3.3. Optimized restricted dynamic wind farm layouts

In this section, the dynamic layout optimization problem is solved using sequential and nested optimization.

3.3.1. Sequential optimization

Optimization approach

To investigate the full potential of turbine repositioning in increasing the AEP of the wind farm, several movable range sizes will be studied. These sizes range from $C = 0.01$ to $C = 20.0$, where C is the ratio between the circular movable range boundary radius and the rotor diameter (see Equation 2.1). Here, 0.01 means there is nearly no movement possible for the wind turbines, and 20.0 means the wind turbines are allowed to move anywhere in the circular wind farm boundary. For $C = 0$, the sequential optimization becomes a static layout optimization since there is no movable range. For $C = 20.0$, the sequential optimization is similar to the unrestricted optimization; in both cases, the turbines can move anywhere in the wind farm.

In solving the sequential WFLOP, use is made of the CMA-ES algorithm for both steps of the optimization. The tolerance of the function value 'tolfun' is set to 1×10^{-2} for the first step of the optimization and to 1 in the second step of the optimization. This is mainly done to reduce the computational time but still obtain a decent wind farm layout.

For each movable range size, the sequential WFLOP is solved 10 times. In Figure 3.6, CMA-ES did not consistently converge to the same optimum for a loose tolerance in the function value ('tolfun' = 1). Thus, by running the optimizer multiple times, a better optimum can be found. Therefore, the sequential optimization is run multiple times as well.

The wind farm efficiency for different sizes of the movable range is shown next, followed by the resulting wind farm layout for a selected movable range size.

Wind farm efficiency for increasing movable range

The best found wind farm efficiency values obtained by solving the sequential WFLOP 10 times are shown in Figure 3.10.

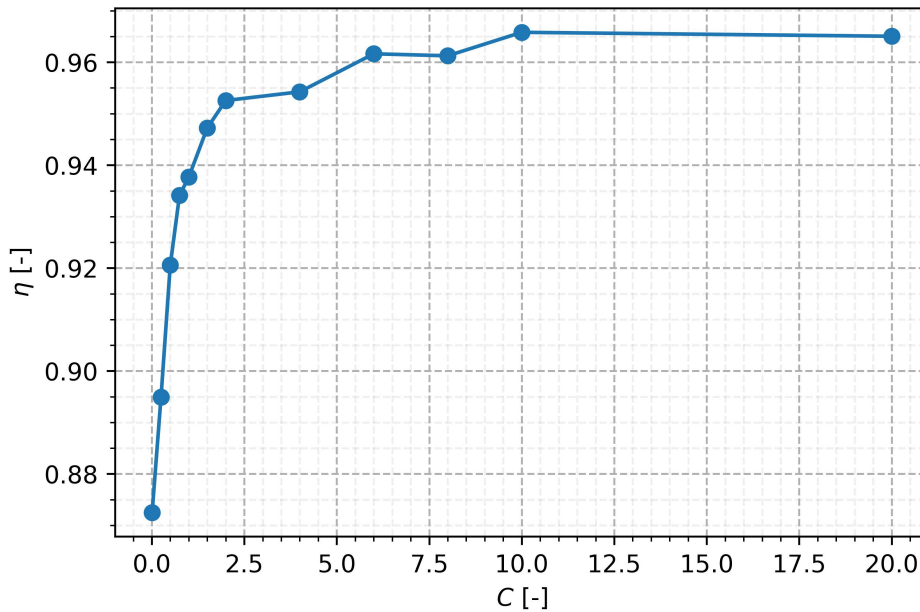


Figure 3.10: Wind farm efficiency for various movable range sizes obtained by solving the sequential WFLOP.

There are several observations that could be made:

- An increase in the movable range size results in an increase in wind farm efficiency;
- The potential of dynamic wind farm layouts to increase wind farm efficiency is large;
- The steepest increase in wind farm efficiency is in the range from $C = 0.01$ to $C = 2.0$;
- For a movable range larger than $C = 2.0$, a large increase in the movable range is required for a minor improvement in the wind farm efficiency.

For $C = 0$, the sequential WFLOP reduces to a static WFLOP. The best found static optimum in terms of wind farm efficiency (0.880) is close to that of the sequential optimization for $C = 0.01$ (0.872).

For $C = 20.0$, the optimization problem that is solved in the second step is similar to the unrestricted dynamic WFLOP: all wind turbines are allowed to move to any location in the wind farm. The result of the sequential optimization (0.965), however, is inferior to the result of the unrestricted optimization (0.998). The difference between the optimizations is in the tolerance of the function value ('tolfun') of the CMA-ES algorithm, which is chosen much stricter for the unrestricted optimization.

The loose tolerance in the function value might also cause inferior results for the other movable range sizes. It can be expected that for a stricter tolerance of the optimization algorithm in the second step of the sequential WFLO, the wind farm efficiency increases for all considered movable range sizes.

Wind farm layout for a selected movable range

In the following, the best found wind farm layout for $C = 2.0$ is presented. The selection of this size is mainly due to the steep increase seen in the wind farm efficiency up to this point.

The static wind farm layout obtained after solving the first step in the sequential WFLOP is shown in Figure 3.11. The AEP value for this static layout is 402.51 GWh.

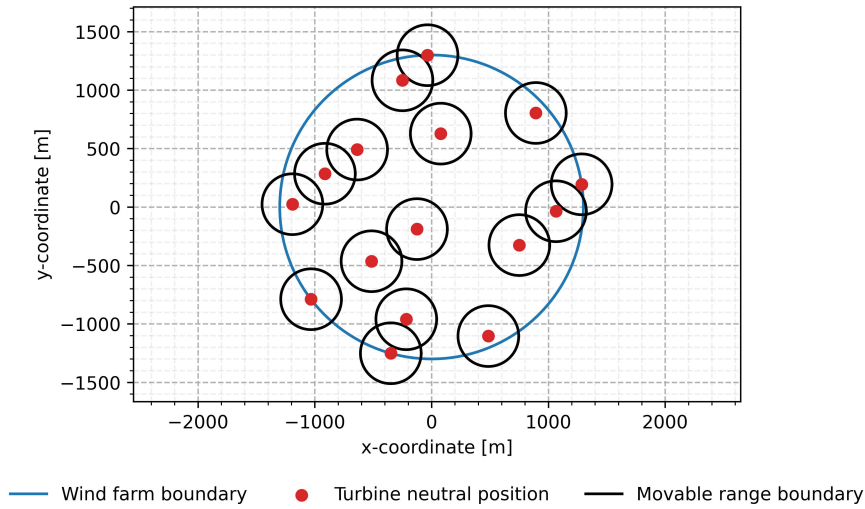


Figure 3.11: Optimized static wind farm layout obtained by solving the sequential WFLOP.

The dynamic wind farm layout is shown in Figure 3.12 for 4 of the 16 different wind directions. The AEP of the dynamic layout is 447.26 GWh.

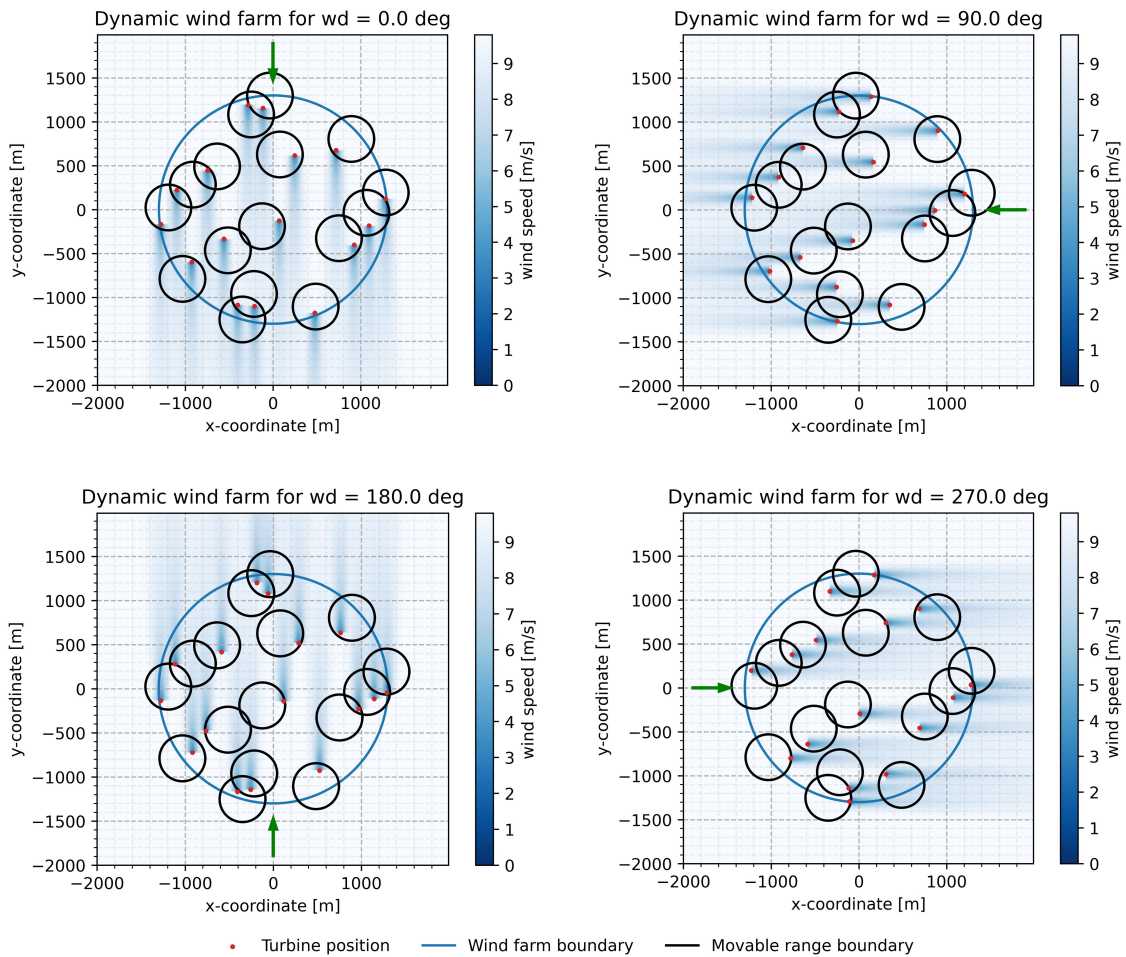


Figure 3.12: Optimized dynamic wind farm layout obtained by solving the sequential WFLOP.

Several observations can be made for the optimal dynamic wind farm layout:

- Some wind turbines have movable range boundaries beyond the wind farm boundary. Because turbines are not allowed to cross the farm boundary, they do not use their full movable range;
- Most movable range boundaries are overlapping;
- Wind turbines are not located in the downstream region of other turbines, where the wake deficit is most prevalent (dark blue flow colour).

3.3.2. Nested optimization

Computational cost of nested optimization

The nested WFLOP is comparable with the sequential WFLOP. In the nested optimization, however, the dynamic layout is assessed for more than one static layout. The total number of static layouts that are generated in the upper level depends on the number of upper level function evaluations required to meet the termination criteria. For example, in Figure 3.6, the minimum number of function evaluations required to meet the termination criteria is around 4,500. It should be noted that this is for a loose tolerance on the function value of the CMA-ES algorithm ('tolfun' = 1). For a stricter tolerance, more function evaluations would be required. If a similar number of function evaluations were required for the upper level of the nested optimization, then there would be at least 4,500 static layouts for which a dynamic layout would be optimized. If this is compared to the sequential optimization, where the dynamic layout is only optimized for one static layout, it could be understood why the nested optimization is much more computationally expensive.

Two measures have been taken to make the study of nested optimization feasible: the selection of only one movable range size ($C = 2.0$) and an assessment of implementation choices and settings that solve the nested WFLOP within a reasonable amount of time. The latter is discussed in more detail next.

Additional implementations for the nested optimization

As previously stated, solving the nested WFLOP is computationally expensive. Several implementations were made to be able to reach convergence at the upper level within a reasonable amount of time (less than 72 h). These implementations are the following:

1. The lower level optimization problem is only solved if the upper level constraints are not violated. Otherwise, the static layout AEP is used as the dynamic layout AEP;
2. There are a total of 16 subproblems in the lower level that are solved in parallel using multiprocessing. Each subproblem corresponds with a specific wind direction;
3. CMA-ES is used as the upper level optimization algorithm, with the maximum number of iterations, 'maxiter', set to 300;
4. COBYLA is used as the lower level optimization algorithm, with the algorithm specific parameter 'rhubeg' (= initial variations to the design variables) set to 100 and 'maxiter' set to 300;
5. If, for a subproblem, COBYLA is unable to find a feasible solution within the 300 iterations, the static layout is used to determine the lower level function value for that subproblem.

The first implementation is a simple way to reduce computational time. The lower level optimization is only run for design variables that do not violate the constraints. Therefore, fewer lower level optimization problems are solved.

The second implementation is of great importance for the nested optimization. By solving the 16 subproblems in parallel instead of in sequence, the computational resources are better utilized. This implementation could also be used for the unrestricted or sequential optimization method.

The third implementation is to use a maximum number of iterations of 300. This number is based on the earlier mentioned minimum number of function evaluations (4,500) that were required for CMA-ES to converge for the static WFLOP (see Figure 3.6). A maximum number of iterations of 300 for the CMA-ES algorithm for 32 design variables, approximately equals 4,500 upper level function evaluations. Even though this is not a performance termination criterion and more iterations might give a better outcome, this implementation was still made to reduce the computational effort.

The fourth implementation is based on additional convergence studies performed for the IEA37 example layout for a movable range of $C = 2.0$ (see Appendix A). The lower level problem has to be solved for each upper level evaluation. There are many iterations required to solve the upper level problem (see third implementation). Therefore, to reduce the computational costs, the lower level problem must be solved quickly. With these settings for 'rhobeg' and 'maxiter', COBYLA is a quick-converging algorithm well suited for the lower level optimization problem.

The fifth implementation is made because COBYLA might not always find a feasible function value within 300 iterations. This occurred frequently, and more information is provided in Appendix A. Therefore, instead of accepting an infeasible function value as the optimum of the subproblem, the static layout is used to compute the function value for this subproblem. Due to the first implementation, this static layout is always feasible.

Wind farm layout of a selected movable range

Before presenting the resulting wind farm layout obtained by solving the nested WFLOP for $C = 2.0$, the convergence rate of the optimization is shown. Figure 3.13 depicts the convergence path of both the static and dynamic layout. Each generated static layout at the upper level that is feasible has a corresponding dynamic layout. It should be noted that the negative function value is the negative AEP value. In Section 2.4.4 it was mentioned that the static layout was evaluated based on its ability to generate an optimum dynamic wind farm layout, not on its ability to generate an optimum static layout. This can be clearly seen since the dynamic layout function value is decreasing while the static layout function value is not. The AEP value for the final static layout is 331.75 GWh, and the corresponding AEP value for the dynamic layout is 452.99 GWh. The optimization took around 2 days and 6 hours to complete on a laptop (8.0 GB ram) with an Intel Core i7-6700HQ Processor.

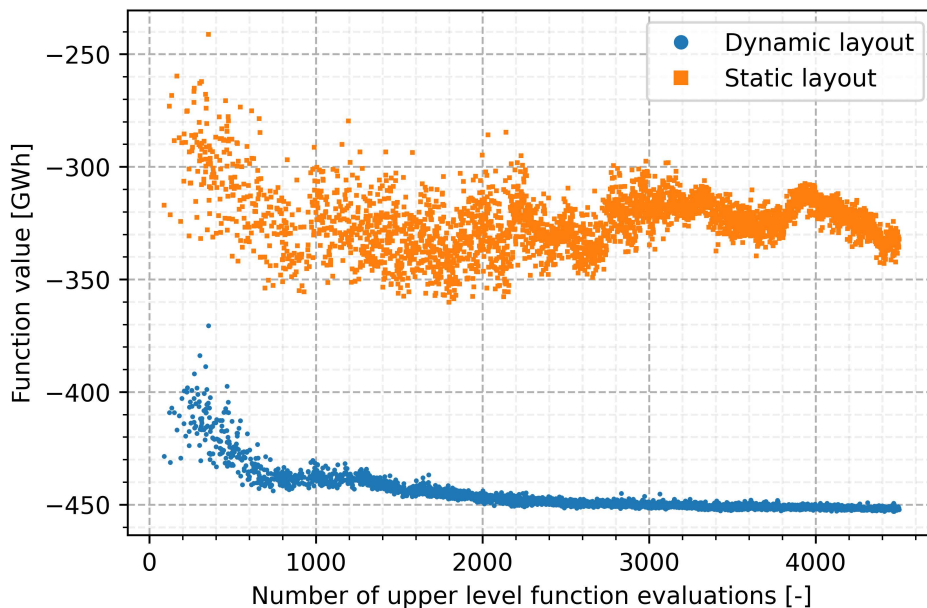


Figure 3.13: Convergence path of the feasible static layouts and their corresponding dynamic layouts, obtained by solving the nested WFLOP.

The final static layout that results in the best dynamic layout is illustrated in Figure 3.14. The observations that are made are the following:

- The wind turbines form clusters: almost all turbines have at least one wind turbine located closely;
- There are large open spaces in the wind farm where there is no turbine at all;
- Most wind turbines are near the wind farm boundary.

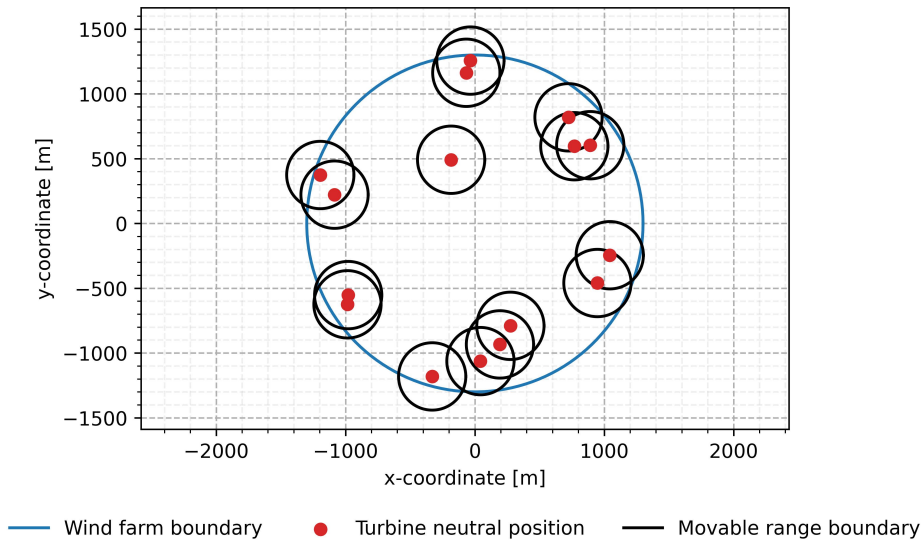


Figure 3.14: Final static wind farm layout obtained by solving the nested WFLOP.

Figure 3.15 demonstrates the dynamic layout for 4 of the 16 considered wind directions.

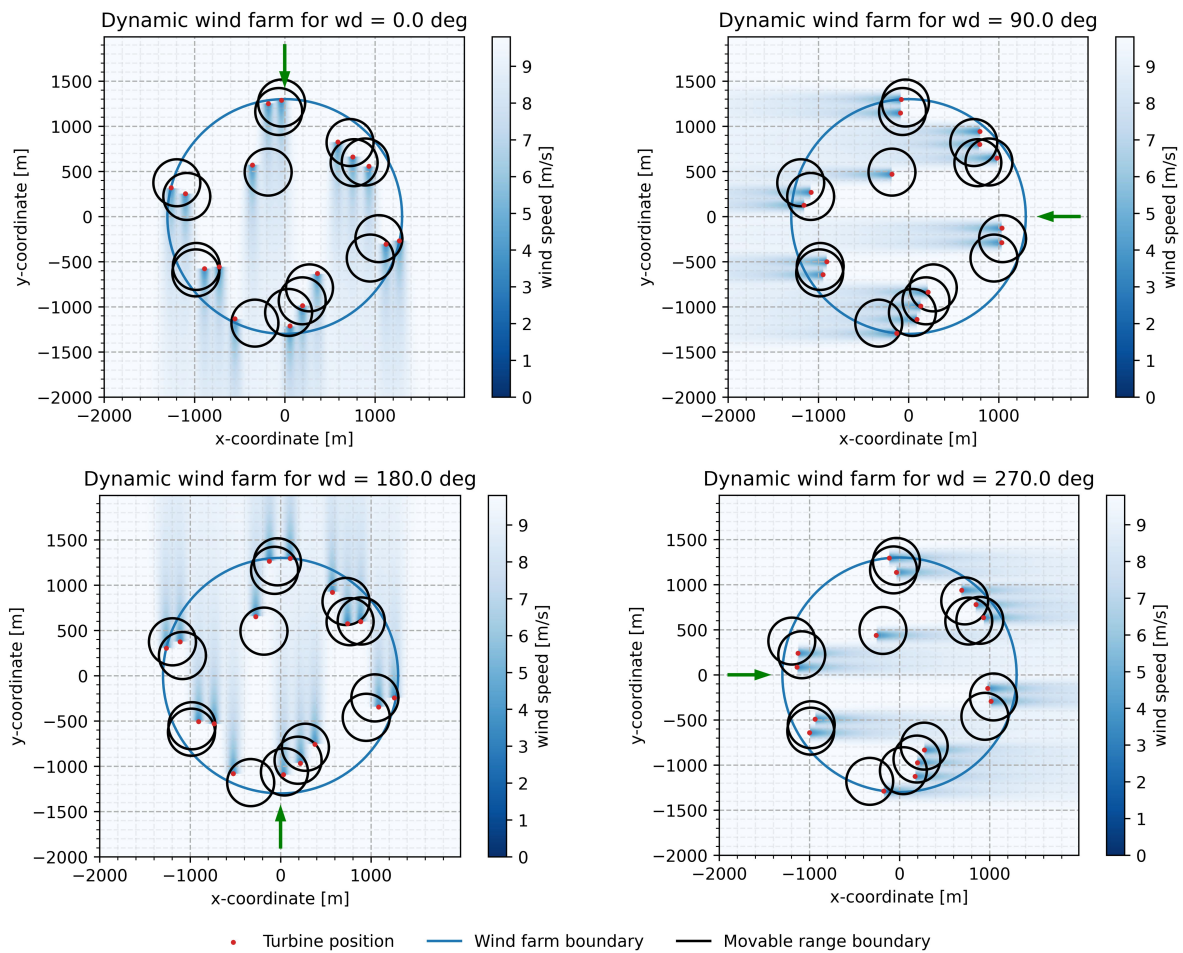


Figure 3.15: Optimized dynamic wind farm layout obtained by solving the nested WFLOP.

There are two observations that could be made:

- The wakes of the clusters do not interfere much with each other;
- Some turbines in these clusters align themselves in the crosswind direction. This same behaviour was seen in the unrestricted dynamic layout (see Figure 3.9).

Both observations are beneficial for the wake loss reduction and therefore the increase in the AEP of the dynamic layout.

3.4. Optimized dynamic wind layouts for three different static layouts

In this section, the dynamic layouts for three predefined static layouts are optimized: the IEA37 example layout (Figure 2.9); the static layout found by solving the sequential WFLOP (Figure 3.11); and the static layout found by solving the nested WFLOP (Figure 3.14).

3.4.1. Introduction to the optimization study

Up until now, the settings for the dynamic WFLO were compromised by the fact that multiple dynamic layouts needed to be optimized (for various movable range sizes in the case of the sequential optimization and for the lower level in the case of the nested optimization). The sequential and nested optimization are thus never run until a strict termination criterion is met, mainly due to the computational time. If a dynamic WFLO is only performed once, much stricter settings can be used since computational time is less of an issue. Therefore, the main reason for performing the optimization once is to determine what can be achieved with one good dynamic layout optimization.

3.4.2. Optimization approach

The dynamic layout is found by only solving the second step of the sequential WFLOP. The static layout is, thus, already established and supplied to the second step. The dynamic layout is optimized for three predefined static layouts:

1. IEA37 example layout (Figure 2.9);
2. Static layout found by solving the sequential WFLOP (Figure 3.11);
3. Static layout found by solving the nested WFLOP (Figure 3.14).

The optimization algorithm selected to solve the dynamic layout optimization is the trust-constr. All algorithm-specific settings are kept at their default values.

The choice of this algorithm is based on convergence studies performed on the IEA37 layout with four different algorithms (see Section A.1) for a movable range of $C = 2.0$. The trust-constr algorithm resulted in the best AEP value for the dynamic layout.

The following three subsections present the resulting dynamic layouts (for $C = 2.0$) for the three predefined static layouts. Hereafter, a comparison of the numerical results of this chapter for various dynamic layout optimizations will be given in Section 3.5.

3.4.3. Dynamic layout for IEA37 example layout

The dynamic layout for IEA37 example layout is presented in Figure 3.16. The resulting AEP value for the dynamic layout is 452.14 GWh. The observations that could be made are the following:

- The wind turbines are located at the boundaries of the movable range most of the time;
- No wind turbine is located in the part of another turbine's wake where the velocity deficit is most prevalent (dark blue).

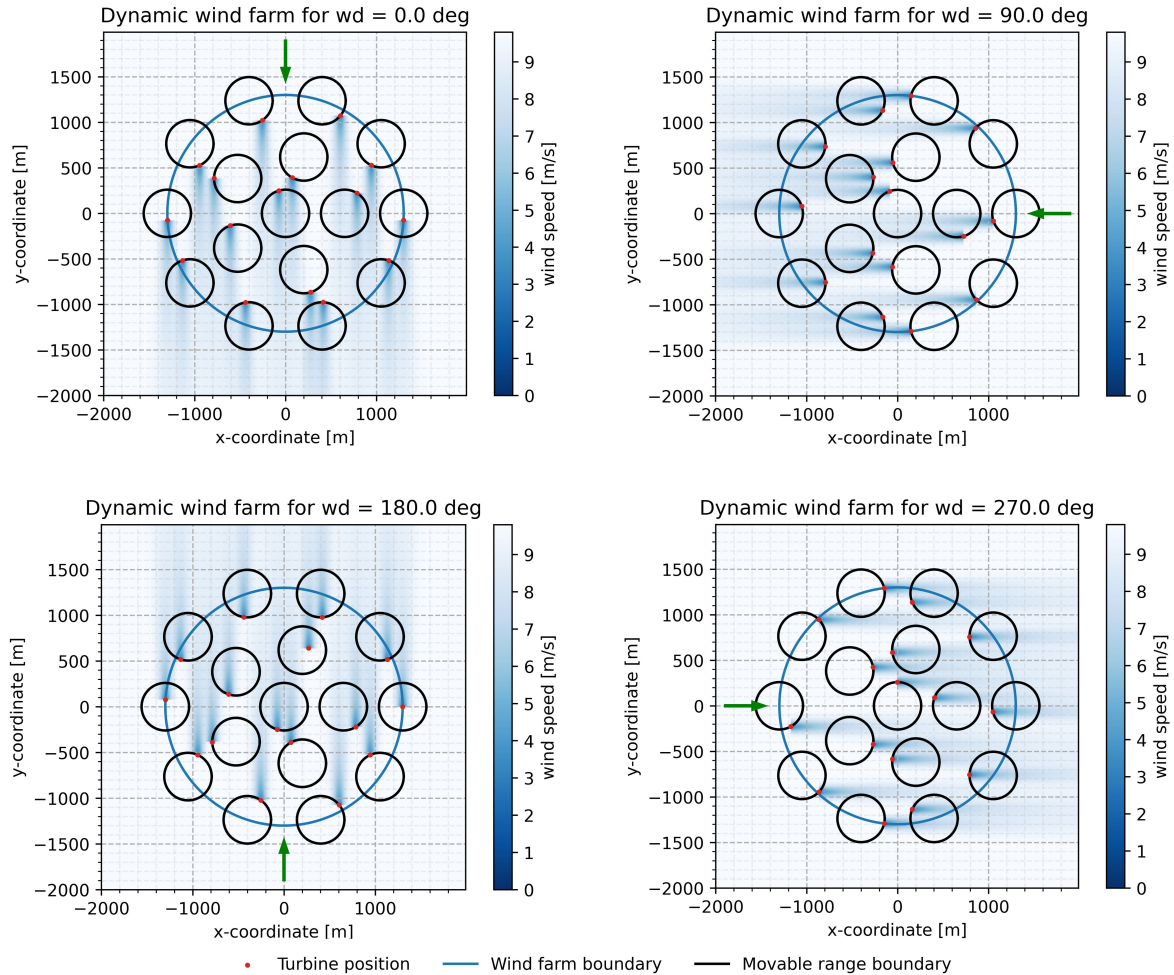


Figure 3.16: Optimized dynamic wind farm layout for the IEA 37 example layout.

3.4.4. Dynamic layout for sequential optimization static layout

The improved dynamic layout for the static layout found by solving the sequential WFLOP for $C = 2.0$ is shown in Figure 3.17. The AEP value for this improved dynamic layout is 454.62 GWh (it was 447.26 GWh). There are no additional observations made, besides that the dynamic layout is not the same as it was previously.

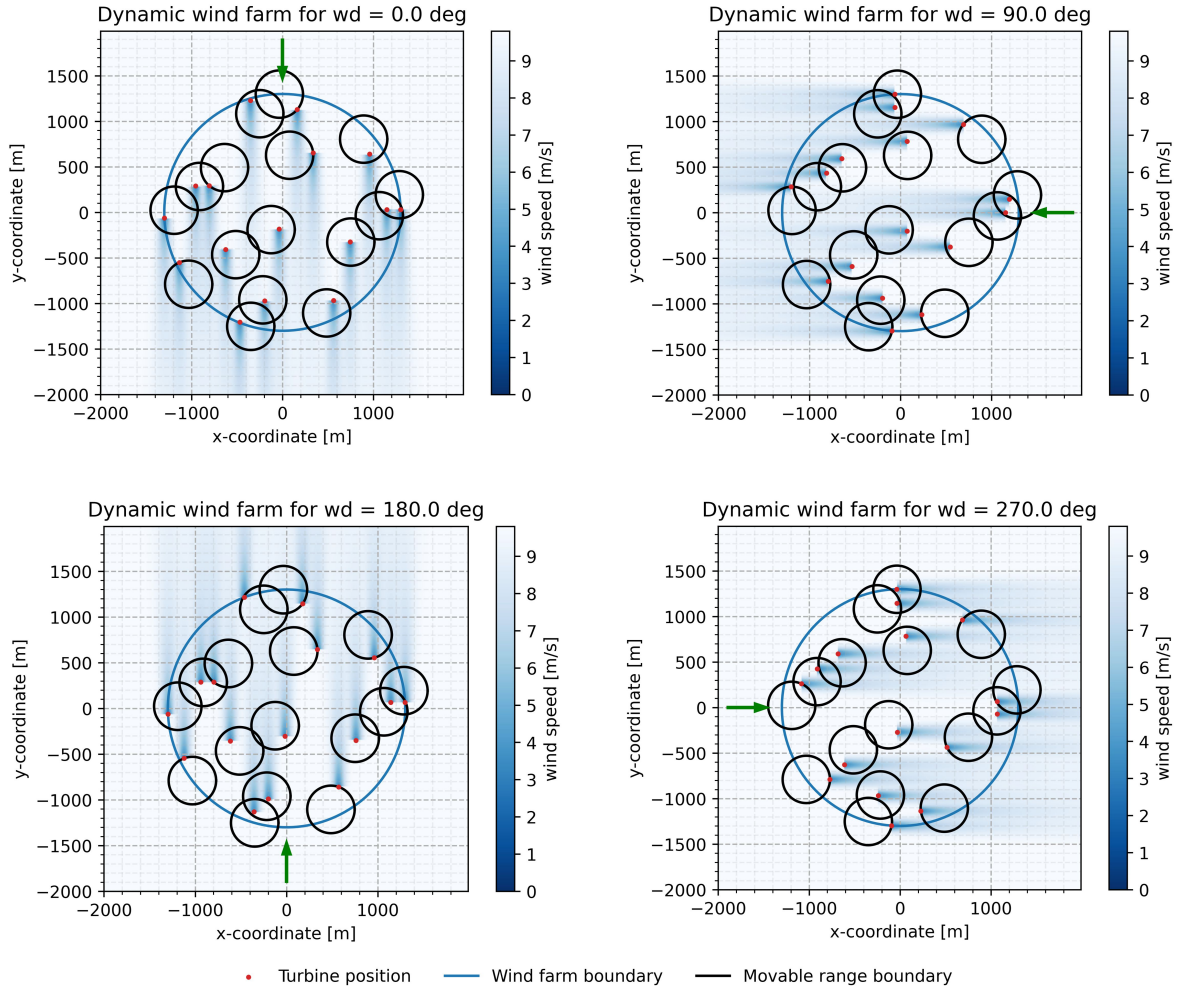


Figure 3.17: Optimized dynamic wind farm layout for the static layout obtained by solving the sequential WFLOP.

3.4.5. Dynamic layout for nested optimization static layout

The improved dynamic layout for the final static layout obtained by solving the nested WFLOP is displayed in Figure 3.18. The AEP for this dynamic layout did improve slightly to 456.34 GWh (it was 452.99 GWh). The improved dynamic layout did not change much from the final dynamic layout obtained by solving the nested WFLOP. Therefore, no additional observations are made for this dynamic layout.

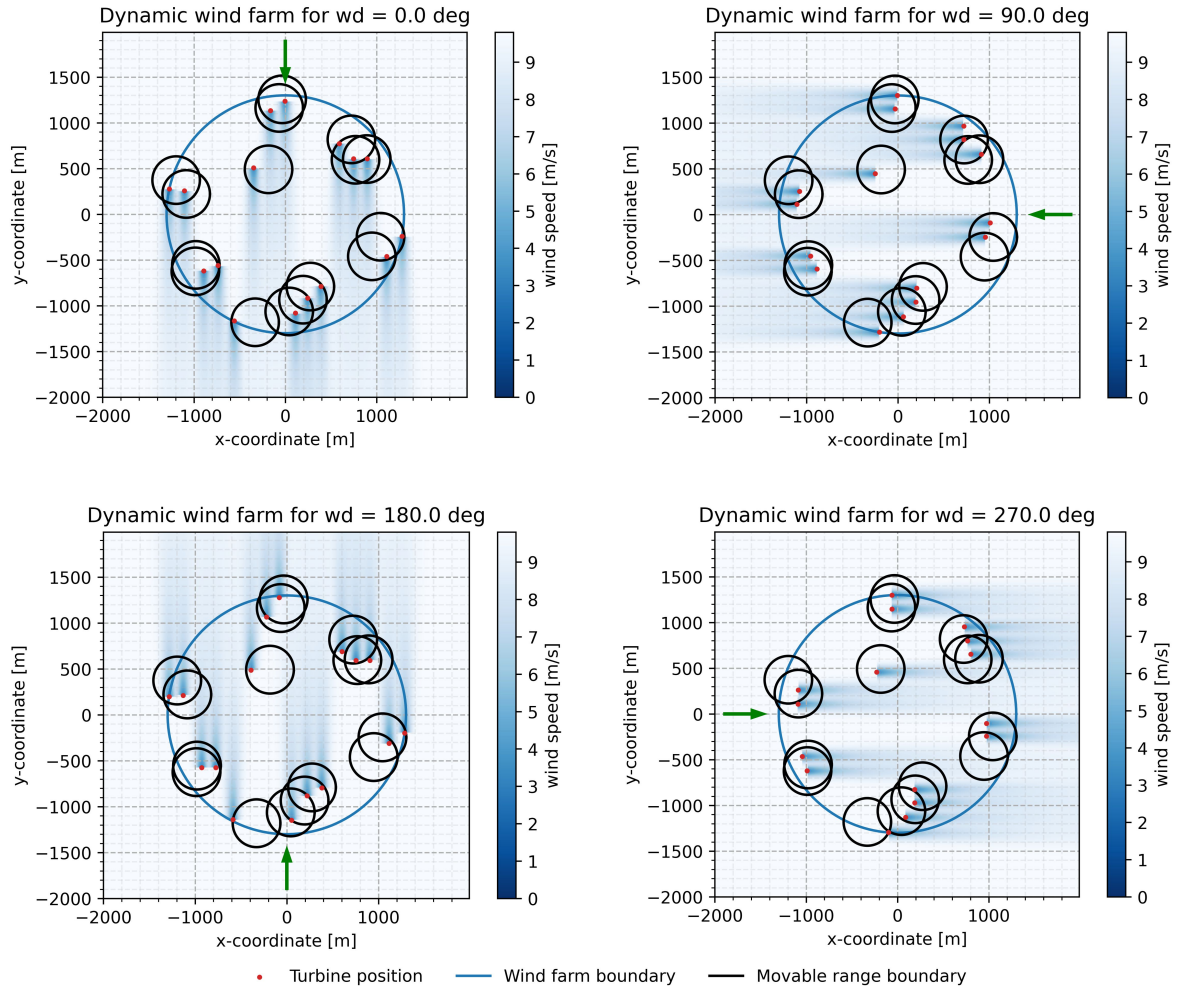


Figure 3.18: Optimized dynamic wind farm layout for the static layout obtained by solving the nested WFLOP.

3.5. Comparison of dynamic layout optimization results

The wind farm efficiency helps in comparing the various dynamic layout optimization results. Figure 3.19 shows the wind farm efficiency for the various optimization studies done in this work.

In Section 3.2, two reference optimizations are performed to provide a lower and upper bound for the dynamic layout optimization: static layout optimization and unrestricted dynamic layout optimization. It should be noted that in unrestricted optimization, the wind turbines can move anywhere in the wind farm and have an unlimited movable range. Therefore, the result of the unrestricted optimization is shown for $C = 20.0$, which also implies that the wind turbines can move anywhere in the wind farm.

In Section 3.3, dynamic layouts are optimized with two different methods: sequential and nested optimization.

In Section 3.4, a dynamic layout optimization is performed once for various static layouts: the IEA 37 example layout; the final static layout for the sequential optimization; and the final static layout for the nested optimization. The latter two can be recognized in the legend with the term “improved”.

From the optimized wind farm efficiencies, several observations can be made:

- The sequential optimization shows the potential of movable turbines for various movable ranges to improve the efficiency of a wind farm;
- Wind farm efficiency can be increased until around $C = 2.0$;
- The nested optimization finds a significantly better wind farm efficiency than the sequential optimization for $C = 2.0$;
- The unrestricted optimization finds a better wind farm efficiency than the sequential optimization for $C = 20.0$ (see Section 3.3.1 for the explanation);
- The results of performing dynamic layout optimization once for three predefined static layouts are close to each other and the nested optimization;
- For $C = 2.0$, the highest wind farm efficiency is found by running the dynamic layout optimization once for the static layout obtained from the nested optimization (Nested improved).

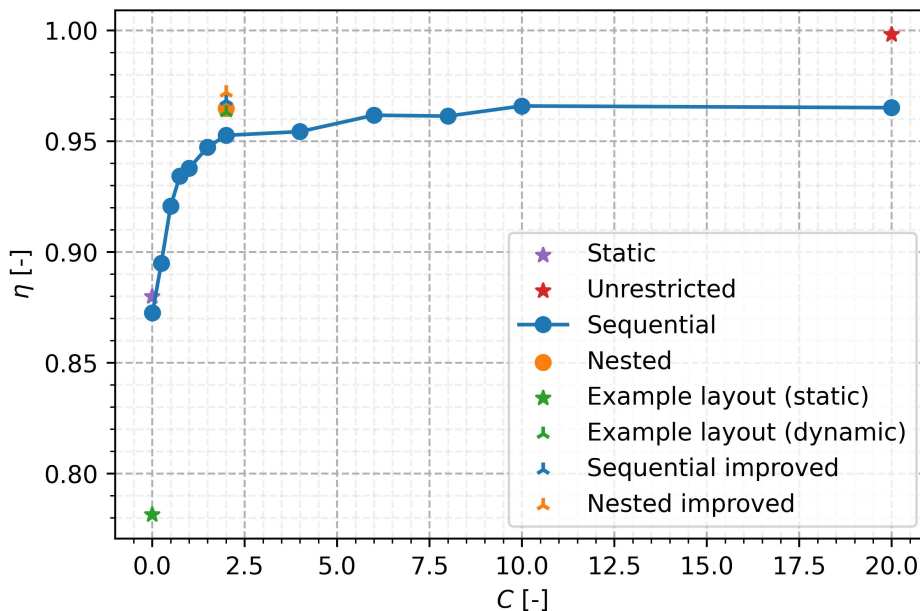


Figure 3.19: Wind farm efficiency for various dynamic layout optimization results.

3.6. Discussion

The important findings in this chapter are discussed and the limitations of the dynamic layout optimization studies are provided.

3.6.1. The interpretations and implications of key findings

The interpretations and implications of key findings for dynamic WFLO for AEP maximization are the following:

- When compared to static layouts, the AEP increases significantly with dynamic layouts.
 - From Figure 3.19, it becomes clear that movable turbines result in a significant increase in wind farm efficiency compared with fixed turbines. The best found layout after solving the static WFLOP resulted in a wind farm efficiency of 0.880. The best found static layout in literature for the same wind farm case study gives 0.892 (for 418.92 GWh) [47]. The best found wind farm efficiency for a movable range size of 2 rotor diameters is 0.972. The gains that can be achieved with dynamic layouts are thus evident when compared to static layouts.
 - Rodrigues et al. (2015) optimized a 6×6 wind farm layout for six different case scenarios [8]. The scenarios include different combinations of whether the installation locations are optimized or not, whether the turbines can move or not, and the number of degrees of freedom (0, 1, or 2). The largest gains in wind farm efficiency in terms of total power output were reported for case scenario 6, where the installation positions are optimized, the turbines can move, and the degrees of freedom are 2 (triangular movable range shape). Although they did not report the exact values, a plot of the wind farm efficiency for the different case scenarios is provided in Fig. 11 of their paper. From the plot, it becomes clear that case scenario 2, where only the installation position is optimized (no movability), has a similar wind farm efficiency as that of case scenario 6. The absolute difference in wind farm efficiency is around 1%. In other words, the static WFLO gave similar results to that of the dynamic WFLO, which is different from what was found in this Master's Thesis (see previous point).
 - The main difference between the results in this Master's Thesis and in the research conducted by Rodrigues et al. (2015), is in the wind farm efficiency obtained from solving the static WFLOP. The best found efficiency for the static layout optimization in this Thesis Project is 0.88, and the efficiency in Fig. 11 of Rodrigues et al. (2015) is a bit below 0.96. Therefore, there is more to gain with movable turbines in this Master's Thesis than in Rodrigues et al. (2015) [6].
 - When considering movable wind turbines in a wind farm, it is suggested to run a static layout optimization in conjunction with a dynamic layout optimization. This way, the results obtained from the dynamic layout optimization gain relevance.
- The nested optimization finds a slightly better dynamic layout than the sequential optimization.
 - When the AEP of the dynamic layout of the sequential optimization (447.26 GWh) is compared with the nested optimization (452.99 GWh), the computationally expensive method finds a slightly better AEP value. From a practical point of view, however, sequential optimization may be a better choice than nested optimization. It is less difficult to set up, less time-consuming, and provides similar results. More importantly, the sequential optimization results in a much better static layout (402.51 GWh) than the nested optimization (331.75 GWh). To reduce risks, it may be best to have both a high AEP value for the static layout and a high AEP value for the dynamic layout.
- For movable turbines, the crosswind component of the displacement has much more impact on the AEP than the downwind component.
 - Figure 3.10 demonstrates that the steepest gains in wind farm efficiency can be obtained up to a movable range of around $C = 2.0$ (the wind turbine can move a distance of 2 rotor diameters in each direction from its neutral position). It is presumed that steep gains are mainly due to the turbine's ability to move in the crosswind direction. After a certain movable range, it is assumed that the largest gains by moving in the crosswind direction have been achieved. Hereafter, the remaining gains are mostly achieved by the ability to shift in the

downwind direction. The ability to shift in the crosswind direction has more of an impact on the power output than in the downwind direction. This has been shown as well by Saadallah and Randeberg (2020) for a two-turbine case scenario [84].

- All dynamic layouts, in Section 3.4, share the same feature as the unrestricted layout: there is no turbine in the part of the wake where the wind speed deficit is greatest. Due to similar crosswind distances between the turbines, it is ensured that no turbine is directly behind another turbine. From this, it becomes clear that the most crucial ability of movable FOWTs is the ability to shift in the crosswind direction.
- For a large movable range, a dynamic layout is almost unaffected by where the turbines are installed.
 - The dynamic layouts for the three different static layouts in Section 3.4, have very similar AEP values. This is not entirely as expected, since one of the static layouts (example layout) used in the study is based on simple spacing rules. The other two layouts were obtained with sequential and nested optimizations. These are more sophisticated methods and were thus expected to result in better dynamic layouts. Therefore, it is argued that for a movable range size of two rotor diameters, turbine relocation is so effective at increasing the AEP that the installation position almost does not matter.
 - It is expected that for smaller movable range sizes, it is less likely that the example layout gives similar results as the static layouts found by solving the sequential and nested optimization problems. Put differently, it is expected that the larger the movable range size, the less the installation position matters for dynamic layout optimization.

3.6.2. Limitations

The limitation of dynamic WFLO for AEP maximization is the following:

- An assumption made in dynamic WFLO is that the wind farm layout changes instantaneously for a different wind direction.
 - As a result, there are no losses due to the time required to switch between layouts or the frequency with which layouts are adjusted. In practice, however, there will be losses. It takes time to establish a new layout, and the layout is not necessarily always in motion.

4

Repositioning mechanism for a movable floating offshore wind turbine

In this chapter, mechanisms for relocating a floating offshore wind turbine are explored. The chapter begins with the formulation of two objectives for a repositioning mechanism (Section 4.1). It then describes and compares several repositioning mechanisms that could achieve these objectives, before selecting one (Section 4.2). Hereafter, the selected repositioning mechanism is further characterized (Section 4.3). Lastly, a novel method is proposed to assess the movability and station-keeping performance of the selected repositioning mechanism and is evaluated through a case study (Section 4.4). Finally, a discussion is included of the important results and the limitations of the study (Section 4.5).

4.1. Repositioning mechanism objectives

The goal of a repositioning mechanism for a movable FOWT is to decrease the wake losses in a wind farm so that the AEP is increased. To accomplish this goal, two objectives are formulated for the repositioning mechanism:

1. To move the wind turbine to the desired position;
2. To keep the wind turbine in the desired position.

In the next section, several repositioning mechanisms are described that could achieve these objectives.

4.2. Description, comparison, and selection of repositioning mechanism(s)

In this section, four different repositioning mechanisms that have previously been proposed in the floating wind and offshore/marine industries are described and compared. Then, one mechanism is selected to be further characterized.

4.2.1. Description of four different repositioning mechanisms

In this Master's Thesis, a total of four different repositioning mechanisms have been considered:

1. Yaw and Induction-based Turbine Repositioning (YITuR);
2. Position Mooring (PM) with mooring line length adjustment capability;
3. Thruster Assisted Position Mooring (TAPM);
4. Dynamic Positioning (DP).

Figure 4.1 illustrates the four different repositioning mechanisms for a floating offshore wind turbine. It must be noted that YITuR and PM with line length adjustment capability (subsequently just referred to as PM) are previously proposed mechanisms for movable FOWTs [6, 85]. The other two concepts, TAPM and DP, have not been considered for FOWTs yet. Although the use of thrusters to reposition wind turbines has been mentioned in the literature [29, 85].

Other hybrid options may be considered as well, such as YITuR and PM with mooring line length adjustment capability; TAPM with mooring line length adjustment capability [86, 87]; YITuR and DP. These options, however, are not considered in this Master's Thesis, but may be further explored in the future.

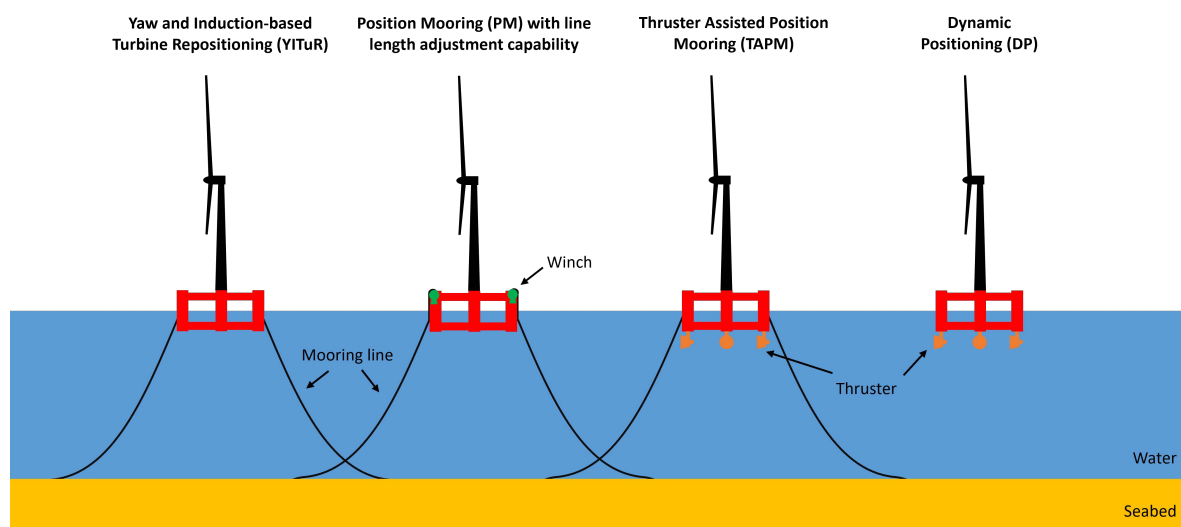


Figure 4.1: Four different repositioning mechanisms for a movable floating offshore wind turbine.

The main idea of YITuR is to adapt the magnitude and direction of the aerodynamic thrust force on the rotor by varying the nacelle yaw angle and the axial induction factor [85, 88]. By adjusting the thrust force, a change in the FOWT position can be realized. The wind turbine must be in a new equilibrium position. This equilibrium is achieved by a force balance between the mooring line tensions and the thrust force. Since YITuR uses actuators that are already present in the wind turbine, no extra components are required.

Position mooring maintains the location of a floating structure or unit [89, 90]. In this Master's Thesis, the main concept underlying PM is to vary the length of the mooring lines through winches. The change in line length results in an imbalance of the mooring line tensions, which causes a displacement of the wind turbine. The mooring line lengths can thus be changed in such a way that a new equilibrium

position is achieved for the FOWT. This concept was assumed by Rodrigues et al. (2015) to achieve mobility of FOWTs in a wind farm [6]. In their work, the repositioning mechanism consists of taut mooring lines, at one end attached to the seabed and at the other end to a winch. Similar mechanisms have been assumed in other applications than FOWTs, but then with catenary mooring lines [91–94]. There are alternative technologies to adjust the mooring line length other than a winch, such as a chain jack and an in-line tensioner [95]. In this Master's Thesis, only winches are considered, due to their speed and continuous operation capability in both haul-in/pull-in (when line length gets shorter) and pay-out (when line length gets longer).

In this work, a mooring system that is assisted by one or more thrusters is referred to as TAPM. The main responsibilities for a TAPM system in other applications are to decrease mooring line tensions, keep position and/or heading, reduce oscillatory motions, and account for imbalances if a mooring line failure occurs [90]. The class notation for this kind of system is named POSMOOR (ATA) by Det Norske Veritas (DNV).

For TAPM, the station-keeping is predominantly provided by the restoring forces of the mooring lines [96]. The mooring system has to oppose the mean components of the environmental forces [97]. Thrusters complement the mooring system, especially in harsh environmental conditions [98, 99]. They aid in lowering mooring line tensions and vessel/unit displacements [100]. For a mobile FOWT, thrusters are the means to move the turbine to desired locations.

Dynamic positioning allows a vessel/unit to automatically keep a position and/or heading by only using its thrusters [101]. There is thus no mooring system, contrary to TAPM. DP systems are usually used in low-speed operations, where the objective is to remain at a certain location or to slowly follow a predefined track [102]. Both functionalities are of great importance when considering a movable FOWT.

4.2.2. Comparison and selection of repositioning mechanism(s)

In Table 4.1, the advantages and disadvantages of each repositioning mechanism, as well as their main means of mobility and station-keeping, are presented.

Method	Mobility	Station-keeping	Advantages	Disadvantages
YITuR	<ul style="list-style-type: none"> Aerodynamic thrust force 	<ul style="list-style-type: none"> Mooring line restoring force 	<ul style="list-style-type: none"> No/minor additional capital costs No additional components 	<ul style="list-style-type: none"> Small movable range Requires slack mooring lines Movable range dependent on wind speed Works against mooring line restoring force
PM	<ul style="list-style-type: none"> Mooring line tension 	<ul style="list-style-type: none"> Mooring line restoring force 	<ul style="list-style-type: none"> Energy efficient Large movable range 	<ul style="list-style-type: none"> Increased capital cost Increased O&M cost
TAPM	<ul style="list-style-type: none"> Thruster force 	<ul style="list-style-type: none"> Mooring line restoring force 	<ul style="list-style-type: none"> Proven technology Maintains position accurately Less energy required compared with DP 	<ul style="list-style-type: none"> Increased capital cost Increased O&M cost Small movable range Requires slack mooring lines Constant power consumption Works against mooring line restoring force
DP	<ul style="list-style-type: none"> Thruster force 	<ul style="list-style-type: none"> Thruster force 	<ul style="list-style-type: none"> Proven technology No installation required Unlimited movable range Operable in deep waters 	<ul style="list-style-type: none"> Increased capital cost Increased O&M cost Higher risk Constant power consumption Has to actively oppose the environmental loads

Table 4.1: Comparison of four different repositioning mechanisms for a movable floating offshore wind turbine.

The selection of a repositioning mechanism mainly depends on the ability to achieve the objectives described in Section 4.1. Even though all mechanisms could, in theory, move to and keep a desired position, PM is the only mechanism that is not working against either the restoring forces of the mooring lines (as do YITuR or TAPM) or the environmental loads (as does DP). This allows the mobile FOWT to move to further positions compared to YITuR or TAPM and to maintain these positions more cost-effectively compared to DP. Therefore, PM is selected to be further characterized next.

4.3. Characteristics of position mooring

In this section, the working principles of position mooring are illustrated and described in more detail. Furthermore, an example of a position mooring system is provided, and its main components are briefly described.

4.3.1. Turbine repositioning using position mooring

The PM system needs to move (objective 1) and keep (objective 2) the floating offshore wind turbine at the desired position (see Section 4.1 for the objectives of a repositioning mechanism). Position mooring has a distinct approach to achieving each objective. Using mooring lines to keep a floating structure on station is a well-known method. Therefore, it is chosen to only illustrate and describe the approach to achieving mobility in more detail. Readers interested in learning more about station-keeping with mooring lines should consult Ma et al. (2019), Chakrabarti (2005), and/or Faltinsen (1993) [103–105].

Figure 4.2 illustrates the PM system for a movable turbine. By altering the mooring line lengths, the turbine moves from its neutral position to a new equilibrium position. For this movement, line A has to increase in length while line B has to decrease in length. The increase in length is done by paying-out extra mooring line (there is extra mooring line on-board), and the decrease in length is done by pulling-in mooring line (storage of mooring line is possible on-board). Each mooring line is attached to a winch (in green), which is responsible for the pay-out or pull-in of the mooring line. The length of the mooring lines determines how much the wind turbine moves; the more line A is increased in length and line B is decreased in length, the more the turbine moves to the right. The movement happens because the change in mooring line lengths causes a change in mooring line tension. This results in an imbalance in the forces acting on the system. To compensate for this imbalance, the turbine is displaced until the line tensions reach an equilibrium point. Hence, the wind turbine is repositioned.

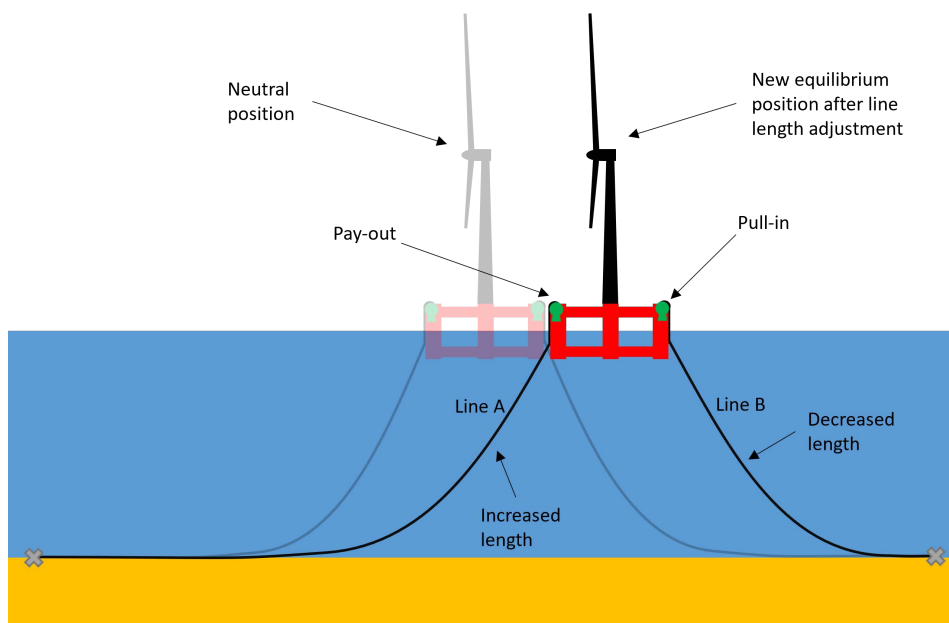


Figure 4.2: Position mooring repositioning mechanism concept for a movable floating offshore wind turbine.

4.3.2. Example position mooring system and its main components

It is important to mention that there is no prior methodology on how to design a PM system for a movable floating offshore wind turbine. The body of research on mooring line tensioning equipment is limited as well [95]. Furthermore, there are many design choices that could be made, such as: mooring configuration; mooring line number; mooring line type; mooring line length; mooring tensioning system; mooring line storage; anchor placement; anchor type; floating platform layout. Besides that, the design is also project location dependent (water depth, environmental conditions, regulations, etc.). Therefore, in this work, the PM system is limited to a basic example design that could realize the movability and

station-keeping of a FOWT.

In Figure 4.3, a basic position mooring design is illustrated together with its main components. The design is inspired by the works of Rodrigues et al. (2015), Zhao et al. (2015), Ma et al. (2019), and Wu et al. (2018) [6, 91, 95, 103]. Starting from the seabed, the anchor can be noticed. The anchor is attached to the mooring line and is responsible for fixing it to the seabed. The catenary mooring lines keep the FOWT on station, and are directed via the fairlead to the winch. The winch is responsible for the pull-in and pay-out of the mooring line, which changes the tensions in the mooring lines required to move the FOWT. The mooring lines can be stored in a chain locker, which has excess mooring lines necessary for the pay-out. It should be noted that there are other options for the anchor, mooring line type, actuator, and line storage that could be considered. The design serves as an example of what a position mooring system for a movable FOWT could look like.

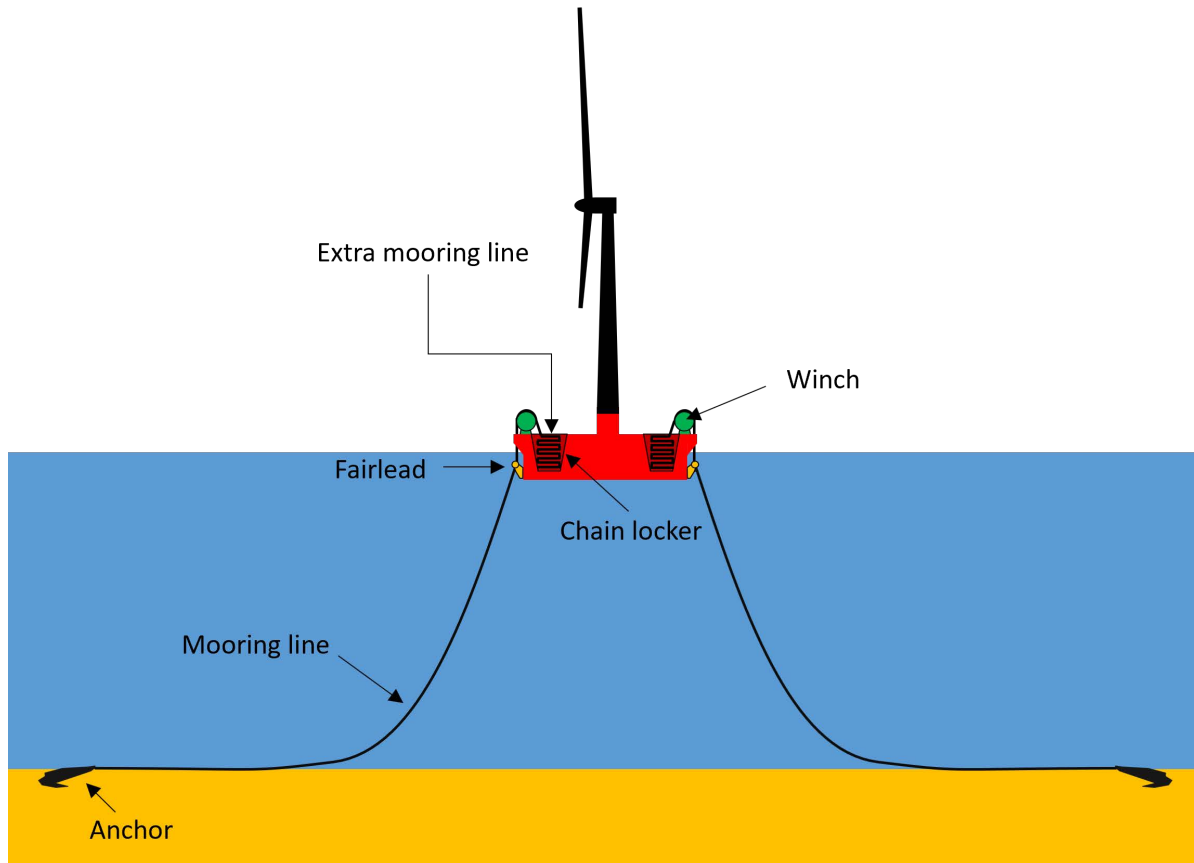


Figure 4.3: Example position mooring system and its main components for a movable floating offshore wind turbine.

4.4. Position mooring performance

A novel method is proposed to assess performance of a position mooring system, which is evaluated with a case study.



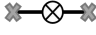

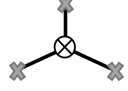

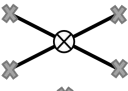


4.4.1. Introduction to position mooring performance assessment

It is important to refer once again to the objectives of a repositioning mechanism: to move and keep the wind turbine at its desired position (see Section 4.1). When the wind turbine neutral position (installation position) and anchor locations are defined, the movable range shape is established. Once the movable range shape is known, it is possible to determine whether the turbine can move and stay anywhere within that range by position mooring.

The movable range shape is directly influenced by the mooring configuration of the FOWT. The mooring configuration also influences the size of the movable range shape. Moving the mooring line anchors

further away expands the movable range size.

In Figure 4.4, various movable range shapes are shown, together with the possible mooring configurations that could allow for such a shape. Out of these movable range shapes, the triangular might be the most probable shape. The reason for this is that many proposed mooring systems in offshore floating wind consist of three mooring lines [103, 106]. However, to increase the redundancy of the mooring systems, more mooring lines could be added. The problem with a low number of mooring lines is that the mooring system might not be able to maintain its station keeping performance once a mooring line fails. According to Campanile et al. (2018), large horizontal offsets on the floater may occur for a mooring system configuration consisting of three mooring lines if one of the mooring lines fails [106]. If a more redundant system is chosen, which includes more mooring lines, the movable range shape comes close to a circular shape.

Motion	Movable range shape	Mooring configuration
Stationary	none	
Linear		
Planar (triangular)		
Planar (rectangular)		
Planar (circular)		




 Wind turbine
 Anchor
 Mooring line

Figure 4.4: Movable range shapes for mobile floating offshore wind turbines for various mooring configurations.

4.4.2. Methodology for position mooring performance assessment

A novel methodology is proposed to assess the mobility and station-keeping performance of position mooring for a FOWT. For this method, it is presumed that the wind turbine neutral position, the anchor positions, and the floater geometry are known in advance. As already mentioned in Section 4.4.1, the neutral position and anchor positions determine the movable range shape. These positions can, for example, be obtained by solving a dynamic WFLOP.

To investigate whether the assumed movable range is the actual movable range, different positions inside the range have to be studied. These positions are referred to as the desired turbine locations. The goal is to determine whether a force equilibrium can be reached at these desired positions by adjusting the mooring line lengths. In this way, it can be assessed whether the wind turbine can be moved to these different locations by position mooring. Figure 4.5 shows the relevant definitions required to assess position mooring.

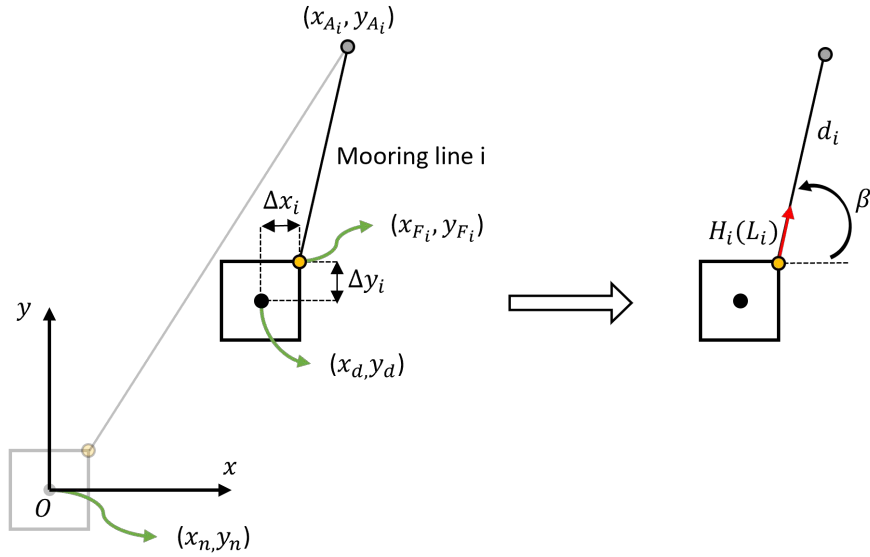


Figure 4.5: Required definitions for a floater (represented by a square) to assess position mooring (top view).

The illustration has two parts. In the left part, the important positions of the moored floater are defined, and in the right part, the necessary definitions to determine the horizontal (xy -plane) forces are provided. It should be noted that the floater is in the shape of a rectangle for illustration purposes only. Any other shape could be used as well.

In the left part:

- x_n and y_n are the floater neutral coordinates;
- x_d and y_d are the floater desired coordinates;
- x_{F_i} and y_{F_i} are the fairlead coordinates;
- x_{A_i} and y_{A_i} are the mooring line anchor coordinates;
- Δx_i and Δy_i are the distances from floater centre to the fairlead;
- i is the mooring line number.

In the right part:

- L_i is the total mooring line length from fairlead to anchor;
- $H_i(L_i)$ is the horizontal component of the mooring line tension at the fairlead as a function of the mooring line length;
- d_i is the horizontal distance (xy -plane) from fairlead to anchor;
- β_i is the mooring line orientation.

As stated already, the neutral and anchor positions are known in advance and are thus fixed, whereas the desired floater position can be freely chosen. This desired position, however, can be defined beforehand as well. In other words, based on the movable range shape, different desired positions could be selected beforehand for which the performance is assessed. It is assumed for these desired positions that there is no change in the yaw angle (rotation around z -axis) for the floater. Now that all positions are fixed or defined in advance, it is possible to calculate d_i and β_i (using geometry).

The horizontal distance from fairlead to anchor can be determined as follows:

$$d_i = \sqrt{(x_{F_i} - x_{A_i})^2 + (y_{F_i} - y_{A_i})^2}, \quad (4.1)$$

where x_{F_i} and y_{F_i} are given by:

$$x_{F_i} = x_d + \Delta x_i \quad (4.2)$$

$$y_{F_i} = y_d + \Delta y_i. \quad (4.3)$$

Therefore, we can write:

$$d_i = \sqrt{(x_d + \Delta x_i - x_{A_i})^2 + (y_d + \Delta y_i - y_{A_i})^2}. \quad (4.4)$$

The mooring line orientation can be computed with the following function:

$$\beta_i = \arctan2((y_{A_i} - y_{F_i}), (x_{A_i} - x_{F_i})). \quad (4.5)$$

The only free variable left is the mooring line length (L_i). By varying this length, the horizontal component of the mooring line tension (H_i) can be altered. Figure 4.6 shows a single catenary mooring, which includes L_i and H_i .

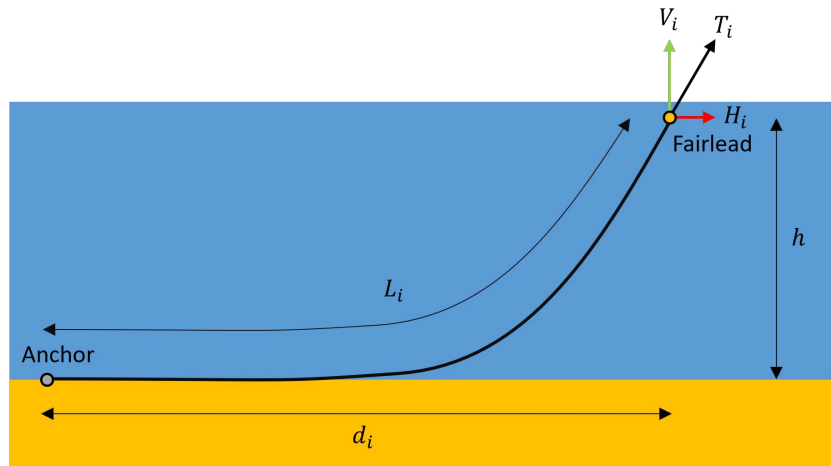


Figure 4.6: Illustration of a single catenary mooring line.

In this illustration, the following is known already:

- Anchor coordinates;
- Fairlead coordinates;
- Horizontal distance from fairlead to anchor (d_i);
- Vertical distance from fairlead to seabed (h).

After determining the mooring line properties and ignoring the environmental loads (i.e., wind, wave, current, ice, and marine growth), the horizontal tension (H_i) for a given mooring line length (L_i) can be calculated using a catenary mooring line model [103].

The horizontal tension has a force component in the x - and y -direction (see Figure 4.5), which can be calculated as follows:

$$H_{i,x} = H_i(L_i) \cos \beta_i \quad (4.6)$$

$$H_{i,y} = H_i(L_i) \sin \beta_i. \quad (4.7)$$

Now that these two components of the mooring line tension can be calculated, it becomes possible to search for a force equilibrium of the system. The following optimization problem is defined to obtain an equilibrium at the desired wind turbine position:

$$\begin{aligned}
& \text{minimize} && |\sum_{i=1}^{n_{ml}} H_{i,x}(L_i)| + |\sum_{i=1}^{n_{ml}} H_{i,y}(L_i)| \\
& \text{by varying} && L_{\min}(d_i) \leq L_i \leq L_{\max}(d_i) \\
& \text{subject to} && H_{\min} - H_i(L_i) \leq 0,
\end{aligned} \tag{4.8}$$

where:

- n_{ml} is the number of mooring lines;
- L_{\min} is the minimum mooring line length;
- L_{\max} is the maximum mooring line length;
- H_{\min} is the minimum horizontal mooring line tension at the fairlead.

The main goal of the optimization is to minimize the resultant forces in the x - and y -direction by varying the mooring line length, subject to a minimum horizontal tension.

The horizontal distance from fairlead to anchor (d_i) determines both the minimum and maximum mooring line length. The maximum length is simply the length when the mooring line is fully slack (i.e., $d_i + h$). The minimum length could be set as the length of a taut mooring line (i.e., $\sqrt{d_i^2 + h^2}$). In this case, there will be a vertical load at the anchor. This, however, is not allowed [104]. Therefore, the minimum line length must be defined such that there is no vertical load at the anchor. This could be done either by simply decreasing the line length and checking whether there is a vertical anchor load or by solving a constraint optimization problem where the line length is minimized while constraining the vertical anchor load. These efforts to determine L_{\min} and L_{\max} are important in order to avoid an ill-defined problem.

The inequality constraint is necessary to avoid obtaining a solution where all mooring lines are slack. In this case, there is no horizontal tension in the mooring lines and the displacement for external forces will be large, which is undesirable. Therefore, a minimum line tension is required. The same value is assumed for H_{\min} as the horizontal component of the pretension in the mooring line when the floater is in its neutral position. The pretension value is typically 0.1 to 0.2 times the line breaking strength [103].

After having solved the Equation 4.8, it may be the case that an equilibrium is found (objective function is zero) or that there is still some imbalance in the system (objective function is non-zero). For the latter, a static equilibrium can be solved to find the actual floater position for the obtained mooring line lengths. For this, the goal is to find the floater position that gives a force equilibrium (net-zero forces). The desired floater position is not reached in this case, but the actual position may still be close to the desired position.

If the optimization problem is solved for multiple desired locations, a contour map spanning the whole movable range could be made to show the error in the desired position (distance between desired and actual positions). The larger the error, the more difficult it is to achieve equilibrium at the desired positions. That makes it possible to assess the movability performance of position mooring for the whole movable range. Additionally, the station-keeping performance can be assessed through the evaluation of the mooring stiffness (force-displacement relationship) per equilibrium position.

It should be noted that for this methodology, several assumptions have been made regarding the position mooring system:

- The tensioning system on the floater is able to pull-in and pay-out the mooring line. In other words, the on-board mechanism can provide the force needed to move the turbine;
- The excess mooring lines can be stored on the floater;
- There is enough extra mooring line on board to reach any position in the movable range;
- The mooring line is fixed to the anchor at one end and to the fairlead at the other end;
- The mooring line follows a straight path from fairlead to anchor. In other words, d_i is a straight line;
- The dynamic power cable (required to export power) is of sufficient length.

4.4.3. Case study: UMaine VoltturnUS-S floater for IEA 15MW turbine

The methodology described in Section 4.4.2 to assess the movability and station-keeping performance of position mooring is evaluated through a case study.

UMaine VoltturnUS-S floater for IEA 15MW turbine

Recently, a 15MW offshore reference wind turbine was designed, which is freely accessible to the public [107]. The reference wind turbine emulates the increasing wind turbine sizes and rated power outputs in the wind energy sector. Not long after, efforts were made to design a reference floater, referred to as UMaine VoltturnUS-S, to support the IEA 15MW turbine [108]. The reference floater is of particular interest for the case study, because it includes a full description of a catenary mooring system.

Figure 4.7 shows illustrations of the floater, including the wind turbine. The mooring system consists of three catenary mooring lines (one line every 120 degrees), with a line length (L_i) of 850 m. The vertical distance from fairlead to anchor (h) is 186 m, and the horizontal distance (d_i) is 779.6 m. For other mooring system characteristics, the reader is referred to Table 6 in Allen et al. (2020) [108].

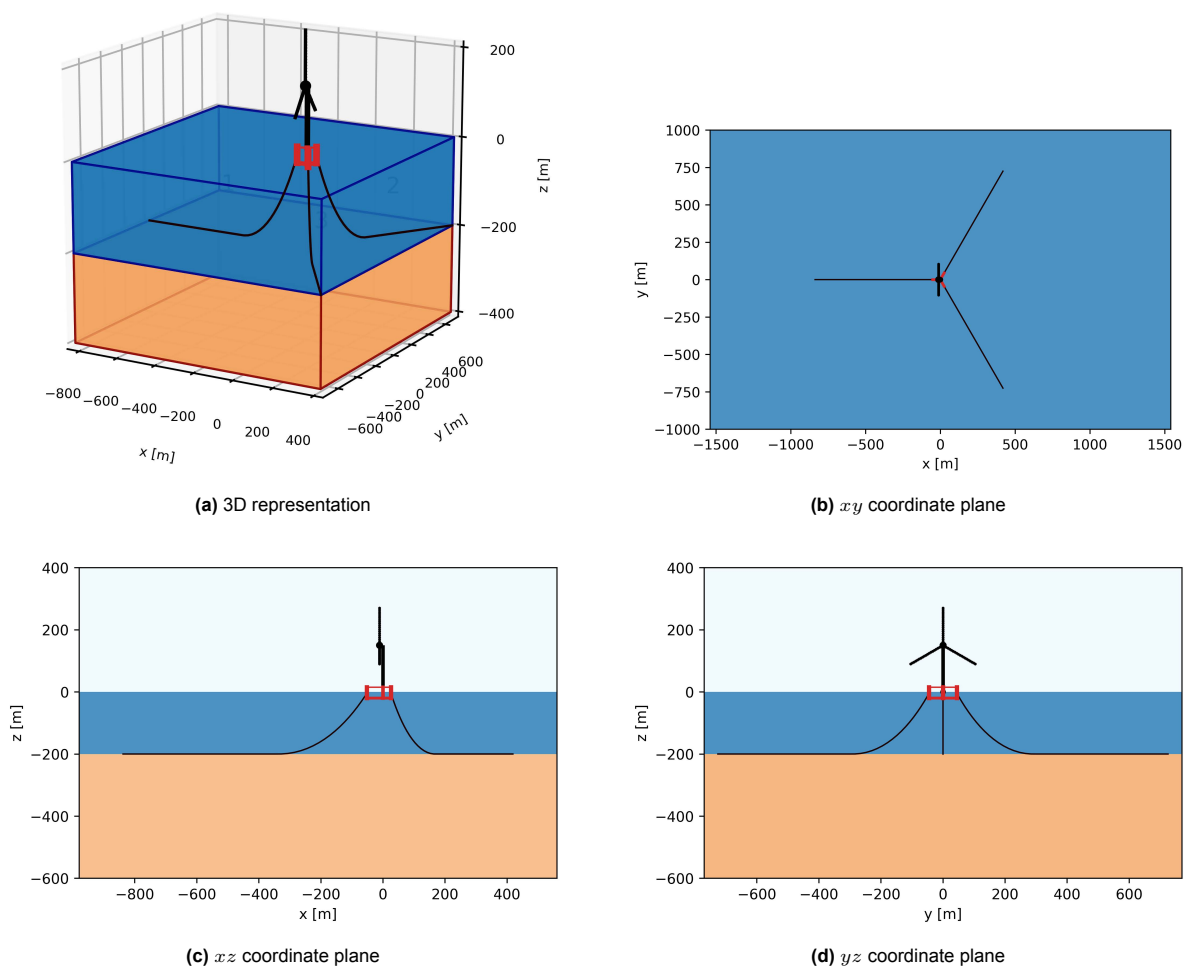


Figure 4.7: Illustrations of the UMaine VoltturnUS-S floater for the IEA 15MW turbine.

Quasi-static mooring analysis using MoorPy

In Section 4.4.2, it was mentioned that once the coordinates, distances, and mooring line properties are defined or known, and the environmental loads are ignored, the horizontal tension (H_i) at the fairlead can be calculated for a given mooring line length (L_i). This can be achieved with a mooring line model.

MoorPy is a model capable of performing quasi-static mooring analysis for moored structures [109]. It is a freely available tool implemented in Python.

MoorPy is used in this Master's Thesis to obtain H_i as a function of L_i in order to solve the optimization problem defined in Equation 4.8. If the optimization is finished and no equilibrium is found (resultant forces are non-zero), the obtained mooring line lengths are used to find an equilibrium state for the system with MoorPy.

The MoorPy model is set up with the UMaine VoltturnUS-S floater for the IEA 15MW turbine. Due to the fact that all mooring system characteristics are known, together with that the pretension and fairlead angle from still water level are provided by Allen et al. (2020) [108], it is possible to verify the model. This fairlead angle is the same as the angle between tension (T_i) and its horizontal component (H_i) at the fairlead.

The results from MoorPy for the UMaine VoltturnUS-S floater's mooring system are:

- Fairlead angle is 56.3511 degrees;
- Fairlead pretension is 2.4364 MN;
- Vertical component of fairlead pretension is 2.0282 MN;
- Horizontal component of fairlead pretension is 1.3500 MN.

As stated already, both the fairlead angle and pretension are known for the floater [108]. The reported fairlead pretension is 2.437 MN and the reported fairlead angle is 56.4 degrees. Very similar results are obtained with the MoorPy model.

Case study methodology implementation

The various steps in the methodology described in Section 4.4.2 are concretely shown for the UMaine VoltturnUS-S floater. For this, the xy coordinate plane will be used, which is illustrated in Figure 4.7b.

In the methodology, it was assumed that the neutral position, anchor positions, and floater geometry were known in advance. That is the case for the UMaine VoltturnUS-S floater. This determines the movable range shape of the FOWT as depicted in Figure 4.8. The obtained shape is triangular. It must be noted that the movable range boundary triangle is not the same as the anchor-to-anchor triangle due to the off-centre position of the fairlead.

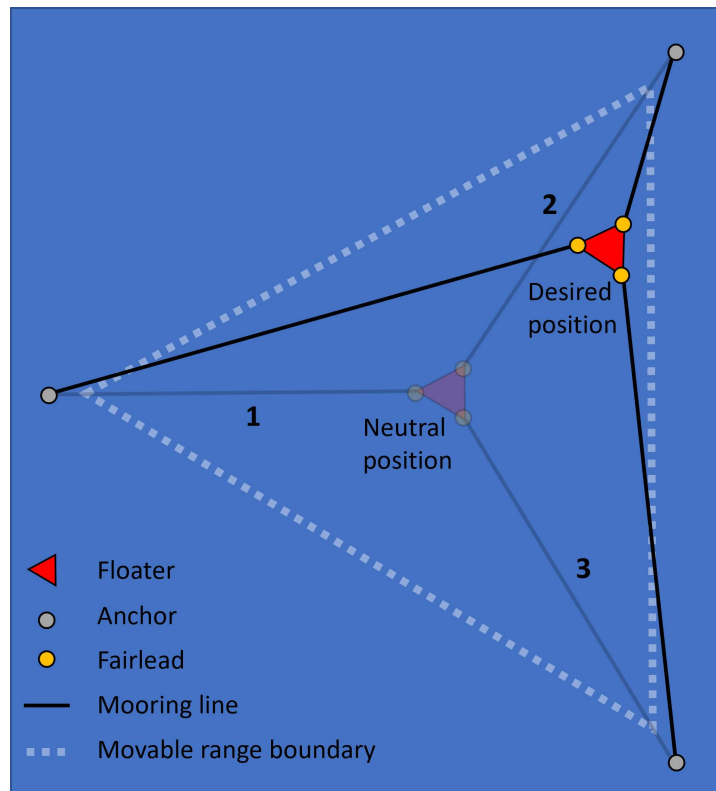


Figure 4.8: Illustration of the position mooring repositioning mechanism concept for the UMaine VoltumUS-S floater.

Once the movable range boundary is obtained, the desired floater positions can be selected. This is done by creating a mesh grid consisting of the desired floater positions. After having created a 30 by 30 mesh grid, it is determined which points are on or inside the movable range triangle. Figure 4.9 depicts the desired turbine coordinates for the triangular movable range shape. Each black dot represents a desired coordinate.

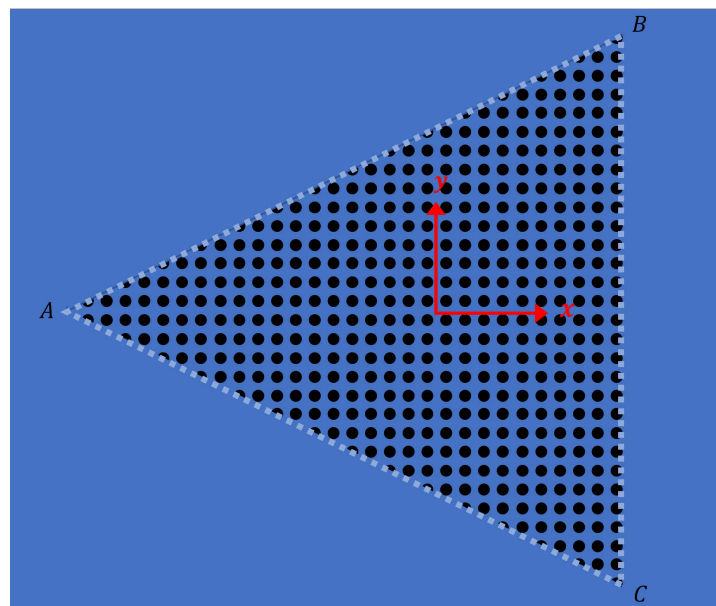


Figure 4.9: Desired coordinates for the UMaine VoltumUS-S floater.

MoorPy can calculate the horizontal tensions at the fairlead based on the mooring line lengths. That makes it possible to compute the x - and y -components of the horizontal tensions with the mooring line orientations (see Equation 4.6 and Equation 4.7). This enables us to search for a force equilibrium in the x - and y -direction, which is achieved by solving the optimization problem in Equation 4.8. The optimization problem is solved with the trust-constr algorithm, which is described in Section 2.6.4. This process is done for all desired positions.

Unless the final function value in the optimization is zero, the system is not in equilibrium. Therefore, an equilibrium has to be found for the obtained mooring line lengths. This can be done with MoorPy by providing the mooring line lengths as an input. A new floater position will be calculated, which is the actual position. An example of this is shown in Figure 4.10.

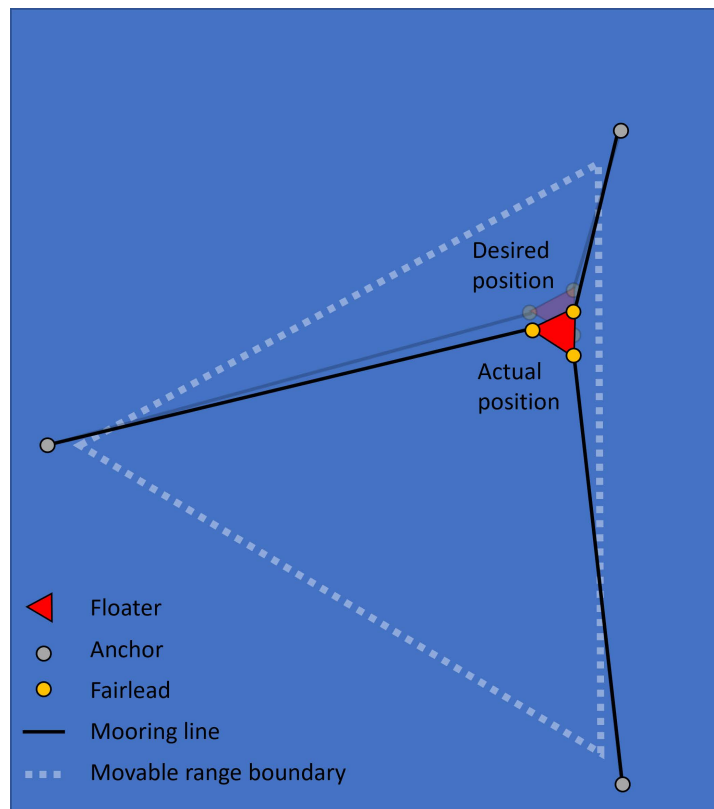


Figure 4.10: Example of a desired position and the actual position for the UMaine VoltumUS-S floater.

Case study results

In the following, the results obtained for the UMaine VoltumUS-S reference floater by using the methodology described Section 4.4.2 are presented. The results are shown with contour plots. The triangle in the plots represents the assumed movable range shape for the floater. Various results are obtained after solving the optimization problem (see Equation 4.8):

1. Mooring line length (L_i);
2. Horizontal tension at the fairlead (H_i);
3. Distance between the desired and actual positions;
4. Vertical tension at the fairlead (V_i);
5. Tension at the fairlead (T_i);
6. Absolute error in the yaw angle (rotation around z -axis) of the floater.

For brevity and relevance, it was chosen not to show all of these results. From the list above, the first three will be presented next, and the last three can be found in Appendix B for the readers that are interested in them.

Figure 4.11 shows the sum of mooring line lengths and the individual contributions of each line to that sum for different desired positions of the floater. The reader is reminded that in the neutral position, the mooring line length for each line is 850 m. The following observations can be made:

- The further the floater is moved from the origin, the larger the sum of the mooring line lengths;
- The further the floater is moved from an anchor, the larger the length of the mooring line connected to that anchor;
- The sum of the line lengths required to achieve large movements of the floater is less than 25% of the total line length in the neutral position.

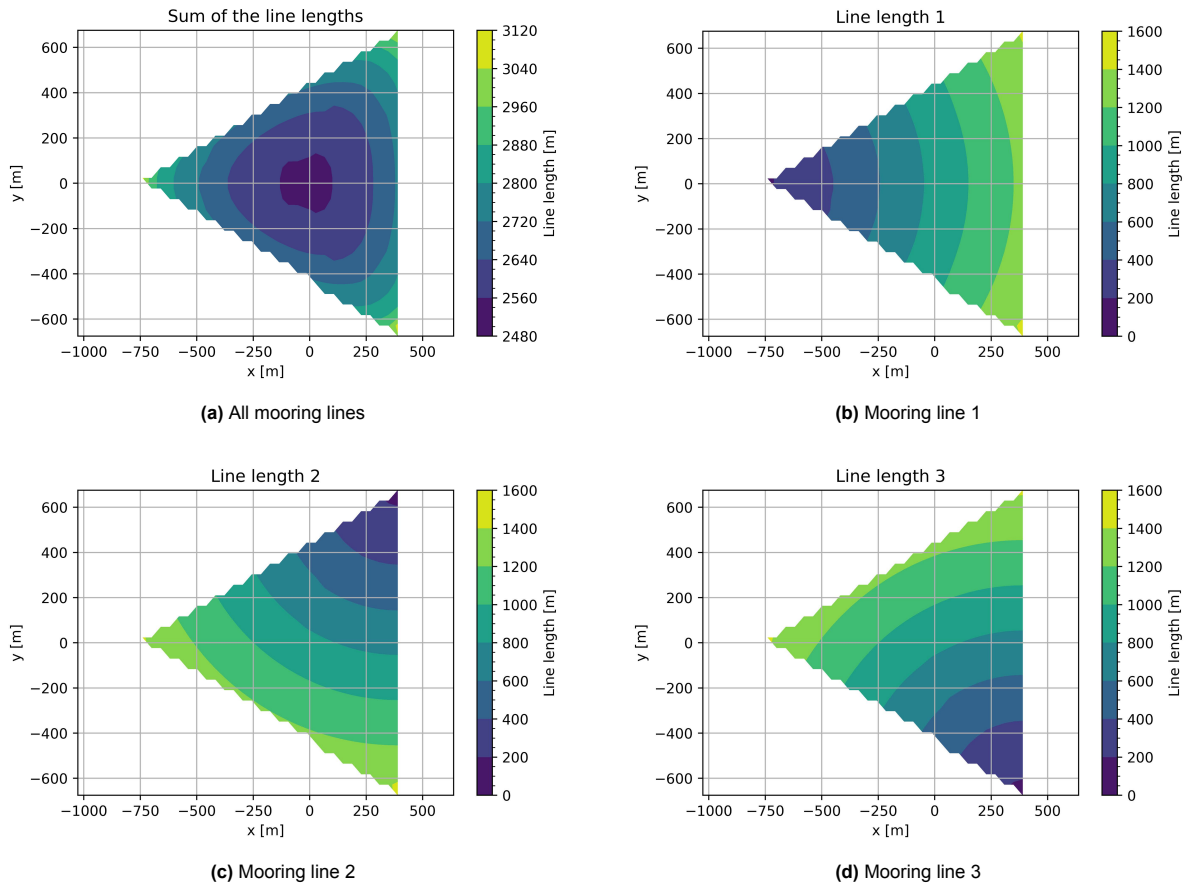


Figure 4.11: Contour plot of the mooring line length for various desired positions.

In Figure 4.12, the horizontal tensions at the fairlead are presented for different desired floater coordinates. It should be noted that these values correspond to the system in equilibrium. In other words, these values are obtained after equilibrating the system with MoorPy for the optimal line lengths (found after solving the optimization problem). Furthermore, it should be noted that the constraints in the optimization problem were that the horizontal tensions must be larger than or equal to the horizontal tensions in the neutral position (1.35 MN). There are two observations made:

- In most cases, the horizontal tensions do not deviate more than 35% from the horizontal tensions in neutral positions.
- The further away the floater is from an anchor, the less likely it is that the mooring line connected to that anchor satisfies the constraint (meaning that the horizontal tension is less than 1.35 MN).

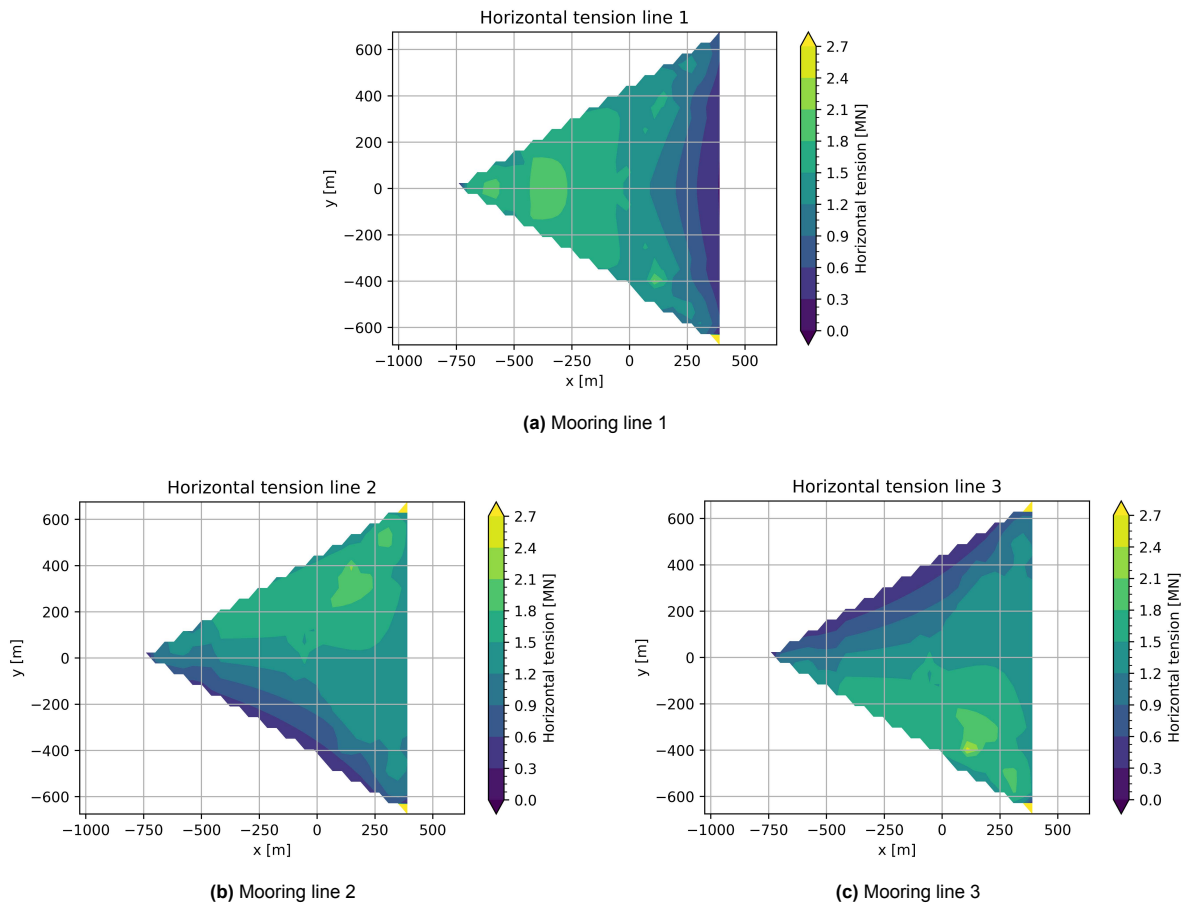


Figure 4.12: Contour plot of the horizontal tension at the fairlead for various desired positions.

Figure 4.13 shows the ability of position mooring to move the floater to a desired position. An error means the optimizer searched for an equilibrium but could not find it because there was none. The smaller the error, the smaller the imbalances in the system after solving the optimization problem, and the larger the error, the larger the imbalances. The imbalances in the system are the smallest along the mooring lines. The results give an indication of what movable range can actually be achieved with position mooring. The actual movable range looks like a star with three points, called a tristar.

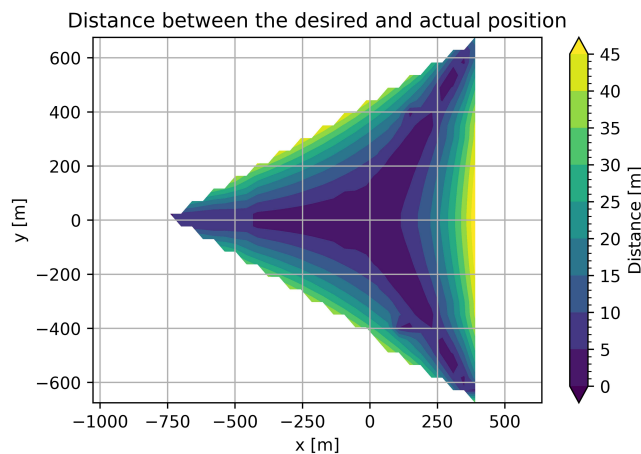


Figure 4.13: Contour plot of the absolute error in position for various desired positions.

4.5. Discussion

The important findings and the limitations of the research in this chapter are discussed in this section.

4.5.1. The interpretations and implications of key findings

The interpretations and implications of key findings for repositioning mechanisms for movable FOWTs are the following:

- A position mooring system is an energy-efficient repositioning mechanism that allows for large movable ranges compared to other alternatives.
 - Due to the fact that the station-keeping is provided passively by the mooring system, there are no additional energy losses to keep the floater at station in the relocated position. The only time energy is required is to move the turbine from its current position to the desired position. Once there, the floater is kept in place by the restoring force of the mooring lines, and no additional energy is required. Therefore, it is recommended to consider position mooring systems for turbine repositioning.
- The movability and station-keeping performance of position mooring can be assessed with the proposed method in Section 4.4.2.
 - Figure 4.13 shows the distance between the desired and actual position and is an indication of what the actual movable range is for the FOWT. There is not necessarily a hard movable range boundary. The boundary depends on what absolute errors in distance are deemed acceptable.
 - Besides that the proposed method can be used to evaluate the movable range of a FOWT, it can also be used to design the movable range. By adding mooring lines or changing the anchor positions, the movable range of the FOWT can be altered;
 - Even though, with the proposed method, the station-keeping performance of position mooring could be assessed, this was not really done. If an equilibrium is found at or near the desired position, then the floater can be kept in place with the mooring lines. However, to determine how well the floater can be kept at station, an additional analysis of the mooring stiffness is required.

4.5.2. Limitations

The limitation of the selected repositioning mechanism is the following:

- There is not much known about position mooring systems for FOWTs.
 - There is not much known about the other alternatives (YITuR, TAPM, and DP) either for FOWTs. The selection and further characterization of one of the options may therefore help in future work that considers turbine repositioning.
 - A basic position mooring system and its main components are provided in Figure 4.3. This design, however, solely serves as a starting point for future position mooring systems. More solutions have to be developed and evaluated.
 - Not all floaters allow for the necessary onboard equipment to reposition the FOWT. In this work, no additional efforts were made to assess what kinds of floaters could and could not accommodate a position mooring system. The floater type must be considered in future studies.

The limitations of the proposed methodology to assess the performance of position mooring are the following:

- The proposed methodology assumes that there is no change in the floater yaw angle in the desired position (see Section 4.4.2).
 - In the objective function shown in Equation 4.8, only the resultant forces are minimized; the resultant moments are neglected. This proved to be a reasonable assumption based on the absolute yaw error, shown in Figure B.3. The error is negligible up until near the anchor points.

- The proposed methodology assumes that the mooring line follows a straight path from fairlead to anchor (see Section 4.4.2).
 - This assumption may hold for small movements, but is expected to cause problems for larger movements. A large part of the mooring line lies on the seabed. Once the floater is moved to the desired position, the part that lies on the seabed may not move with it. Therefore, when looking at the mooring lines in, for example, Figure 4.8 it may be the case that the line follows a curved path instead of a straight one. It is not yet known how this may impact the mooring analysis.

5

Discussion

5.1. Introduction to the discussion

Ideally, for a dynamic wind farm, the increase in AEP and the increase in costs due to the repositioning mechanism are considered together. Both aspects are dependent on the repositioning mechanism. Currently, not much is known about these mechanisms and their characteristics. As a result, evaluating dynamic wind farms based on their ability to reduce LCoE is difficult. Therefore, in this Master's Thesis, two aspects related to dynamic wind farms are considered separately: the ability of movable FOWTs to maximize the AEP of the wind farm and repositioning mechanisms with their characteristics. These two separate parts have one commonality among them: the movable range. In Section 5.2, it is attempted to bring these separate parts together through the movable range. Hereafter, in Section 5.3, the limitations are discussed for dynamic WFLO if position mooring were to be considered as the repositioning mechanism.

5.2. Movable range

Figure 5.1 shows a comparison between the circular movable range shape (used in the dynamic WFLOP) and the movable range shape (for the UMaine VoltumUS-S floater). The size of the circular movable range shape (2 rotor diameters) is based on the movable range size where the steepest gains in wind farm efficiency are seen for the dynamic WFLO in Figure 3.19. It should be noted that the rotor diameter for the IEA 15MW reference turbine is 240 meters [107], and the rotor diameter that is used in the dynamic WFLOP is 130 meters. The circular shape in the illustration corresponds with the rotor diameter of the IEA 15MW turbine.

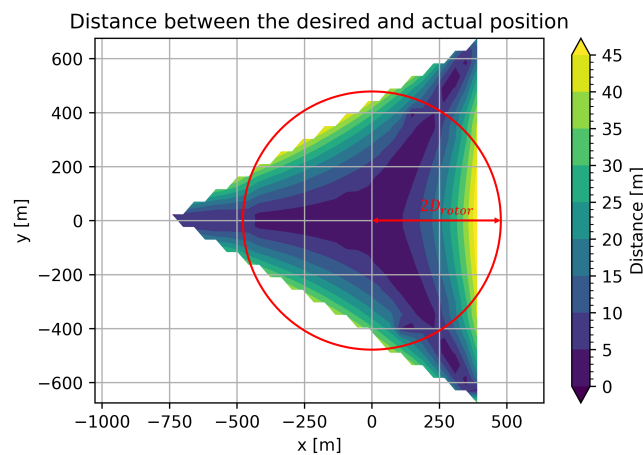


Figure 5.1: Comparison of the circular movable range shape and the movable range shape for the UMaine VoltumUS-S floater.

Even though the movable range shapes (tristar and circular) can not be directly compared, the following insights can be provided:

- A large movable range can potentially be obtained with position mooring;
- If mooring lines are added to the system and/or the anchor points are moved further away, the movable range is expected to increase even more. This allows us to reach an even larger part of the depicted circular movable range shape.

There are also insights that can be provided regarding the wind farm efficiency that can be gained with the tristar shape compared to the circular shape:

- Even though the tristar movable range shape does not cover the full circle, it allows for a large mobility of the turbine. Therefore, a significant wind farm efficiency gain can be expected;
- It has already been established that the crosswind displacement has much more impact on the wind farm efficiency than the downwind displacement. The crosswind displacement can be achieved via the tristar almost as well as via the full circular area. Hence, a wind farm efficiency is expected for the tristar shape that is close to that of the circular shape;
- The minor difference in wind farm efficiency may be mitigated even more by considering the orientation of the shape in dynamic WFLO.

5.3. Limitations

There are several limitations with the dynamic WFLO in this work, if position mooring is considered as the repositioning mechanism:

- The selected objective function for dynamic WFLO is AEP.
 - The AEP gains that could be achieved through position mooring must outweigh the additional capital and O&M costs. At this moment, this cannot be assessed since the detailed characteristics of the mechanism are yet unknown. Once more detailed position mooring systems are developed and evaluated, the effect of movable FOWTs on a wind farm's LCoE may be assessed. The objective function can then be changed from AEP to LCoE.
- The separation distance constraint between the turbines is excluded for the dynamic WFLO.
 - Excluding the separation distance causes dynamic wind farm layouts with overlapping movable ranges (see, for example, Figure 3.17 or Figure 3.18). The overlap in the movable range is not desired from a practical perspective. It might increase the risk of collisions between the turbines; it results in overlapping mooring lines; and it increases the operational difficulty.
 - For future work, it is suggested that the separation distance for the installation position be ascertained, such that there is no overlap in the movable range. Although, with increased know-how, overlapping movable ranges may still be considered.
- The selected movable range shape for the dynamic WFLO is circular.
 - The movable range shape depends on the repositioning mechanism. Currently, not much is known about these mechanisms and their characteristics. Therefore, a movable range shape has to be assumed to solve the dynamic WFLO. A circular shape was chosen for this work, mainly due to its simplicity. This reduces the complexity of the optimization since a design variable is removed (the orientation of the movable range shape). This, in turn, made it possible to study in depth how different movable range sizes affected the AEP.
 - From a practical perspective, triangular (considered by Rodrigues et al. (2015) [6]) or rectangular movable range shapes might be more realistic. For both shapes, the orientation has to be taken into account. This increases the complexity of the optimization problem and the computational time required to solve it.
 - The insights that were obtained from solving the dynamic WFLO with a circular movable range shape are not expected to change if different shapes were considered.

6

Conclusion and further work

6.1. Conclusion

The objectives of this Master's Thesis were twofold:

1. To provide insight into the ability of movable floating offshore wind turbines to increase a wind farm's AEP;
2. To gain an understanding of repositioning mechanisms and their characteristics for movable floating offshore wind turbines.

To achieve the first objective, various wind farm layout optimization problems were solved with AEP as the objective function. Two reference methods have been considered: static layout optimization (no turbine mobility) and unrestricted dynamic layout optimization (unlimited turbine mobility). Static layout optimization provides a lower bound, whereas unrestricted dynamic layout optimization provides an upper bound for wind farm layout optimization with movable turbines. Two realistic dynamic layout optimization methods have been considered as well that do take into account the movable range of the turbines: sequential and nested optimization. Different sizes are considered for the assumed circular movable range shape of the mobile turbine, ranging from a radius of 0.01 rotor diameters (very small turbine mobility) to a radius of 20 rotor diameters (turbine can move anywhere in the wind farm).

For movable turbines, a displacement perpendicular to the wind direction (crosswind) is much more important for the wind farm efficiency in terms of AEP than a displacement parallel to the wind direction (downwind). The steepest gains in efficiency are seen up to a movable range radius of 2 rotor diameters. Up to this point, crosswind displacements account for the majority of efficiency gains. Hereafter, the additional gains, which are minor, come from the downwind displacements. When the sequential and nested optimization are compared for the same movable range size (2 rotor diameters), an absolute difference in the efficiency of around 1% is seen in favour of nested optimization. This method, however, is much more computationally expensive and complex. Further investigations into this size showed that compared to static layouts, which have efficiencies of around 85%-90%, dynamic layouts can increase the efficiency up to around 97%. This brings their efficiency within 3% of a dynamic wind farm with unlimited turbine mobility. Moreover, for this movable range size, movable turbines in a wind farm are so effective in increasing the AEP that the installation positions almost do not affect the efficiency.

To achieve the second objective, various repositioning mechanisms have been explored and one has been selected: position mooring. By adapting the mooring line lengths through winches, the wind turbine can be moved and kept in a new position. A novel method is proposed to assess the movability and station-keeping performance of position mooring. The methodology is evaluated through a case study: the UMaine VoltturnUS-S floater for the IEA 15MW turbine.

When position mooring is considered for the UMaine VoltturnUS-S floater, the assumed movable range shape is triangular. The area in this triangle wherein the floater can easily move looks like a star with three points. This area is called a tristar. More generically, position mooring works well when the

movement of the turbine is in the direction of an anchor.

A comparison between the circular shape with a radius of 2 rotor diameters and the tristar shape for the UMaine VoltturnUS-S floater shows a very promising outlook for the ability of movable turbines to increase a wind farm's AEP. Once the gains in AEP outweigh the additional operational and capital costs of position mooring, movable turbines will decrease the LCoE of floating offshore wind farms. Hence, their competitiveness with other (renewable) energy resources will be increased.

6.2. Further work

The findings in this Master's Thesis for dynamic wind farm layouts are quite promising. This topic, however, is still in its infancy. Therefore, the author identified the following gaps that may be considered in future works:

- The effect of mooring line length adjustment, to enable repositioning, on a floater's mooring stiffness and natural frequencies has not been looked into yet.
- The proposed methodology for position mooring to assess a floater's movability and station-keeping is only used for one case study, with three mooring line lengths. The influence of the anchor positions and the number of mooring lines on the movable range of a floater is unexplored. Additionally, the influence of shared mooring lines on position mooring has not yet been considered.
- For position mooring, only catenary mooring lines were considered. Taut mooring lines can be considered as well, as was done by Rodrigues et al. (2015) [6]. The advantages and disadvantages of both mooring line types regarding turbine repositioning are yet to be determined.
- An example design was provided for the position mooring system. This is a basic design and can be further explored. More detailed designs have not been proposed yet.
- Once more detailed repositioning mechanisms are developed (see previous point, for example) and their properties are well known, the net effect of the additional costs and the increase in AEP on the LCoE can be assessed. The net effect of the trade-off in costs and AEP on the LCoE is yet unknown. This can be done with dynamic WFLO with the LCoE as an objective function.
- A control strategy may be proposed that can actively control the position of the FOWT through mooring line length adjustment. Nguyen et al. (2010) proposed such an active position control strategy for a vessel and can be used as a starting point [93].
- Large gains in the AEP have been shown by movable FOWTs in a wind farm. On the other hand, the effects of movable turbines on the fatigue of structural components are unknown. Fatigue damage can be included in dynamic WFLO as a constraint.

References

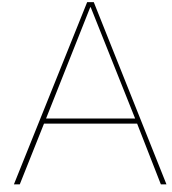
- [1] GWEC. *Global Offshore Wind Report 2021*. Global Wind Energy Council, Brussels, 2021.
- [2] IEA. *Net Zero by 2050: A Roadmap for the Global Energy Sector*. International Energy Agency, Paris, 2021.
- [3] NREL. *Offshore Wind Market Report: 2021 Edition*. National Renewable Energy Laboratory, Golden, CO (United States), 2021.
- [4] L. Ramirez, D. Fraile, and G. Brindley. *Offshore Wind in Europe: Key trends and statistics 2020*. WindEurope, Brussels, 2021.
- [5] IRENA. *Offshore renewables: An action agenda for deployment*. International Renewable Energy Agency, Abu Dhabi, 2021.
- [6] S. Rodrigues et al. "Wake losses optimization of offshore wind farms with moveable floating wind turbines". In: *Energy conversion and management* 89 (2015), pp. 933–941.
- [7] W. Musial. *Overview of Floating Offshore Wind*. National Renewable Energy Laboratory, Golden, CO (United States), 2021.
- [8] S. Rodrigues et al. "Trends of offshore wind projects". In: *Renewable and Sustainable Energy Reviews* 49 (2015), pp. 1114–1135.
- [9] M. Atcheson et al. *Floating offshore wind energy*. Springer, 2016.
- [10] DNV-SE-0422. *Certification of floating wind turbines*. Det Norske Veritas, Norway, 2021.
- [11] M. Lerch et al. "Sensitivity analysis on the levelized cost of energy for floating offshore wind farms". In: *Sustainable Energy Technologies and Assessments* 30 (2018), pp. 77–90.
- [12] A. M. Eltamaly and M. A. Mohamed. "Optimal sizing and designing of hybrid renewable energy systems in smart grid applications". In: *Advances in renewable energies and power technologies*. Elsevier, 2018, pp. 231–313.
- [13] J. Simpson, E. Loth, and K. Dykes. "Cost of Valued Energy for design of renewable energy systems". In: *Renewable Energy* 153 (2020), pp. 290–300.
- [14] T. Stehly and P. Duffy. *2020 Cost of Wind Energy Review*. Tech. rep. National Renewable Energy Lab.(NREL), Golden, CO (United States), 2021.
- [15] M. Shields et al. "Impacts of turbine and plant upsizing on the levelized cost of energy for offshore wind". In: *Applied Energy* 298 (2021), p. 117189.
- [16] J. F. Manwell, J. G. McGowan, and A. L. Rogers. *Wind energy explained: theory, design and application*. John Wiley & Sons, 2010.
- [17] NZWEA. *Benefits of wind farms*. New Zealand Wind Energy Association, Wellington, 2013.
- [18] P. Fleming et al. "Simulation comparison of wake mitigation control strategies for a two-turbine case". In: *Wind Energy* 18.12 (2015), pp. 2135–2143.
- [19] M. Samorani. "The wind farm layout optimization problem". In: *Handbook of wind power systems*. Springer, 2013, pp. 21–38.
- [20] G. Ren et al. "The analysis of turbulence intensity based on wind speed data in onshore wind farms". In: *Renewable energy* 123 (2018), pp. 756–766.
- [21] F. Koch et al. "Consideration of wind farm wake effect in power system dynamic simulation". In: *2005 IEEE Russia Power Tech*. IEEE. 2005, pp. 1–7.
- [22] F. Porté-Agel, M. Bastankhah, and S. Shamsoddin. "Wind-turbine and wind-farm flows: a review". In: *Boundary-Layer Meteorology* 174.1 (2020), pp. 1–59.
- [23] I. Neunaber et al. "Distinct turbulent regions in the wake of a wind turbine and their inflow-dependent locations: The creation of a wake map". In: *Energies* 13.20 (2020), p. 5392.

- [24] L.J. Vermeer, J. N. Sørensen, and A. Crespo. “Wind turbine wake aerodynamics”. In: *Progress in aerospace sciences* 39.6-7 (2003), pp. 467–510.
- [25] R. J. Barthelmie et al. “Modelling and measurements of power losses and turbulence intensity in wind turbine wakes at Middelgrunden offshore wind farm”. In: *Wind Energy: An International Journal for Progress and Applications in Wind Power Conversion Technology* 10.6 (2007), pp. 517–528.
- [26] G.A.M. Van Kuik et al. “Long-term research challenges in wind energy—a research agenda by the European Academy of Wind Energy”. In: *Wind energy science* 1.1 (2016), pp. 1–39.
- [27] T. Knudsen, T. Bak, and M. Svenstrup. “Survey of wind farm control—power and fatigue optimization”. In: *Wind Energy* 18.8 (2015), pp. 1333–1351.
- [28] S. Boersma et al. “A tutorial on control-oriented modeling and control of wind farms”. In: *2017 American control conference (ACC)*. IEEE. 2017, pp. 1–18.
- [29] A. C. Kheirabadi and R. Nagamune. “A quantitative review of wind farm control with the objective of wind farm power maximization”. In: *Journal of Wind Engineering and Industrial Aerodynamics* 192 (2019), pp. 45–73.
- [30] A. Tesauro, P. E. Réthoré, and G. C. Larsen. “State of the art of wind farm optimization”. In: *Proceedings of EWEA* (2012), pp. 1–11.
- [31] C. Han and R. Nagamune. “Platform position control of floating wind turbines using aerodynamic force”. In: *Renewable Energy* 151 (2020), pp. 896–907.
- [32] P. Asaah, L. Hao, and J. Ji. “Optimal placement of wind turbines in wind farm layout using particle swarm optimization”. In: *Journal of Modern Power Systems and Clean Energy* 9.2 (2021), pp. 367–375.
- [33] M. R. Patel and O. Beik. *Wind and solar power systems: design, analysis, and operation*. CRC press, 2021.
- [34] F. Azlan et al. “Review on optimisation methods of wind farm array under three classical wind condition problems”. In: *Renewable and Sustainable Energy Reviews* 135 (2021), p. 110047.
- [35] M. A. Lackner and C. N. Elkinton. “An analytical framework for offshore wind farm layout optimization”. In: *Wind Engineering* 31.1 (2007), pp. 17–31.
- [36] K. E. Johnson and N. Thomas. “Wind farm control: Addressing the aerodynamic interaction among wind turbines”. In: *2009 American Control Conference*. IEEE. 2009, pp. 2104–2109.
- [37] J. F. Herbert-Acero et al. “A review of methodological approaches for the design and optimization of wind farms”. In: *Energies* 7.11 (2014), pp. 6930–7016.
- [38] G. Mosetti, C. Poloni, and B. Diviacco. “Optimization of wind turbine positioning in large wind-farms by means of a genetic algorithm”. In: *Journal of Wind Engineering and Industrial Aerodynamics* 51.1 (1994), pp. 105–116.
- [39] J. S. González et al. “A review and recent developments in the optimal wind-turbine micro-siting problem”. In: *Renewable and Sustainable Energy Reviews* 30 (2014), pp. 133–144.
- [40] J. R. R. A. Martins and A. Ning. *Engineering design optimization*. Cambridge University Press, 2021.
- [41] N. F. Baker et al. *Wake Model Description for Optimization Only Case Study: IEA Task 37 on System Engineering in Wind Energy*. Tech. rep. Tech. rep., International Energy Agency, <https://github.com/byuflowlab> ..., 2019.
- [42] A. Migdalas, P. M. Pardalos, and P. Värbrand. *Multilevel optimization: algorithms and applications*. Vol. 20. Springer Science & Business Media, 1998.
- [43] S. A. Gabriel et al. *Complementarity modeling in energy markets*. Vol. 180. Springer Science & Business Media, 2012.
- [44] N. F. Baker et al. *Wind Farm Layout Optimization Case Studies 3 & 4: IEA Task 37 on System Engineering in Wind Energy*. Tech. rep. Tech. rep., International Energy Agency, <https://github.com/byuflowlab> ..., 2019.

- [45] M. M. Pedersen et al. "DTUWindEnergy/PyWake: PyWake". In: (2019). DOI: 10.5281/zenodo.2562662.
- [46] N. F. Baker et al. *Wind Farm Layout Optimization Case Studies: IEA Task 37 on System Engineering in Wind Energy*. Tech. rep. Tech. rep., International Energy Agency, <https://github.com/byuflowlab> ..., 2018.
- [47] N. F. Baker et al. "Best practices for wake model and optimization algorithm selection in wind farm layout optimization". In: *AIAA Scitech 2019 forum*. 2019, p. 0540.
- [48] A. P. J. Stanley and A. Ning. "Massive simplification of the wind farm layout optimization problem". In: *Wind Energy Science 4.4* (2019), pp. 663–676.
- [49] N. Hansen, Y. Akimoto, and P. Baudis. "CMA-ES/pycma on Github". In: *Zenodo*, DOI:10.5281/zenodo.2559634 (2019).
- [50] P. Virtanen et al. "SciPy 1.0: fundamental algorithms for scientific computing in Python". In: *Nature methods 17.3* (2020), pp. 261–272.
- [51] Z. Michalewicz. *Genetic algorithms + data structures = Evolution Programs*. 1996.
- [52] I. Rechenberg. *Evolutionsstrategie—Optimierung technischer Systeme nach Prinzipien der biologischen Information*. 1973.
- [53] Hans-Paul Schwefel. *Numerical optimization of computer models*. John Wiley & Sons, Inc., 1981.
- [54] N. Hansen, D. V. Arnold, and A. Auger. "Evolution strategies". In: *Springer handbook of computational intelligence*. Springer, 2015, pp. 871–898.
- [55] H. Georg. Beyer and B. Sendhoff. "Covariance matrix adaptation revisited—the CMSA evolution strategy—". In: *International Conference on Parallel Problem Solving from Nature*. Springer. 2008, pp. 123–132.
- [56] N. Hansen, A. Ostermeier, and A. Gawelczyk. "On the Adaptation of Arbitrary Normal Mutation Distributions in Evolution Strategies: The Generating Set Adaptation." In: *ICGA*. Citeseer. 1995, pp. 57–64.
- [57] N. Hansen and A. Ostermeier. "Completely derandomized self-adaptation in evolution strategies". In: *Evolutionary computation 9.2* (2001), pp. 159–195.
- [58] A. Auger and N. Hansen. "Tutorial CMA-ES: evolution strategies and covariance matrix adaptation". In: *Proceedings of the 14th annual conference companion on Genetic and evolutionary computation*. 2012, pp. 827–848.
- [59] M. J. D. Powell. "Direct search algorithms for optimization calculations". In: *Acta numerica 7* (1998), pp. 287–336.
- [60] M. J. D. Powell. "A view of algorithms for optimization without derivatives". In: *Mathematics Today-Bulletin of the Institute of Mathematics and its Applications 43.5* (2007), pp. 170–174.
- [61] M. J. D. Powell. "A direct search optimization method that models the objective and constraint functions by linear interpolation". In: *Advances in optimization and numerical analysis*. Springer, 1994, pp. 51–67.
- [62] R. H. Byrd, M. E. Hribar, and J. Nocedal. "An interior point algorithm for large-scale nonlinear programming". In: *SIAM Journal on Optimization 9.4* (1999), pp. 877–900.
- [63] D. Kraft. "A software package for sequential quadratic programming". In: *Forschungsbericht-Deutsche Forschungs- und Versuchsanstalt für Luft- und Raumfahrt* (1988).
- [64] C.L. Lawson and R.J. Hanson. "Solving least squares problems". In: (1974).
- [65] IEA Task 37. *IEA Wind TCP Task 37: Systems Engineering in Wind Energy*. 2022. URL: <https://iea-wind.org/task37/> (visited on 06/02/2022).
- [66] M. K. McWilliam et al. "IEA Wind Energy Task 37-System Engineering-Aerodynamic Optimization Case Study". In: *AIAA Scitech 2021 Forum*. 2021, p. 1412.
- [67] P. Bortolotti et al. *IEA Wind TCP Task 37: Systems engineering in wind energy-WP2. 1 Reference wind turbines*. Tech. rep. National Renewable Energy Lab.(NREL), Golden, CO (United States), 2019.

- [68] R. Wiser et al. "Expert elicitation survey predicts 37% to 49% declines in wind energy costs by 2050". In: *Nature Energy* 6.5 (2021), pp. 555–565.
- [69] N. O. Jensen. "A note on wind generator interaction". In: (1983).
- [70] I. Katic, J. Højstrup, and N. O. Jensen. "A simple model for cluster efficiency". In: *European wind energy association conference and exhibition*. Vol. 1. 1986, pp. 407–410.
- [71] G. C. Larsen. *A simple wake calculation procedure*. Risø National Laboratory, 1988.
- [72] T. Ishihara, A. Yamaguchi, and Y. Fujino. "Development of a new wake model based on a wind tunnel experiment". In: *Global wind power* 6 (2004).
- [73] S. Frandsen et al. "Analytical modelling of wind speed deficit in large offshore wind farms". In: *Wind Energy: An International Journal for Progress and Applications in Wind Power Conversion Technology* 9.1-2 (2006), pp. 39–53.
- [74] M. Bastankhah and F. Porté-Agel. "A new analytical model for wind-turbine wakes". In: *Renewable energy* 70 (2014), pp. 116–123.
- [75] L. Tian et al. "Development and validation of a new two-dimensional wake model for wind turbine wakes". In: *Journal of Wind Engineering and Industrial Aerodynamics* 137 (2015), pp. 90–99.
- [76] S. Xie and C. Archer. "Self-similarity and turbulence characteristics of wind turbine wakes via large-eddy simulation". In: *Wind Energy* 18.10 (2015), pp. 1815–1838.
- [77] X. Gao, H. Yang, and L. Lu. "Optimization of wind turbine layout position in a wind farm using a newly-developed two-dimensional wake model". In: *Applied Energy* 174 (2016), pp. 192–200.
- [78] T. Ishihara and G. W. Qian. "A new Gaussian-based analytical wake model for wind turbines considering ambient turbulence intensities and thrust coefficient effects". In: *Journal of Wind Engineering and Industrial Aerodynamics* 177 (2018), pp. 275–292.
- [79] H. S. Dhiman, D. Deb, and A. M. Foley. "Bilateral Gaussian wake model formulation for wind farms: A forecasting based approach". In: *Renewable and Sustainable Energy Reviews* 127 (2020), p. 109873.
- [80] C. L. Archer et al. "Review and evaluation of wake loss models for wind energy applications". In: *Applied Energy* 226 (2018), pp. 1187–1207.
- [81] J. K. Kaldellis, P. Triantafyllou, and P. Stinis. "Critical evaluation of Wind Turbines' analytical wake models". In: *Renewable and Sustainable Energy Reviews* 144 (2021), p. 110991.
- [82] P. Hou et al. "A review of offshore wind farm layout optimization and electrical system design methods". In: *Journal of Modern Power Systems and Clean Energy* 7.5 (2019), pp. 975–986.
- [83] J. J. Thomas and A. Ning. "A method for reducing multi-modality in the wind farm layout optimization problem". In: *Journal of Physics: Conference Series*. Vol. 1037. 4. IOP Publishing, 2018, p. 042012.
- [84] N. Saadallah and E. Randeberg. "Dynamic repositioning in floating wind farms". In: (2020).
- [85] A. C. Kheirabadi and R. Nagamune. "Real-time relocation of floating offshore wind turbine platforms for wind farm efficiency maximization: An assessment of feasibility and steady-state potential". In: *Ocean Engineering* 208 (2020), p. 107445.
- [86] O. M. Aamo and T. I. Fossen. "Controlling line tension in thruster assisted mooring systems". In: *Proceedings of the 1999 IEEE International Conference on Control Applications (Cat. No. 99CH36328)*. Vol. 2. IEEE, 1999, pp. 1104–1109.
- [87] M. Nakamura, W. Koterayama, and H. Kajiwara. "Model experiments on thruster assisted mooring system". In: *The Fifth International Offshore and Polar Engineering Conference*. OnePetro, 1995.
- [88] C. Han, J. R. Homer, and R. Nagamune. "Movable range and position control of an offshore wind turbine with a semi-submersible floating platform". In: *2017 American Control Conference (ACC)*. 2017, pp. 1389–1394. DOI: 10.23919/ACC.2017.7963147.
- [89] ABS. *Guide for Position Mooring Systems*. American Bureau of Shipping, 2022.
- [90] DNV-OS-E301. *Position Mooring*. Det Norske Veritas, Norway, 2021.

- [91] Y. Zhao et al. "Global Benefits and Operational Challenges of Vessel Relocation". In: *International Conference on Offshore Mechanics and Arctic Engineering*. Vol. 56499. American Society of Mechanical Engineers. 2015, V003T02A059.
- [92] E. Falkenberg et al. "Mooring a Drilling Semi Over a Pre-Installed Riser System-West Alpha at Snorre B". In: *The Eleventh International Offshore and Polar Engineering Conference*. OnePetro. 2001.
- [93] D. H. Nguyen et al. "Control of marine riser end angles by position mooring". In: *Control Engineering Practice* 18.9 (2010), pp. 1013–1021.
- [94] J. Cheng, P. Cao, and S. Xiang. "Wet Tree Semi-Submersible With SCRs for 4,000 ft Water Depth in the Gulf of Mexico". In: *International Conference on Offshore Mechanics and Arctic Engineering*. Vol. 44335. 2011, pp. 675–683.
- [95] Y. Wu et al. "Mooring Tensioning Systems for Offshore Platforms: Design, Installation, and Operating Considerations". In: *Offshore Technology Conference*. OnePetro. 2018.
- [96] R. Skjetne and Z. Ren. "A survey on modeling and control of thruster-assisted position mooring systems". In: *Marine Structures* 74 (2020), p. 102830.
- [97] X. Zhu. "Thruster-Assisted Mooring". In: *Encyclopedia of Ocean Engineering*. Ed. by W. Cui, S. Fu, and Z. Hu. Singapore: Springer Singapore, 2019, pp. 1–9. ISBN: 978-981-10-6963-5. DOI: 10.1007/978-981-10-6963-5_144-1. URL: https://doi.org/10.1007/978-981-10-6963-5_144-1.
- [98] J. P. Strand, A. J. Sørensen, and T. I. Fossen. "Design of automatic thruster assisted mooring systems for ships". In: (1998).
- [99] D. T. Nguyen and A. J. Sørensen. "Switching control for thruster-assisted position mooring". In: *Control Engineering Practice* 17.9 (2009), pp. 985–994.
- [100] J. Bjørnø et al. "Modeling, parameter identification and thruster-assisted position mooring of c/s in ocean cat i drillship". In: *International Conference on Offshore Mechanics and Arctic Engineering*. Vol. 57748. American Society of Mechanical Engineers. 2017, V07BT06A019.
- [101] IMO. *Guidelines for vessels with dynamic positioning systems*. 1994.
- [102] A. J. Sørensen. "A survey of dynamic positioning control systems". In: *Annual reviews in control* 35.1 (2011), pp. 123–136.
- [103] K. T. Ma et al. *Mooring system engineering for offshore structures*. Gulf Professional Publishing, 2019.
- [104] S. Chakrabarti. *Handbook of Offshore Engineering (2-volume set)*. Elsevier, 2005.
- [105] O. Faltinsen. *Sea loads on ships and offshore structures*. Vol. 1. Cambridge university press, 1993.
- [106] A. Campanile, V. Piscopo, and A. Scamardella. "Mooring design and selection for floating offshore wind turbines on intermediate and deep water depths". In: *Ocean Engineering* 148 (2018), pp. 349–360.
- [107] E. Gaertner et al. *IEA wind TCP task 37: definition of the IEA 15-megawatt offshore reference wind turbine*. Tech. rep. National Renewable Energy Lab.(NREL), Golden, CO (United States), 2020.
- [108] C. Allen et al. *Definition of the UMaine VoltornUS-S reference platform developed for the IEA Wind 15-megawatt offshore reference wind turbine*. Tech. rep. National Renewable Energy Lab.(NREL), Golden, CO (United States); Univ. of ..., 2020.
- [109] M. Hall et al. *Moorpy (quasi-static mooring analysis in python)*. Tech. rep. National Renewable Energy Lab.(NREL), Golden, CO (United States), 2021.



Optimized dynamic layout for IEA 37 example layout

In this appendix, the results of several convergence studies are presented. These studies were done on the IEA37 example layout (shown in Figure 2.9).

A.1. Convergence study with four different optimization algorithms

The goal of the convergence study is to maximize the AEP of the dynamic layout for the IEA37 example layout. The static layout is, thus, predefined and fixed, and only a dynamic WFLOP is solved for a movable range of $C = 2.0$. In other words, only the problem in the second step of the sequential dynamic layout optimization is solved.

Four different optimization algorithms (described in Section 2.6) are used to solve the dynamic layout optimization. All algorithm specific parameters are kept at their default values except for: 'maxiter', which was set to a high value, such that the algorithms do not terminate too early; and 'tolfun' of the CMA-ES algorithm, which was set to 1×10^{-6} .

Figure A.1 shows the convergence study of the dynamic layout optimization for four different algorithms. It should be noted that the negative function values correspond with the wind farm's power output for that specific wind direction. The maximum power output per wind direction for sixteen 3.35MW wind turbines is 53.6 MW. Therefore, the lowest attainable function value, i.e., no wake losses, is -53.6 MW. These power outputs are used to evaluate the AEP of the dynamic layout with Equation 2.9. The final feasible AEP values for the four different optimization algorithms are shown in Table A.1.

Algorithm	AEP [GWh]
CMA-ES	451.16
COBYLA	451.63
SLSQP	409.72
trust-constr	452.14

Table A.1: Best found AEP values of the dynamic wind farm layout for the IEA37 example layout.

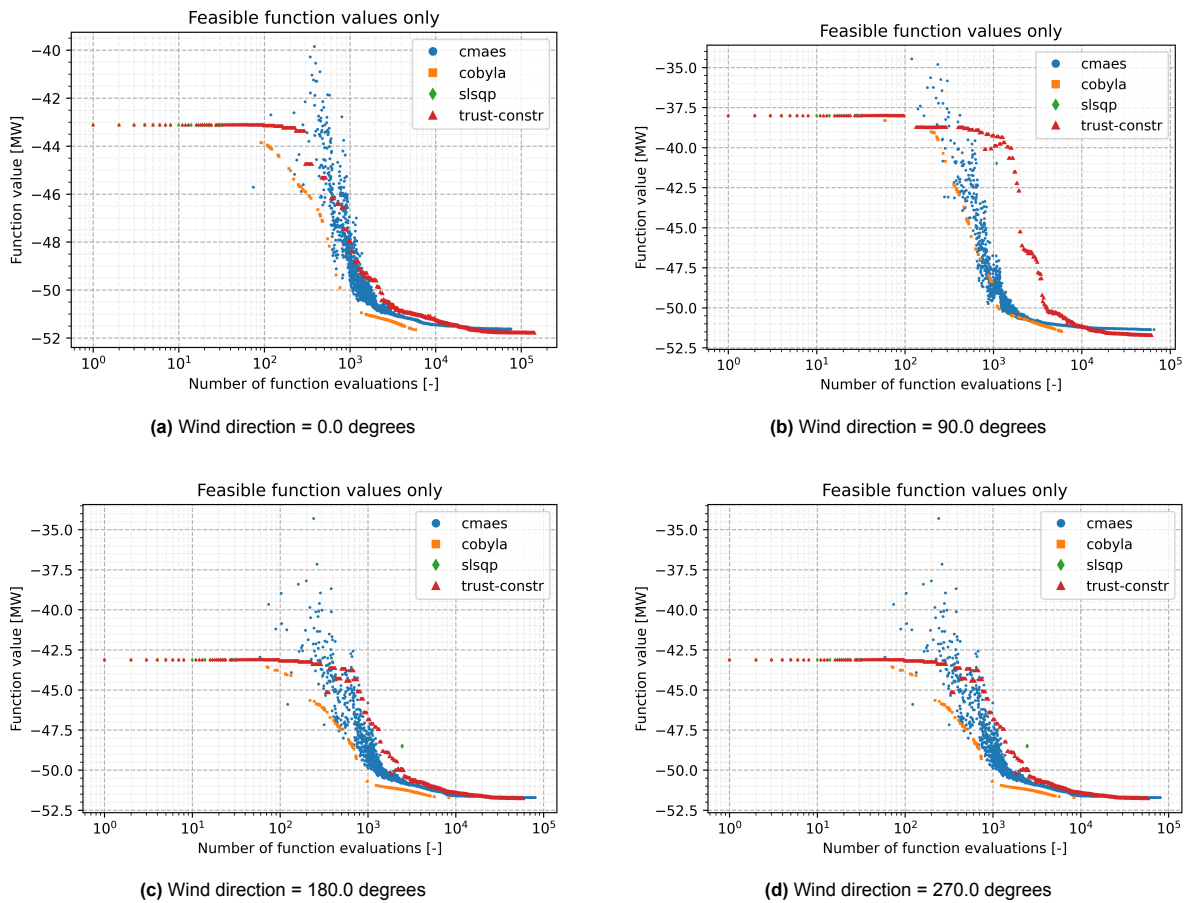


Figure A.1: Convergence study of the dynamic layout for 4 of the 16 wind directions, only showing the feasible function values.

Readers interested in the same convergence study but with a looser tolerance on the constraint violations are encouraged to see Figure A.2. Here, an exceedance of 1 meter of the constraint radii (R_B and R_{mr}) is tolerated. No additional efforts were made to calculate the AEP, but it can be noted that both COBYLA and SLSQP would benefit from the looser tolerance.

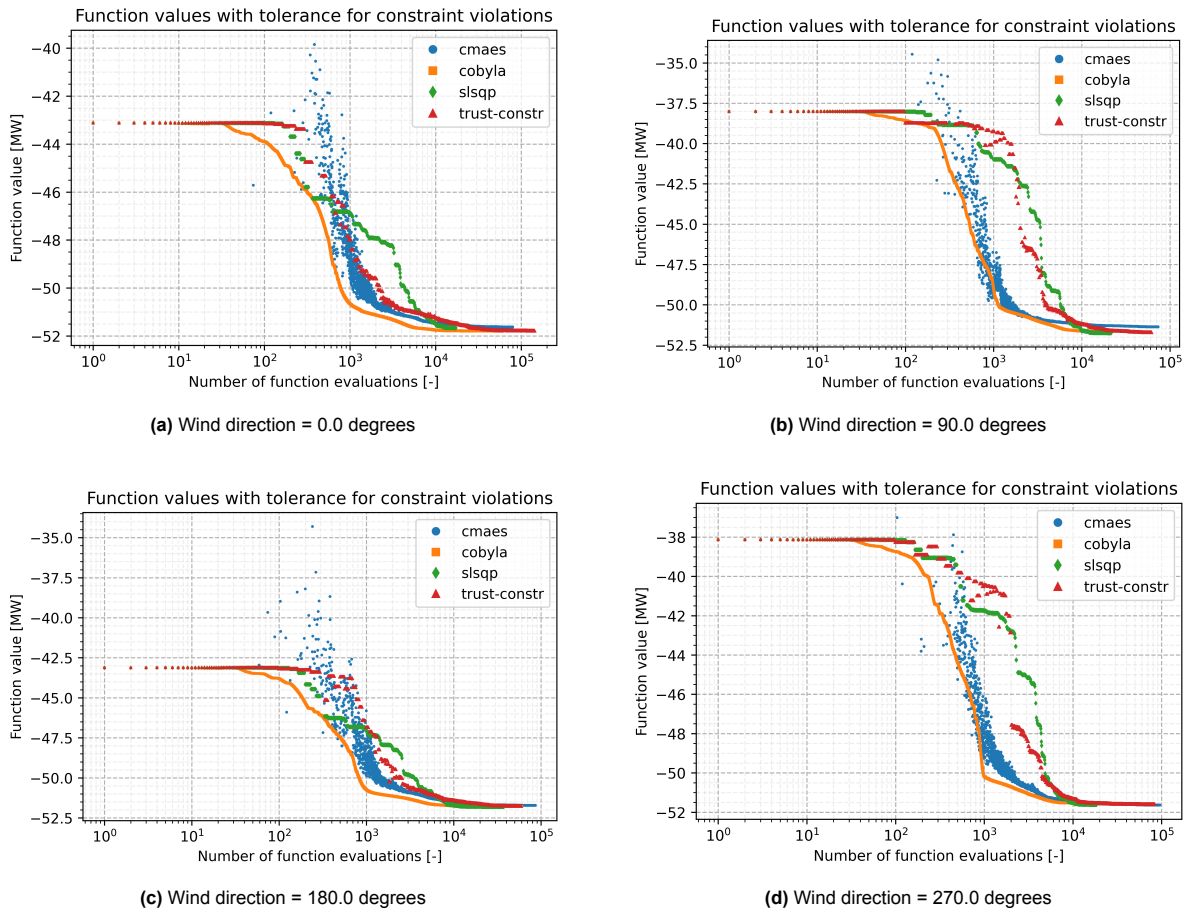


Figure A.2: Convergence study of the dynamic layout for 4 of the 16 wind directions, with a looser tolerance on the constraint violations.

A.2. Convergence study with COBYLA for different parameter values

In the following, a similar convergence study is performed as in the previous section, but only for the COBYLA optimization algorithm. Of the four different optimization algorithms in the previous section, COBYLA has the steepest convergence rate for the first 1000 function evaluations.

In this convergence study, efforts are made to reach even quicker convergence for the first 1000 function values. This is done by changing the COBYLA algorithm specific parameter 'rhubeg', which is the initial change to the design variables. The default value is 1.0. To achieve quicker convergence, it is assumed that larger values are required for this parameter.

Figure A.3 shows the results of the convergence study for 4 of the 16 wind directions, only for the feasible function values. The gaps in the lines for different 'rhubeg' values indicate that there are many infeasible function values. In Figure A.4 the same convergence study but with all function values is shown (including infeasible function values).

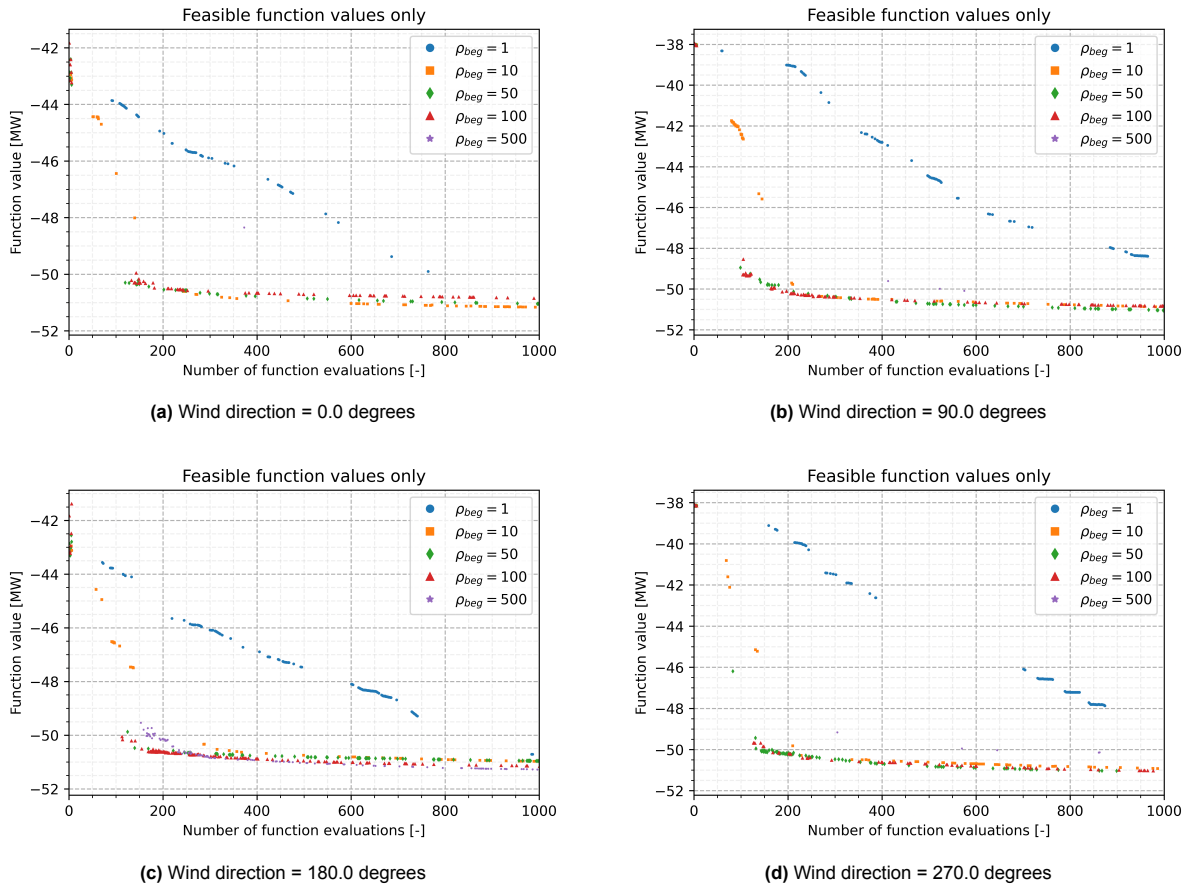


Figure A.3: Convergence study of the dynamic layout for 4 of the 16 wind directions using the COBYLA algorithm, only showing the feasible function values.

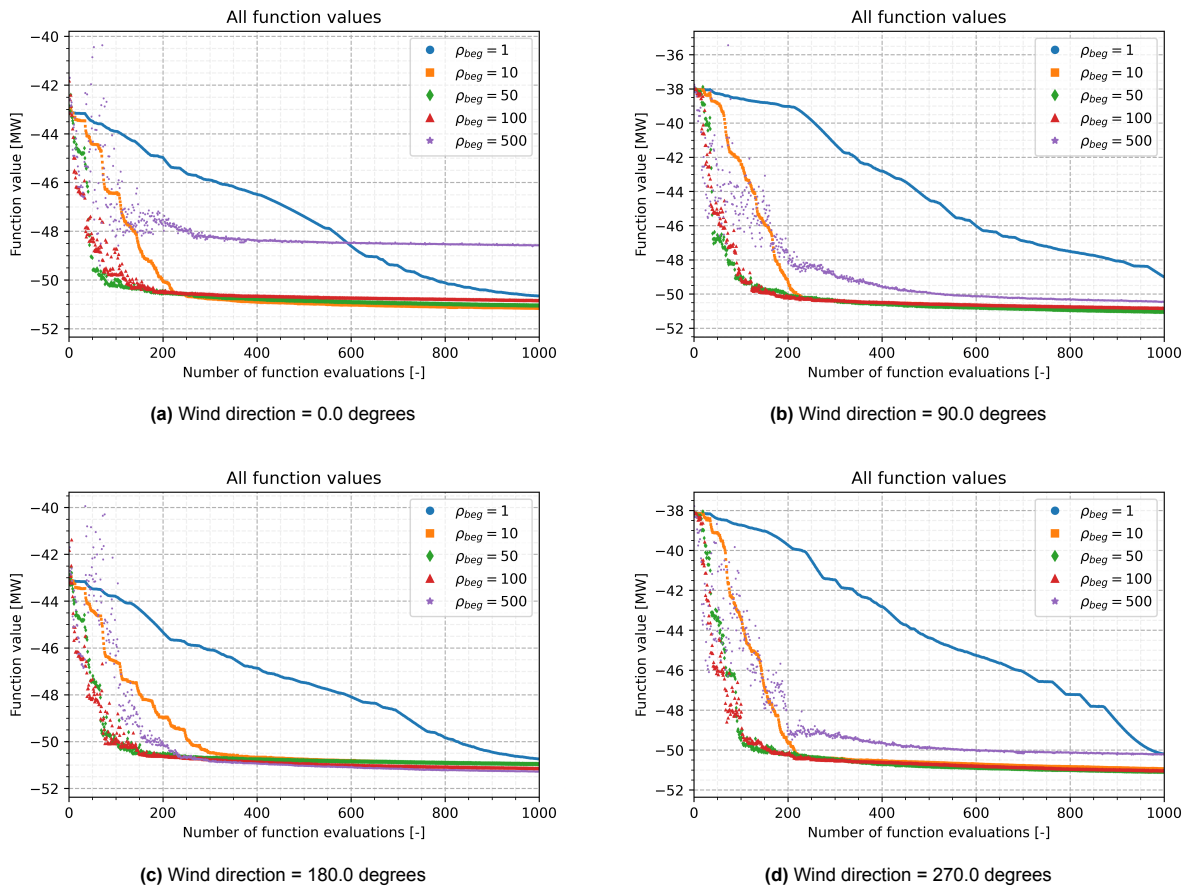


Figure A.4: Convergence study of the dynamic layout for 4 of the 16 wind directions using the COBYLA algorithm, showing all function values (including infeasible function values).

B

Additional results for position mooring of UMaine VolturnUS-S

In this chapter, additional results are displayed for the UMaine VolturnUS-S case study (see Section 4.4.3). The results are in the form of a contour plot, with the triangle (present in all plots) corresponding to the assumed movable range shape for the case study. First, the tensions at the fairlead are presented (Section B.1). Next, the vertical component of the fairlead tensions are shown (Section B.2). Lastly, the absolute errors in the yaw angle of the floater are displayed (Section B.3).

B.1. Fairlead tension

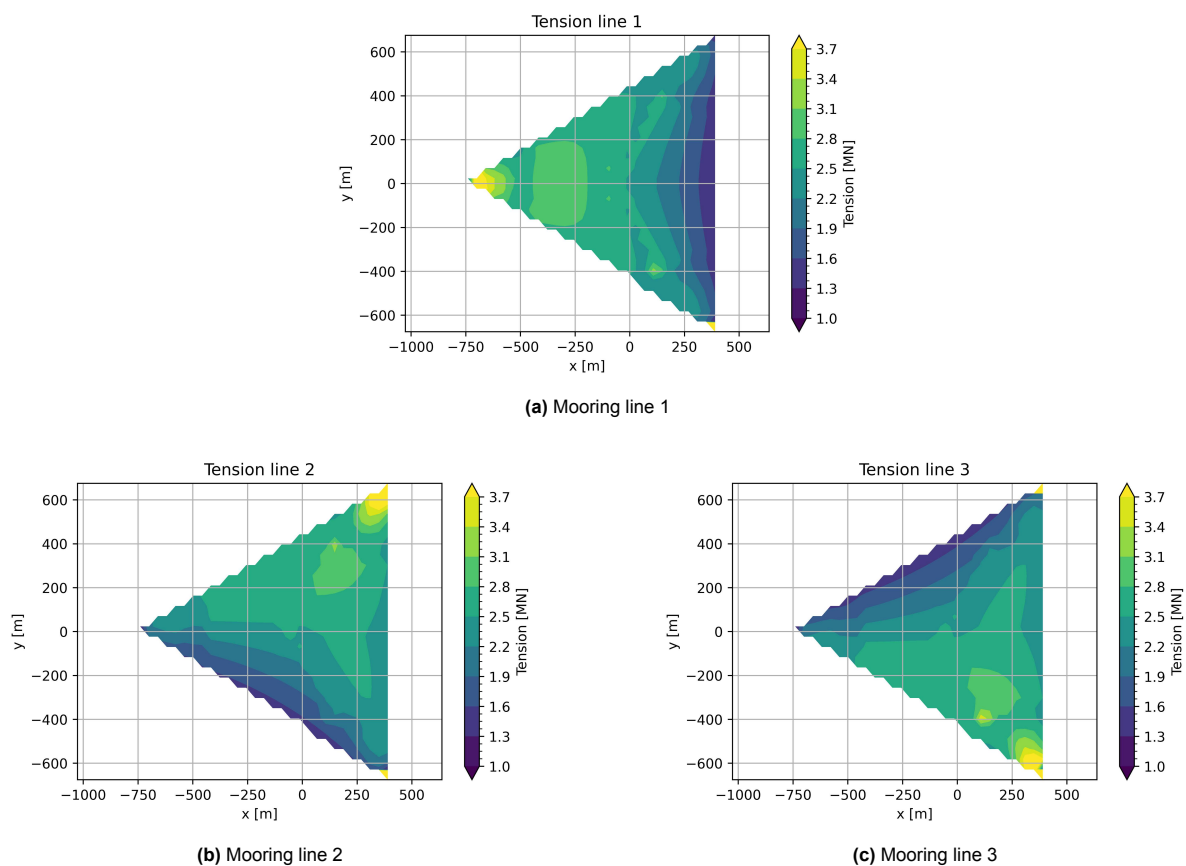


Figure B.1: Contour plot of the tension at the fairlead for various desired positions.

B.2. Vertical fairlead tension

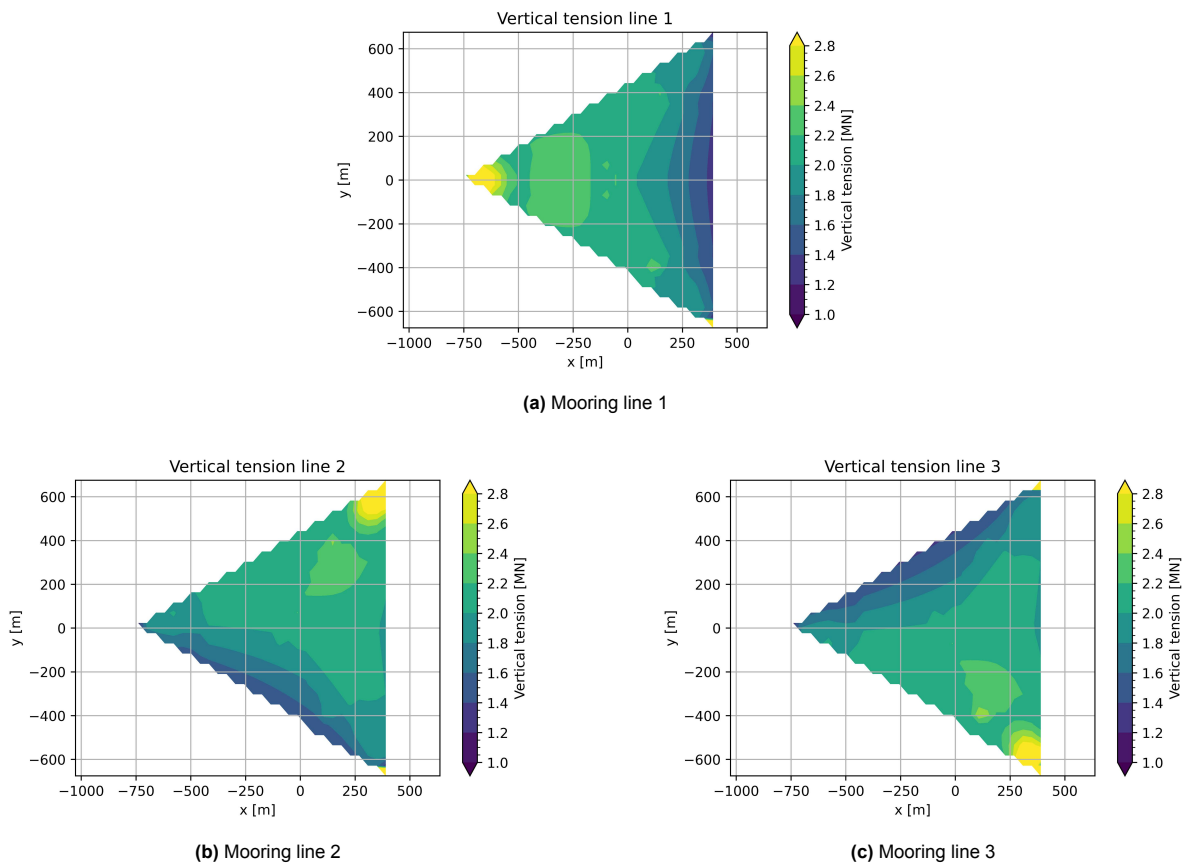


Figure B.2: Contour plot of the vertical tension at the fairlead for various desired positions.

B.3. Absolute error in yaw angle

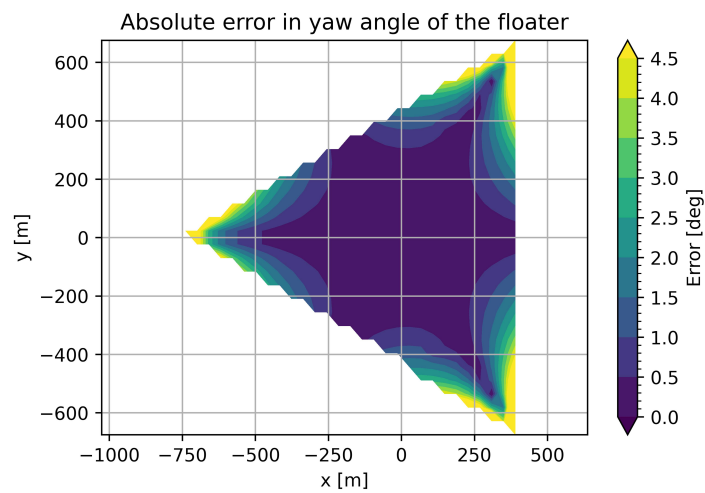


Figure B.3: Contour plot of the absolute error in yaw angle (rotation around z -axis) for various desired positions.